Loyola University Chicago
Loyola eCommons

Dissertations | Theses and Dissertations

2020

Metal Ions Impact on Shewanella Oneidensis MR-1 Adhesion to Ito Electrode and the Enhancement of Current Output

Aisha Awad Alshahrani

Follow this and additional works at: https://ecommons.luc.edu/luc_diss

 Part of the Analytical Chemistry Commons

Recommended Citation

Alshahrani, Aisha Awad, "Metal Ions Impact on Shewanella Oneidensis MR-1 Adhesion to Ito Electrode and the Enhancement of Current Output" (2020). *Dissertations*. 3769.
https://ecommons.luc.edu/luc_diss/3769

This Dissertation is brought to you for free and open access by the Theses and Dissertations at Loyola eCommons. It has been accepted for inclusion in Dissertations by an authorized administrator of Loyola eCommons. For more information, please contact ecommons@luc.edu.

This work is licensed under a Creative Commons Attribution-Noncommercial-No Derivative Works 3.0 License.
Copyright © 2020 Aisha Awad Alshahrani

LOYOLA UNIVERSITY CHICAGO

METAL IONS IMPACT ON SHEWANELLA ONEIDENSIS MR-1 ADHESION TO ITO ELECTRODE AND THE ENHANCEMENT OF CURRENT OUTPUT

A DISSERTATION SUBMITTED TO

THE FACULTY OF THE GRADUATE SCHOOL

IN CANDIDACY FOR THE DEGREE OF

DOCTOR OF PHILOSOPHY

PROGRAM IN CHEMISTRY

BY

AISHA AWAD. AL SHAHRANI

CHICAGO, IL

AUGUST 2020

Copyright by Aisha Awad. Al Shahrani, 2020
All rights reserved.

ACKNOWLEDGEMENTS

I would like to express my sincere gratitude to my research advisor Professor Alanah Fitch for the opportunity to conduct research under her guidance as well as her continuous support, motivation, and encouragement throughout my Ph.D. research. I appreciate her advice during my research as well as writing my dissertation.

In addition to my advisor, I would like to thank my committee members Professor Dali Liu and Professor Daniel Graham for their guidance, insightful comments, advice, and continuous support toward my projects and during my research.

My sincere thanks also go to Professor Rasha Abbasi, for her willingness to serve on my dissertation committee.

I would like to thank Professor John Al-Bazi and the Department of Chemistry at Northeastern Illinois University for providing the HPLC instrument for my sample analyses.

I am deeply indebted to the graduate program director Professor Jacob W. Ciszek who allowed me to use a scanning electron microscope and I appreciate his time spent training me for the same. This research utilized a scanning electron microscope, which was funded by the NSF, Major Research Instrumentation (MRI) Program via Award No. 1726994.

I would like to thank the Department of Biology at Loyola University Chicago and Mr. Joseph Schiluep for providing an Olympus Compound Microscope BH2-RFCA.

I would like to thank the Chair of the Chemistry and Biochemistry Department at Loyola University Chicago Professor Miguel Ballicora and all faculty members for the knowledge that I

have obtained through my interactions with them. I am extremely grateful to and sincerely acknowledge Albaha University for awarding me a scholarship for the doctoral program.

In particular, I would like to thank my family and express my love and gratitude to my parents, Awad Abdullah Alshahrani and Huda Ahmad Alasiri, who are my first teachers; they have been role models as well as an inspiration in my life. I would like to thank them for their love, prayers, and spiritual support throughout my study that has helped in the successful completion of my study and research. I am extremely grateful to my brother Bandar Alshahrani who has supported me during my studies and who deserves my sincere appreciation. In addition, I am grateful to my brothers Nayef Alshahrani, Abdullah Alshahrani, Nawaf Alshahrani, Abdulmajeed Alshahrani, and Ahmed Alshahrani and sister Dareen Alshahrani for their support and valuable prayers.

TABLE OF CONTENTS

LIST OF TABLES

LIST OF FIGURES

LIST OF ABBREVIATIONS

MFC	Microbial fuel cell
EET	Extracellular electron transfer
PEM	Proton-exchange membrane
R	External resistance
FMN	Flavin mononucleotide
RF	Riboflavin
OM	Outer membrane
IM	Inner membrane
CM	Cytoplasmic membrane
LPS	Lipopolysaccharides
EPS	Extracellular polysaccharides
ATP	Adenosine triphosphate
Cyt-c	Cytochrome-c
DET	Direct electron transfer
MET	Mediated electron transfer
SH	Sulfhydryl
ITO	Indium tin oxide
CPE	Controlled potential electrolysis
CV	Cyclic voltammetry

E_i	Initial potential
E_{sw}	Switching potential
I_{pa}	Anodic peak current
I_{pc}	Cathodic peak current
E_{pa}	Anodic peak potential
E_{pc}	Cathodic peak potential
HPLC	High-performance liquid chromatography
NP-HPLC	Normal-phase HPLC
RP-HPLC	Reversed-phase HPLC
UV-Vis	Ultraviolet-Visible spectrophotometer
SEM	Scanning electron microscopy
SE	Secondary electron detector
BSE	Backscattered electron detector
TSB	Tryptic soy broth
$CaCl_2$	Calcium chloride
$PbCl_2$	Lead chloride
$CdCl_2$	Cadmium chloride
$MgCl_2$	Magnesium dichloride
WE	Working electrode
RE	Reference electrode
CE	Counter electrode
DI	Deionized
OD_{650}	Optical density at 650_{nm}

ABSTRACT

The goal of this study is to enhance the efficiency of bacterial extracellular electron transfer (EET) in *Shewanella oneidensis* MR-1 by enhancing adhesion to the electrode's surface. Our results clearly show a major difference in the attachment and behavior of *Shewanella oneidensis* MR-1 for Ca^{2+}, Pb^{2+}, Cd^{2+}, and Mg^{2+}, compared to the control. The final microbial coverage, as measured by confocal microscopy and cathodic peak charge in cyclic voltammetry (Q_{pc}), increases with increasing metal ion concentrations. We found the cells attached to the electrode increased more with the addition of metal ion concentrations in the following order of metals: $Ca^{2+} > Pb^{2+} > Cd^{2+} > Mg^{2+}$, compared to the control. The effect of metal ions on the bacteria's metabolism was tested via riboflavin production and glucose consumption. Metabolic activity mirrored the same order of the activity as the electrochemical results.

CHAPTER ONE

INTRODUCTION

In this research, the aim is to investigate whether metal ions enhance the efficiency of bacterial extracellular electron transfer (EET) in *Shewanella oneidensis* MR-1 by enhancing adhesion to the electrode surface for improving the current output of microbial fuel cells. Adhesion of bacteria has been shown to be affected by metal ions. In this work, the electrochemical behavior is investigated by the variation of metal ions such as Ca^{2+}, Pb^{2+}, Cd^{2+}, and Mg^{2+} and their concentrations. This chapter provides a review of the field of MFC and previous work on metal ions.

Microbial fuel cells (MFCs)

Among modern research communities, energy requirement is one of the extremely important topics that is progressively predominant and is of global interest. Microbial fuel cells (MFCs) constitute one of the modern, effective alternative energy sources.[1-2]

MFC is an interesting field of science and technology. The field of MFCs is the combination of physical and biological catalytic redox activities.[3] Recent studies on the development of MFCs have predominantly focused on the enhancement of power output, which can achieved by the design change of MFCs to surmount barriers of charge (electrons/protons) transport. Alternatively, the power output of MFCs can be enhanced via the increase in the surface area and modification of electrodes.[1, 4]

In 1910, Potter established the initial concept of MFCs.[5] MFCs are bioelectrochemical devices that use bacteria as the catalysts to convert the chemical energy of a fuel (such as organic compounds) to electrical energy under anaerobic conditions.[3, 5-7] In MFCs, bacteria oxidize a substrate and generate a potential via the transfer of electrons to the electrode. The current generation of MFCs has been reported to be dependent on the bacterial cell concentration and electrode surface area.[8-10]

Microbial fuel cells components

Figure 1 shows the schematic of a typical MFC for producing electricity. MFCs comprise anode and cathode chambers, separated by a proton-exchange membrane (PEM), such as Nafion. The anode, or the anaerobic chamber, comprises an electrode, metal-reducing microorganisms (see below), and a substrate. The cathode, or an aerobic chamber, comprises an electrode, an electron acceptor, and a catalyst.[11-13]

In the anode chamber of the MFC, metal-reducing microorganisms oxidize the substrate and produce electrons and protons.[5, 14] The electrons are collected by the anode and flow from the anode via an external circuit to the cathode chamber. The protons pass through the PEM or a salt bridge to the cathode chamber.[7, 15-17] The PEM permits the flow of protons to the cathode while simultaneously blocking the diffusion of oxygen into the anodic chamber.[1, 5] The protons and electrons reacting in the cathode combine with oxygen to form water. A platinum catalyst is typically used to catalyze the reduction at the cathode. Alternatively, an oxygen reducing microorganism can replace such an expensive catalyst.[13, 17-19]

An example of the anodic and cathodic reactions is as follows:[17, 20]

Anodic reaction: $CH_3COO^- + 2H_2O \rightarrow 2CO_2 + 7H^+ + 8e^-$ ($E°' = -0.29$) (1)

Cathodic reaction: $O_2 + 4e^- + 4H^+ \longrightarrow 2H_2O$ ($E°' = +0.82$) (2)

The standard reduction potentials ($E°'$) above have indicated that the redox reaction of the combined 1 and 2 reactions have a maximum attainable MFC potential of +1.11 V at pH7.[17, 20] This means that energy is released. The potentials achieved to date remain below 0.62 V during the generation of a current.[20]

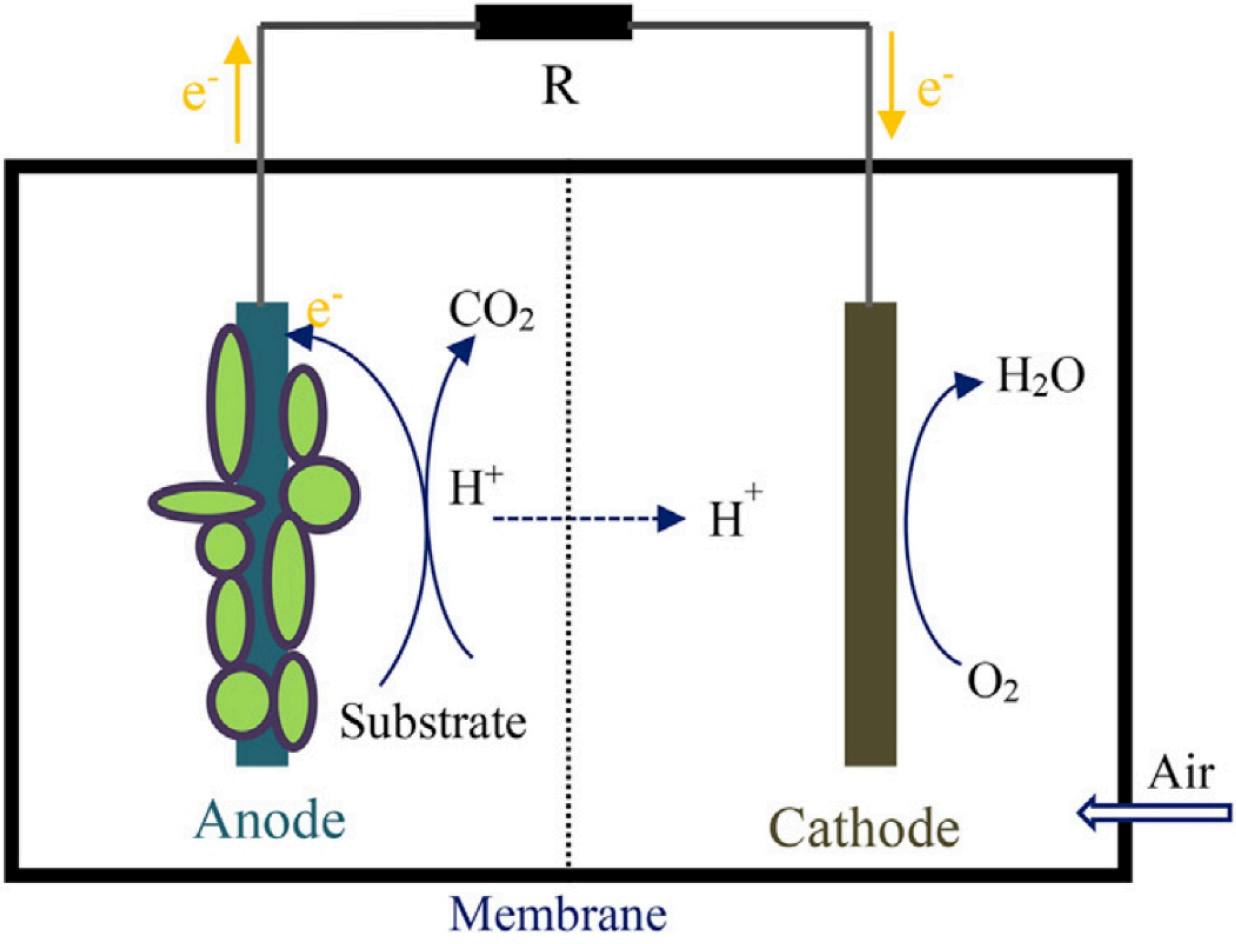

Figure 1. Schematic of a typical microbial fuel cell (MFC) comprising two chambers (i.e., anodic and cathodic chambers, respectively), a proton-exchange membrane (PEM), and external resistance (R) applied for producing electricity.[17]

Table 1 summarizes the description of the basic components of the MFC and materials used for construction.

Table 1. Basic components of microbial fuel cells.[5]

Items	Materials	Remarks
Anode	Carbon paper, carbon cloth, Pt, Pt black, graphite, graphite felt.	Necessary
Cathode	Carbon paper, carbon cloth, Pt, Pt black, graphite, graphite felt.	Necessary
Anodic chamber	Polycarbonate, Plexiglas, glass	Necessary
Cathodic chamber	Polycarbonate, Plexiglas, glass	Optional
Proton-exchange system	Nafion, Ultrex, porcelain septum, salt bridge, or only electrolyte.	Necessary
Electrode catalyst	Polyaniline, Pt, Pt black, Fe^{3+}, electron mediator immobilized on anode.	Optional

Microbial fuel cell applications

In recent decades, a MFC system can be used for different applications, including electricity generation, biohydrogen production, and wastewater treatment, as well as biosensor.

Electricity generation

Electricity generation is the most commonly studied application of MFC technology. Bacteria can be used in an MFC to generate electricity via the converting of chemical energy

stored in a chemical compound to electrical energy.[21-22] The first step toward the current generation in MFCs is the adjustment of electrochemically active bacteria in the anode chamber. Thus, the bacteria in the anode chamber form a conductive biofilm on the electrode surface.[23-24] The production of a biofilm by bacteria is a characteristic that varies from other bacteria or microorganisms. The assembly of adhesives promotes the biofilm formation on the electrode surface from the single bacterial cell.[25-26]

Biohydrogen production

In addition, MFCs can be used in the form of hydrogen for energy sources. MFCs can be easily adjusted to generate hydrogen gas (H_2) instead of electricity generation. An external potential is applied to increase the cathode potential in the MFC circuit. In this mode, under anaerobic conditions, protons and electrons formed by the anodic reaction move to the cathode and produce hydrogen.[22, 27-29]

Wastewater treatment

As an energy source, wastewater demonstrates considerable potential due to the rich variety of organic compounds.[30-31] MFC technology can be used for wastewater treatment due to the use of wastewater as a substrate by bacteria. At the same time, the end products of the oxidation, i.e. electrons and protons, can generate sustainable bioelectricity.[32] In the late nineteenth century, Habermann and Pommer used MFCs for about 5 years of continuous wastewater treatment.[33] Different wastewaters, including sanitary wastes, food-processing wastewater, and swine wastewater, have been reported to provide energy in the form of biodegradable organic matter that can fuel MFCs.[5, 22, 34]

Biosensors

Batteries exhibit a limited lifetime and must be changed or recharged. In contrast MFCs can be continuously be utilized as power source. Thus, MFCs are suitable for powering electrochemical sensors. MFCs can be small telemetry systems used to transmit the obtained signals to remote receivers.[35] MFCs have been reported to be effective biosensors for organic compounds and contaminants for wastewater sensing.[36-37] MFCs can be possibly used as biological oxygen demand (BOD) sensors. In addition, MFC-based BOD sensors have been reported to exhibit extreme operational sustainability and reproducibility and continuous operation for 5 years.[22]

Electrochemically active bacteria

More than 100 years ago, the ability of a microorganism to create an electrochemical potential was discovered.[38] The ability to transfer electrons to extracellular electron acceptors has been reported to occur naturally in several microbes.[39] In an anaerobic environment, bacteria-mediated metal reduction is an important biogeochemical process. Metal-reducing bacteria can transfer electrons generated during respiration to an electron acceptor, such as Fe(III).[40]

The *Shewanella* group is an example of metal-reducing bacteria.[41] Thus far, several bacterial organisms have been used in MFCs. Recently, MFCs have been developed by the two main groups of iron-reducing bacteria: *Shewanella* and *Geobacter*.[42] Extracellular electron transfer (EET) mechanisms in *Shewanella* and *Geobacter* have been examined.[43]

The following bacteria from the *Shewanellaceae* family have been examined: *Shewanella oneidensis* MR-1,[44] *Shewanella frigidimarina*,[44] *Shewanella oneidensis* MR-4,[45] *Shewanella putrefaciens* W3-18-1,[46] *Shewanella putrefaciens* IR-1,[8] *Shewanella putrefaciens* SR-21,[8]

Shewanella loihica PV-4,[47] *Shewanella decolorationis* NTOU1,[48] *Shewanella japonica* KMM 3299,[49] *Shewanella frigidimarina* NCIMB400[50] and *Shewanella marisflavi* EP1.[51]

In our research, *Shewanella oneidensis* MR-1, which is a typical rod shaped bacterium, 2-3 μm in length, and 0.4-0.7 μm in diameter,[52] is utilized (Figure 2). *Shewanella oneidensis* MR-1 was first isolated in 1988 from Lake Oneida, NY, and it was identified in a various environments, including soil, sediments, water column, and clinical isolates.[53-54]

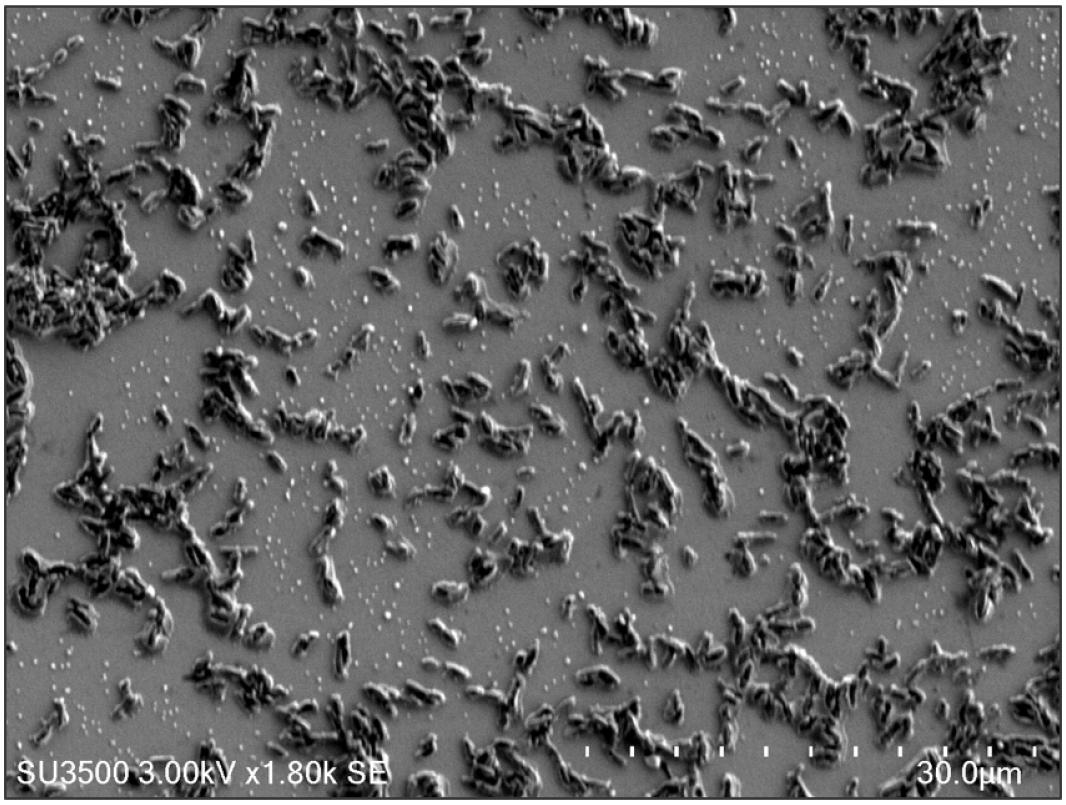

Figure 2. Scanning electron microscopy image of *Shewanella oneidensis* MR-1.[55]

Shewanella oneidensis MR-1 1 is a gram-negative bacterium, previously referred to as *Shewanella putrefaciens* MR-1.[53] Gram-negative bacteria stain red due to a thinner peptidoglycan layer during decoloring; hence, these bacteria do not retain crystal violet.[56]

Gram-negative cells contain three layers (Figure 3). The first layer comprises an inner

membrane (IM), which is also known as the cytoplasmic membrane (CM). The second layer comprises a peptidoglycan layer within the periplasmic space, which is outside the cytoplasmic membrane. The peptidoglycan is located between the outer and inner membranes. Several membrane proteins, known as lipoproteins, form a special chemical union between the outer membrane and peptidoglycan layer of gram-negative cells. Lipoproteins contain lipid tails that are deeply inserted into the hydrophobic domain of the membrane. A portion of the protein is linked to the peptidoglycan layer by either covalent or electrostatic bonds. The third layer is the outer membrane (OM) containing porins, which permit the movement of small molecules through the membrane.[57-60]

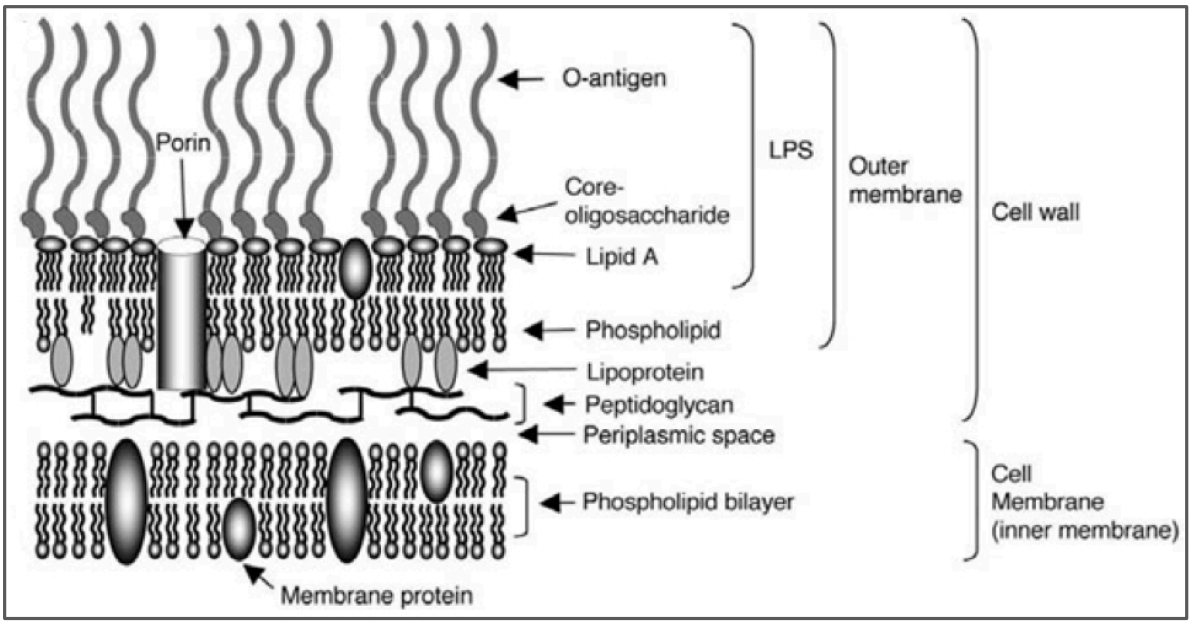

Figure 3. Representation of a gram-negative cell envelope structure, comprising an outer membrane bound by lipoproteins to a thin peptidoglycan layer. The peptidoglycan layer is present within the periplasmic space that is created between the outer and inner membranes. The outer membrane comprises lipopolysaccharide molecules that extend into the extracellular space and porins.[61]

The external membrane surface is filled with lipopolysaccharides (LPS), which extend into the extracellular space and O-antigens.[57, 60] LPS molecules comprise two main regions:

polysaccharide and lipid regions. The polysaccharide region comprises two parts: core oligosaccharide and O-antigens. The schematic in Figure 3 shows the lipid region, indicated as lipid A.[57, 62] LPS exhibit high-affinity binding sites on the surface of gram-negative bacteria for divalent cations.[63] Metal ions bind to extracellular polysaccharides (EPS) and can affect their adhesion mechanism. Negatively charged groups in O-antigen species have been reported to mediate Ca^{2+} dependent cell adhesion.[64-65]

Respiration pathway of *Shewanella oneidensis* MR-1

The *Shewanella oneidensis* MR-1 belongs to a specific class of microorganisms that exhibit a unique ability to transfer electrons from its metabolic pathways to extracellular minerals.[66] *Shewanella oneidensis* MR-1 cell comprises outer membrane (OM) cytochromes. Cytochromes on the cell surface can facilitate the direct transfer of electrons to electron acceptors.[39, 67-69] *Shewanella oneidensis* MR-1 is a facultative microbe, implying that it can grow in an environment in the presence or absence of oxygen.[70-71]

Under anaerobic conditions (in the absence of oxygen), glucose is converted to two pyruvate molecules in cytosol (glycolytic cycle), generating either ethanol or lactic acid (Figure 4). Ethanol production occurs by fermentation. Meanwhile, under aerobic conditions (in the presence of oxygen), the microbe uses an aerobic electron-transport pathway. Respiration mainly occurs in the mitochondrion, producing up to 38 Adenosine triphosphate (ATP) molecules per glucose and two pyruvate molecules (Figure 4). Oxygen is the terminal electron acceptor, producing water.[72]

These processes can be harvested for energy. The respiratory chain (Figure 5) process in the microbial fuel cell has a maximum potential of ~1.11 V (see above). The maximum available

potential, on the other hand, is estimated to be about 0.49 V, while the remaining energy (0.62 V) can be used for electricity generation in an MFC.[17, 20, 24] The typical output of microbial fuel cells using *Shewanella* is in the range of 0.1–2 μA/cm^2.[48, 73-76]

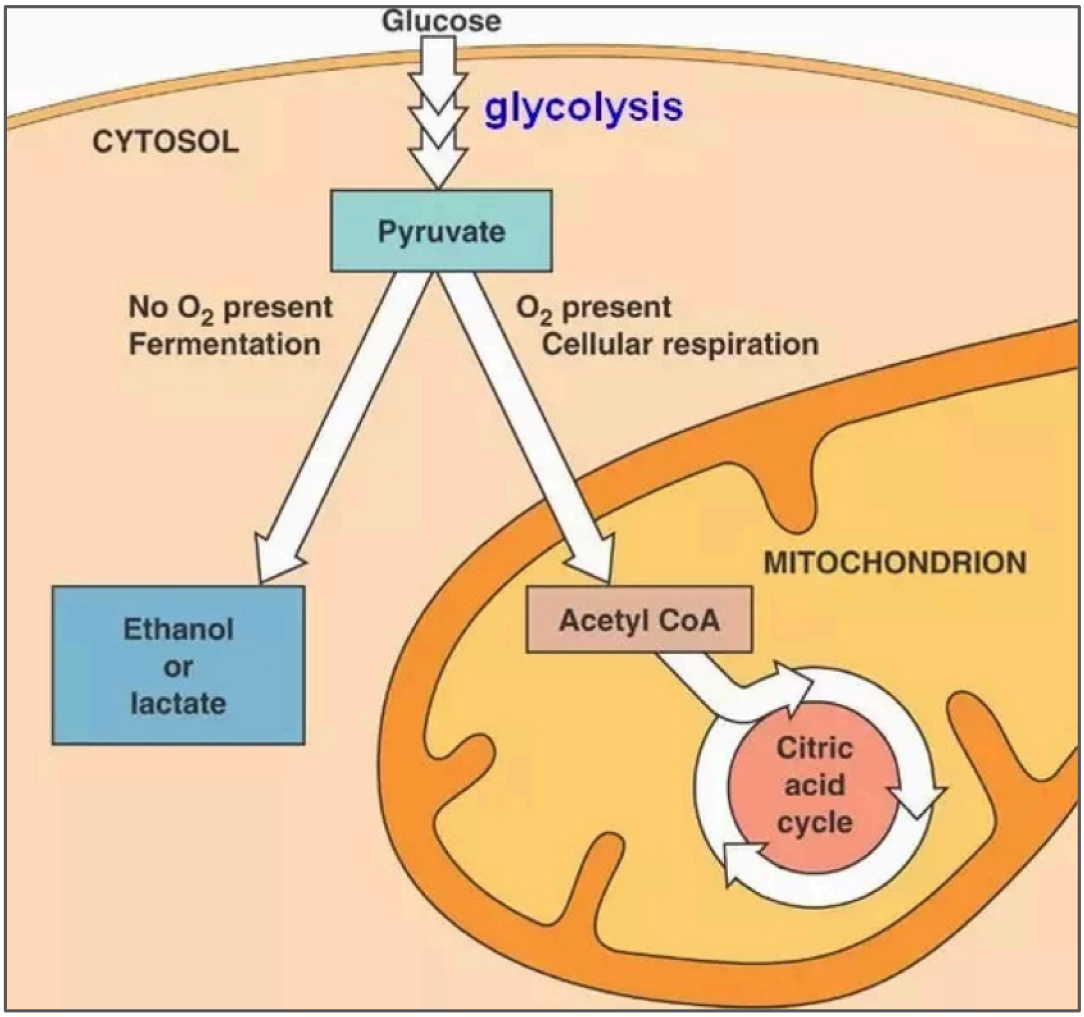

Figure 4. Schematic showing cellular respiration and fermentation. Pyruvate is the "fork" in metabolic pathways. Typically, pyruvate goes through one of these two pathways in a facultative anaerobe (which is capable of aerobic cellular respiration and fermentation) depending on the presence or absence of oxygen.[72]

Under anaerobic respiration, bacteria use a transmembrane electron-transfer pathway, transporting electrons from the cell interior to the extracellular surface (Figure 5). Genetic and biochemical studies have revealed that under anaerobic conditions, respiration can deliver electrons to Fe(III) oxides or anodes.[9]

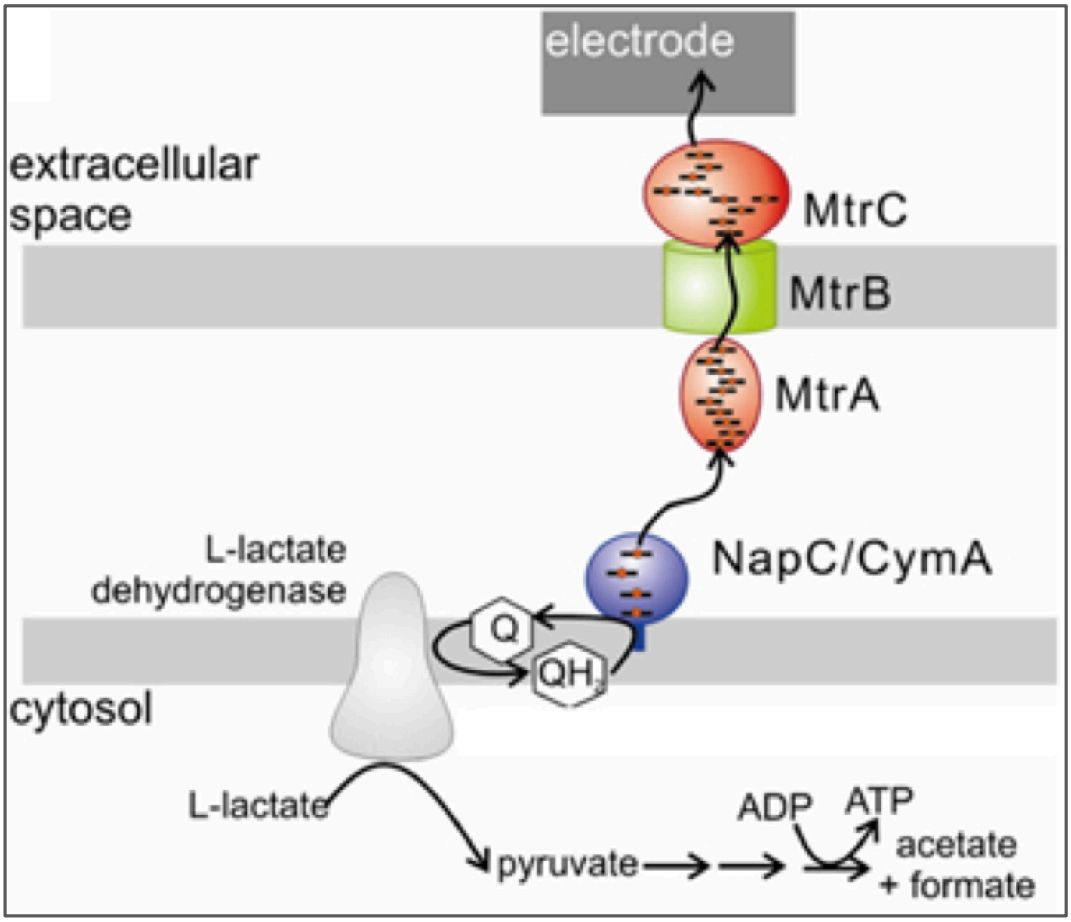

Figure 5. Respiration pathway of *Shewanella oneidensis* MR-1. There are main components of the electron-transfer pathway through a series of intermolecular electron transfers. Electrons are derived from lactate to an anode via the Mtr pathway. The route for the electrons starts from menaquinol to CymA, from CymA to MtrA, and from MtrA through the MtrB pore membrane to MtrC. Electrons are transferred from MtrC to the extracellular space. In *Shewanella oneidensis* MR-1, CymA accepts electrons from menaquinol. In *Escherichia. coli*, NapC accomplishes this task. [77]

L-lactate dehydrogenase oxidizes L-lactate to pyruvate in the cytosol, which is converted to formate and acetate. The produced lactate transfers electrons from the cytosol to the inner

membrane (IM) cytochrome CymA. Electrons are transferred from CymA to the periplasm (MtrA) via menaquinol (MQH_2) and from MtrA to the extracellular surface (MtrC and OmcA) in the outer membrane (OM). From MtrC and OmcA, electrons can be transported to terminal electron acceptors via redox shuttles (e.g., flavins) or by direct contact by proteins on the cell surface (e.g., MtrC and OmcA).[77] This pathway permits cell respiration via the exchange of electrons with solid minerals instead of oxygen or metallic electrodes. In the process, due to the flow of electrons through electrodes, cells produce electrochemical currents.[66]

Extracellular electron-transfer mechanisms of *Shewanella oneidensis* MR-1

Different microorganisms have developed variable electron-transfer mechanisms to complete respiration via an extracellular pathway.[78] Three electron-transfer mechanisms from the microbe to the electrode surface exist (Figure 6).[17, 79-80]

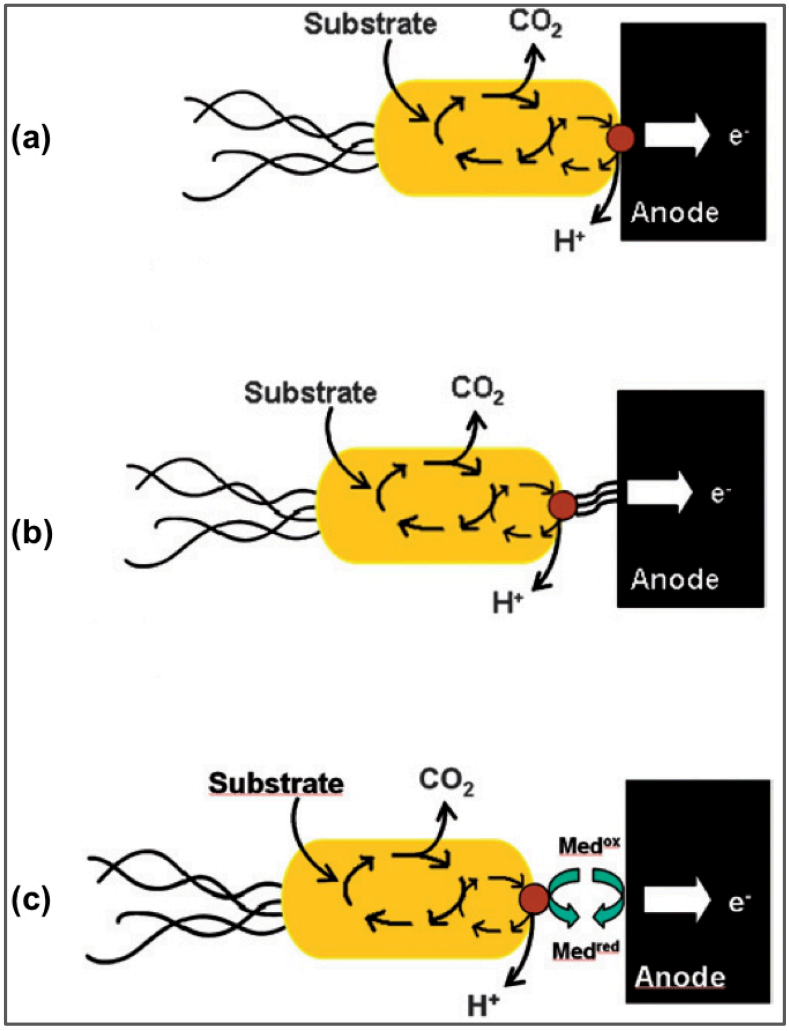

Figure 6. Schematic showing the role of three extracellular electron-transfer mechanisms at the anode. (a) Direct electron transfer via the outer membrane cytochromes. (b) Electron transfer via electrically conductive "nanowires" (pili). (c) Indirect electron transfer by mediated electron transfer via redox shuttle mediators.[80]

Direct electron transfers by c-type cytochromes

Figure 6(a) shows the first direct electron-transfer mechanism by the physical/electrical contact between the bacterial cell membrane and anode substrate. This mechanism requires the microorganisms to contain OM redox macromolecules, e.g., cytochromes. A cytochrome enables the transfer of electrons to the anode surface.[80] Metal-reducing bacterium *Shewanella*

putrefaciens MR-1 has been reported to contain cytochromes in its outer membrane (OM). Under anaerobic conditions, in the absence of terminal electron acceptors, these electron charge carriers (i.e., cytochromes) can generate an anodic current.[81-82]

The c-Type cytochromes (CTCs) are typical heme-containing proteins in metal-reducing bacteria. CTCs have been considered to be one of the most effective electron-transfer strategies for the production of current by electrochemically active bacteria. Cytochromes comprise a large family of proteins. Most of these proteins contain c-haem cytochromes, referred to as cytochrome-c (cyt-c). Cytochrome-c comprises iron coordinated by protoporphyrin IX, which is covalently linked to a peptide by thioether bonds (Figure 7(a)). These bonds typically arise from the binding of Cys-His amino acids, providing a histidine axial ligand to the haem iron. The axial position of histidine amino acid ligands maintains the correct direction of the cytochromes (Figure 7(b)).

Correct orientation requires the rapid transfer of electrons between two or more c-haems (multiheme proteins) that are arranged to get adjacent iron within a distance of 15.5 A° from each other. These c-haems support the rapid electron transfer (ET) via a series of intraprotein electron transfer steps, involving the ferric/ferrous redox couple.[83]

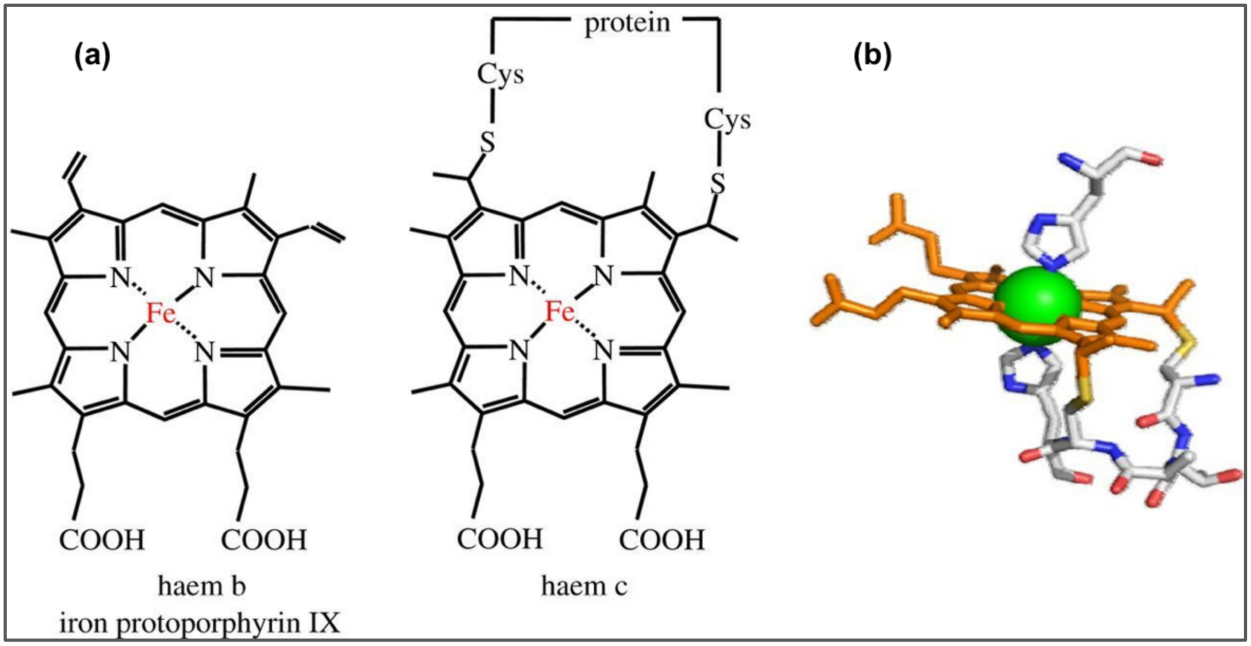

Figure 7. Diagram showing (a) two types of haem found in biological systems, i.e., haem b and haem c, respectively, where haem c includes covalent thioether linkages to the protein. (b) haem c binding through the Cys–His binding motif (providing the proximal axial histidine ligand) and with histidine as the distal axial ligand.[83]

Shewanella oneidensis MR-1 contains 42 generally considered c-type cytochromes.[84-85] Five c-type cytochromes can be expressed : OmcA, MtrC/OmcB, MtrD, MtrA, and MtrF.[86] MtrC and OmcA are two decaheme c-type cytochrome lipoproteins, which are known to be terminal extracellular reductases of *Shewanella oneidensis* MR-1. MtrC and OmcA play an important role in the direct electron transfer (DET) mechanism.[39, 87]

Electron transfer by conductive nanowires

Figure 6(b) shows the second mechanism of the direct electron transfer via conductive nanowires (pili). Some microbes have been reported to develop electronically conducting nanowires to create physical or electrical connections with an electrode.[80] Pili are referred to as microbial nanowires. Bacterial nanowires have found in *Shewanella oneidensis* MR-1 and some other bacteria.[85, 88] These pili are long proteinaceous filaments of 1 μm, extending from its outer

surface to the extracellular matrix. These pili can participate in extracellular electron transport mechanisms, due to their long filament-like structure and conductive properties. Msh-pili, type IV pili, and flagella are found in *Shewanella oneidensis* MR-1. Type IV pili play a key role in adhesion between the bacterial species and electrode surface.[2, 85]

Indirect electron transfer via electron shuttles

Figure 6(c) shows the third mechanism of indirect electron transfer through mediators. Mediated electron transfer (MET) can be either via the added (exogenous) soluble redox or secreted (endogenous) mediators. Any electron mediator must satisfy the following requirements. First, it must exhibit physical contact with the electrode surface. Second, it must exhibit electrochemical activity. Third, it must contain a standard potential similar to the redox potential of the substrate.[80] Soluble mediators are recycled by simultaneous reduction (accepting electrons from the cell) and oxidation (donating electrons to anode), which can be achieved in MFCs. When the reduced form of the shuttle comes into contact with an appropriate catalytic substrate such as the anode, the electrons are passed to suitable external acceptors, such as insoluble Fe(III) oxides or the MFC anode. Hence, the addition of exogenous electron shuttle compounds leads to the improved current production in MFCs.[89-90]

Shewanella oneidensis MR-1 and *Geobacter sulfurreducens* predominantly produce two flavin molecules: riboflavin (RF) and flavin mononucleotide (FMN). These molecules are considered to serve as electron shuttles to the electrode, which function as cofactors for cytochromes such as OmcA and MtrC. FMN comprises the binding sites for MtrC, whereas RF serves as a cofactor for OmcA. RF-OmcA and FMN-MtrC increase the enhancement of the electron transfer to the electrode surface.[13, 25]

Instead of exogenous mediators, endogenous redox mediators can act as shuttles, which are secreted by the bacteria itself as secondary metabolites.[80, 91] *Pseudomonas*, *Lactobacillus*, and *Enterococcus* have been reported to produce endogenous electron shuttles, such as phenazines in the case of *Pseodomonas aeruginosa*, which promote the transfer of electrons to the anode. In addition, this same electron shuttle mechanism has been reported for *Shewanella oneidensis* in extracellular Fe^{3+} reduction. Expression of natural mediators, such as pyocyanin and riboflavin (RF), is an energy-intensive process that is generated by bacteria under strain.[81]

Strategies for the efficiency improvement of extracellular electron transfer

Extracellular electron transfer efficiency is a key topic in MFCs. Several strategies exist for the improvement of the extracellular electron transfer efficiency and MFC power output.

As described above MFC efficiencies are affected by electrode modification,[92] anode structure design,[93] cell configuration,[94] electrolyte compositions,[95] and nutritional substrates.[70]

Electrolyte composition is a key factor and can affect various aspects of MFCs, including power output, surface attachment, and biology. Environmental factors, such as pH, metal ions, among others, have been used to enhance performance due to their cost-effectiveness and operational ease. Some electrochemically active bacteria prefer alkaline electrolytes,[96] whereas others can function in an acidic environment.[97] Electrolyte pH optimization is key for the development of MFC performance.[98]

Effects of electrolyte composition on microbial fuel cell power output

Metal ions such as Fe^{3+}, Ca^{2+}, Cu^{2+}, Cd^{2+}, and Na^{+} have been reported to enhance the MFC activity.[99] For example, Wu et al.[100] have reported that the addition of 10 mM Fe^{3+} to *Shewanella oneidensis* MR-1 solution leads to a minimal 1.1 times increase in power output of

MFCs compared to the control. Kim et al.[101] have reported that the addition of 100 mM Fe^{3+} in the leads to the 80% increase in the power output of MFCs. Furthermore, Fitzgerald et al.[102] have reported that the addition of Ca^{2+} at the concentration of 1.4 mM increased the current density by more than 80% in *Shewanella oneidensis* MR-1. In addition, heavy metals can increase power output. As an example, Xu et al.[99] found that the addition of 5-6 nM Cu^{2+} and Cd^{2+} increased the power output of MFCs by 1.3-1.6 times.

One possibility is that metal ions have non-specific effect solution properties. Metal ions are known to increase the conductivity of electrolytes, decrease their internal resistance, and increase the power output of MFCs.[103] Electrolyte concentrations (related to ionic strength) affect the MFC power output. Liu et al.[104] have reported that the addition of Na^{+} leads to the improved MFC power output via the increase in the solution ionic strength from 100 to 400 mM. Lefebvre et al.[105] observed that Na^{+} (20 g L^{-1}) improved the maximum power output of MFCs by 30%.

Effects of electrolyte composition on surface attachment

Outside of MFC research, electrolytes have been reported to affect surface attachment. The classical Derjaguin–Landau–Verwey–Overbeek (DLVO) theory has been applied to describe bacterial adhesion to different surfaces. DLVO is a model that describes for electrostatic repulsion and van der Waals attractive (V_A) forces between a cell and a flat surface. The repulsive interaction from the electrical double layer (V_R) is due to the negative charge of the cells and substrate.

$$V_{TOT} = V_A + V_R \quad (3)$$

$$V_A = -\frac{Ar}{6d} \quad (4)$$

Where A is the Hamaker constant, which describes the strength of the V_A interaction between two particles, or between a particle and a substrate, d is the separation distance between the cell and the substratum, and r is the cell radius.

The double-layer interaction is the result of the interactions between charged molecules, and the presence of surrounding ions strongly impacts its strength and range.[106] The species of opposite charge are attracted to a charged surface, while species of the same charge are repelled, thus forming a compact region close to the surface and a loose region away from the surface. The double-layer consists of a Helmholtz or Stern layer and a diffuse layer. The Stern layer is a layer of ions that are bound to the surface and to form a compact layer, whereas the diffuse layer is made up of ions that are loosely free ions that are affected by the electrostatic force of the charged surface.[106-107]

The electric double layer can be related to the surface potential Ψ, the distance between the cell and the surface d and the Debye length κ, as shown in the equation (5):

$$V_R \propto \Psi^2 e^{-kd} \tag{5}$$

The inverse Debye length, $1/\kappa$, which for an electrolyte is defined in the equation (6):

$$\kappa = \sqrt{\frac{2000e^2 N_A C}{\varepsilon\varepsilon_0 kT}} \tag{6}$$

where N_A is Avogadro's constant, C is the concentration (in mol 1^{-1}) of the ions of the electrolyte, ε is the dielectric constant of the solution, ε_0 is the dielectric permittivity of free space, k is the Boltzmann constant, e is the electronic charge, and T is the absolute temperature. The inverse Debye length values depend on ionic strength (I).

There are a range of laboratory studies on the effect of electrolyte concentration on

compressing the double layer and the causes of bacterial adhesion. Natural surfaces have a net negative charge[106, 108] and the net charge of bacteria is negative as well.[106, 109] Consequently, at high ionic strength, the double-layer interaction is compressed.[106, 110] The presence of metal ions in a solution leads to the passive increase in the bacterial attachment to soil surfaces.[111] Research has revealed that the electrolyte affects bacterial adhesion to Teflon,[112] metal surface wettability,[113] hydroxyapatite,[114] glass, and metal oxide[63] surface by increasing the ionic strength.[63] Choi et al.[115] have investigated the attachment and detachment of bacteria under various ionic strengths by using a quartz sand surface. McEldowney et al.[116] have been studied the effect of physicochemical factors that affect the adhesion of bacteria onto a polystyrene substrata.

It was suggested that an ion compresses the double layer, making it easy for the microbes to approach the electrode and attach to the surface.[117] This consists of a non-specific impact of the metal ion on bacteria adhesion.

Effects of electrolyte composition on biology

Biological effects have been reported for electrolytes such as metal ions. Metal ions can affect the adhesion of bacteria to a surface in different species, such as *Shewanella oneidensis* MR-1. Ca^{2+} binding proteins impact cell-cell aggregation.[64, 118] The association of Ca^{2+} with *Shewanella oneidensis* MR-1 has been reported to affect extracellular electron transfer due to the presence of Ca^{2+} ions near cytochromes as observed in the recent crystal structure of MtrF. One of these Ca^{2+} has been located close to heme 3 in the crystal structure.[119-120] Ca^{2+} and Mg^{2+} can affect bacterial adhesion and biofilm formation via the effects on electrostatic interactions and physiology-dependent attachment processes.[121-122] Ca^{2+} and Mg^{2+} are attracted to the negative

charge of the of the bacterial cell wall. These metals are strongly bound, and there is only a small portion of metal ions remain in the solution.[123]

Lipopolysaccharide (LPS) has been reported to contain high-affinity binding sites for divalent cations on a gram-negative bacterial surface.[63] It has been suggested that negatively charged groups in the O-antigen are able to mediate Ca^{2+} dependent cell adhesion as well.[64-65] These extracellular polysaccharides (EPS) play an important role in mediating the surface bacterial colonization and cell adhesion.[124] Bacterial metabolism has been observed to affect the adsorption of Cd^{2+} on cell-wall functional groups. Cd^{2+} binding occurs at a great distance from the inner plasma membrane of gram-negative cells.[125] Xing et al.[126] have found carboxyl and phosphate groups are predominantly responsible for the adsorption of Cd^{2+} on bacterial cells and affect the affinity between the bacterial cells and metal ions.

Microbial-driven electrochemical enhancement by metal ions may be offset by toxic biological effects. Metal ions tend to bind to a sulfhydryl (SH) group inside the cell. Metals can prevent the activity of sensitive enzymes via binding to the sulfhydryl groups.[127] In plants, they can affect photosynthesis, gaseous exchange, and nutrient absorption of plants. In addition, heavy metals interact with plant antioxidant levels and reduce the nutritive value of the product.[128]

CHAPTER TWO

TECHNIQUES AND METHODS

This chapter provides a detailed description of general electrochemical concepts, voltammetry, potential step chronoamperometry, and cyclic voltammetry (CV), high-performance liquid chromatography (HPLC), UV–visible double beam spectrophotometer, confocal microscopy, and scanning electron microscopy (SEM), as well as chemicals, microbes, and culture conditions, electrochemical cell setup and measurements, and analysis of glucose consumption and riboflavin production by using HPLC in this Ph.D. project.

General Electrochemical Concepts

Electrochemistry involves the study of chemical changes that occur by the passage of an electric current and the generation of electrical energy by a chemical reaction. Current results from the transfer of charges across the electrode–solution interface, which can occur when species undergo electrochemical reactions on the electrode surface. This process is collectively referred to as faradaic processes as these reactions are controlled by Faraday's law. For example, the extent of chemical reaction caused by the flow of current is proportional to the amount of electricity passed.[129]

Electron transfer can occur between molecules or between electrodes and molecules. In an electrochemical system, energy is applied to a solution in the form of an electrode potential, subsequently leading to current measurement.

Generally, the energy available in the electrochemical system depends on the redox potential, as shown in equation (7):[129-130]

$$\Delta G = -nFE \quad (7)$$

where ΔG is the energy applied in joules (coulomb-volts), n is the number of equivalents (electrons per mole), F is the Faraday constant in coulombs (9.64846×10^4 C/eq), and E is the applied voltage (V). The number of equivalents (electrons per mole) is expressed by the reduction reaction shown in equation (8):

$$Ox + en \leftrightarrow Red \quad (8)$$

where *Ox* is the oxidized species, n is the number of electrons transferred, and *Red* is the reduced species.

The electrochemical system comprises two key electrodes. The first electrode comprises some charge conducting material that can be placed in a conductive media. The second electrode is connected to a voltage (energy) source. The solution is in equilibrium with the distribution of ions in the oxidized and reduced states before ΔG (energy) is applied to the electrode surface.[131] For an electrode reaction, equilibrium is characterized by the Nernst equation for the equilibrium potential across an electrode-electrolyte interface.[130-131]

$$E = E^\circ - \frac{RT}{nF} \ln \frac{C_R}{C_O} \quad (9)$$

where E° is the formal potential, R is the molar gas constant, T is the temperature (K), n is the number of electrons exchanged, F is Faraday's constant (96,485.3 C/mol), and C_R and C_O are the bulk concentrations.

Some factors can enhance the advantages and disadvantages of electrochemical methods, including heterogeneity of the solution, rate of the electron-transfer event, and the coupling of

chemical processes. Most of the voltammetric techniques are based on all of these factors. Cyclic voltammetry is an extremely popular technique used by most electrochemists.

Voltammetry

Voltammetry comprises a group of electroanalytical methods that provide information about an analyte, which is obtained by measuring the current as a function of the applied potential. The current is obtained under conditions that encourage the polarization of an indicator or a working electrode. Generally, to enhance polarization, working electrodes are microelectrodes with surface areas of at most a few square millimeters and a few square micrometers or less in some applications.[132] Several voltammetry methods exist, two of which are employed in this dissertation: chronoamperometry and cyclic voltammetry. A voltage or a series of voltages are applied to the electrode, and the corresponding flow of current is monitored.[133]

Electrochemical Techniques

Potential Step Chronoamperometry

In chronoamperometry, potential is applied to the working electrode. The potential is stepped from one potential to another; this potential step affords a current, which is monitored as a function of time.[134] Figure 8 shows the basic waveform and current–time curve in potential step chronoamperometry.[135] The initial potential (E_1) is maintained constant for a specific time. Then, the potential is stepped to the final potential (E_2), as shown in Figure 8(a). This potential can cause electrolysis or electrochemical reactions of the electroactive species on the electrode surface. Therefore, a plot of current as a function of time is obtained (Figure 8(b)).

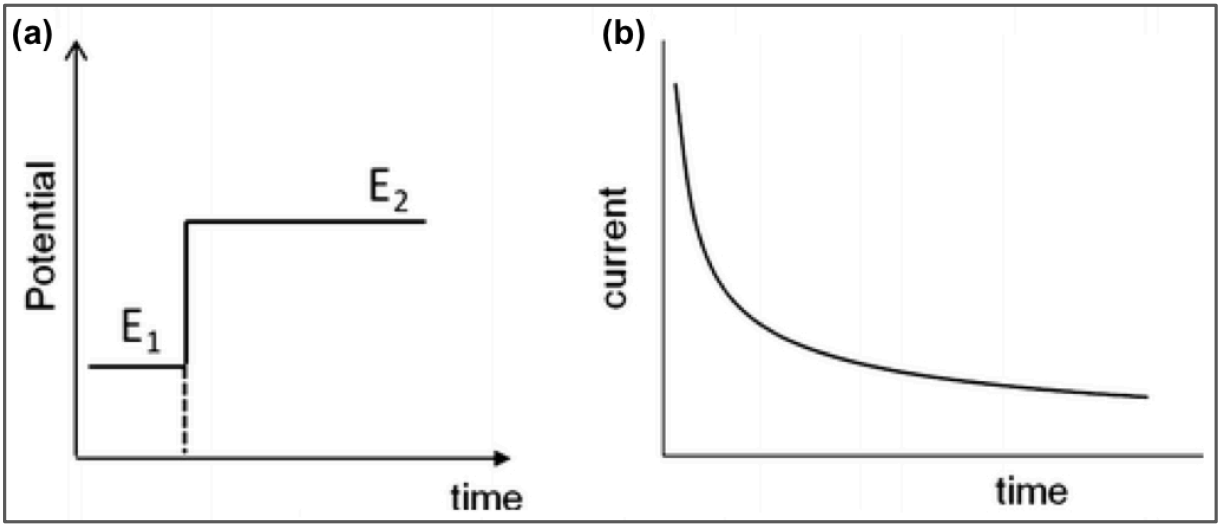

Figure 8. Typical input (waveform) potential change as a function of time (a) (output) and current change as a function of time (b).[135]

Controlled potential electrolysis (CPE) is an application of chronoamperometry. In CPE, the working electrode is maintained at a constant potential until the electrolysis of the solution is completed. If only the oxidized species is present at the start, the potential is then set at a constant value that is sufficiently negative to cause rapid reduction and is maintained at this value until only the reduced species is present in the solution. The current is integrated to calculate the total charge passed during CPE (equation 10).

$$Q = \int_0^t I\mathrm{d}t \tag{10}$$

Where I is the current at time (t), and Q is the charge or number of electrons passed during electrolysis. This equation also can be expressed as follows:

$$\mathrm{N} = \mathrm{Q}/\mathrm{nF} \tag{11}$$

Where (N) is the amount of material electrolyzed in moles, (F) is Faraday's constant (96,485 Cmol^{-1}), and (n) is the number of electrons transferred per molecule.[136]

Cyclic Voltammetry

Cyclic voltammetry (CV) is the most widely used electroanalytical technique for investigating electroactive species. CV can be employed for examining a compound, a biological material, or an electrode surface. Typically, it is employed to observe redox processes of molecular species over a wide potential range.[137-138] In CV, the applied potential is first linearly scanned from an initial potential to a switching potential, then and then a second switching potential is applied where the cycle is repeated (Figure 9(a)).

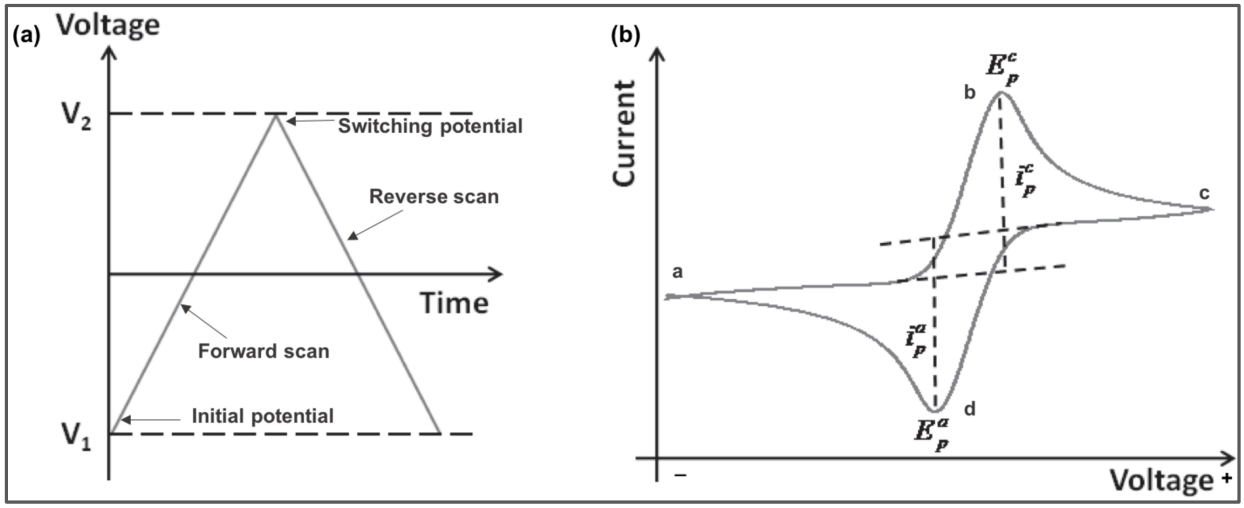

Figure 9. Cyclic voltammetry waveform (a) and a typical cyclic voltammogram (b). Parameters Epc, Epa and Ipc, Ipa are the potential and current at the cathodic and anodic peaks, respectively.[139]

Key parameters in CV include the anodic peak current (Ipa), cathodic peak current (Ipc), anodic peak potential (Epa), and cathodic peak potential (Epc), as shown in Figure 9b. The current is measured at the working electrode during the potential scans, and a cyclic voltammogram is obtained. Reduction begins from the initial potential (a) to the switching potential (c). In this region, the potential scans negatively to cause reduction, affording Ipc and Epc at (b). When all of the substrate on the electrode surface is reduced, Epc is reached.

Oxidation occurs from the switching potential (c) to the initial potential (a). The potential scans positively to cause oxidation, affording Ipa and Epa at (d). When all of the substrate on the electrode surface is oxidized, Epa is reached.[138]

Two experiments in CV include diffusion voltammetry or adsorption on the electrode surface, respectively (Figure 10).

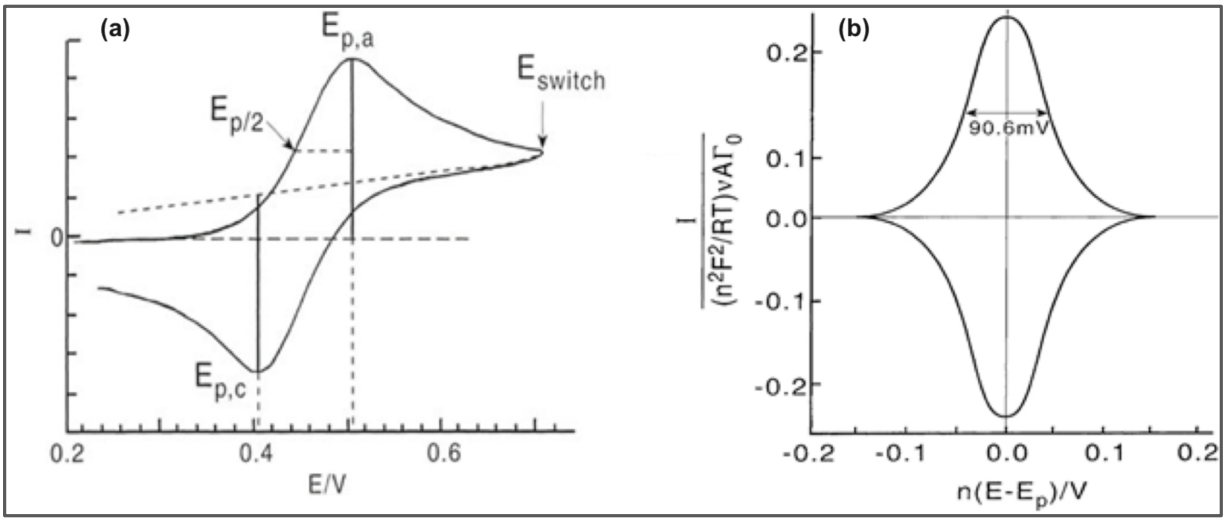

Figure 10. Types of cyclic voltammetry considered: (a) diffusing voltammetry and (b) adsorbed voltammetry.[140]

The peak current dependence on the scan rate for reversible electron-transfer processes is described by the Randles–Sevcik equation (equation 12).[138]

$$i_p = (2.69\times10^5)n^{3/2}AD^{1/2}Cv^{1/2} \quad (12)$$

where i_p is peak current (A), n is the number of electrons transferred, A is the electrode surface area (cm^2), and D is the diffusion constant (cm^2/s), C is the concentration of solution species (mol/cm^3), and v is the scan rate (Vs^{-1}). The peak current (I_p) linearly increases with the square root of the scan rate $\upsilon^{1/2}$ (Vs^{-1}) for the diffusing redox species. Ip in the adsorbed species is directly proportional to the scan rate (Vs^{-1}). One feature of diffusion-controlled cyclic

voltammograms is the determination of the number of electrons transferred in the electrode reaction (n) from the separation between the peak potentials (ΔE_p), as can be observed by the following equation:[138]

$$\Delta E = E_{pa} - E_{pc} = \frac{0.059}{n} \quad (13)$$

The peak potential is separated and shifted with the scan rate due to the diffusion of the analyte from the electrode. Notably, the reversibility of the redox couple depends on the selected scan rate. The peak separation increases in case of a rapid scan rate. Values for the cathodic and anodic peak currents of a simple reversible rapid redox couple should be identical (equation 14).[138]

$$\frac{i_{pa}}{i_{pc}} = 1 \quad (14)$$

In contrast, the cyclic voltammogram of an adsorbed species should be symmetric with respect to the I = 0 axis. The width $E_{1/2}$ = 90 mV at the half-height of the peak.[137, 141] The formal reduction potential ($E°$) is centered between E_{pa} and E_{pc} for a reversible couple (equation 15).[138]

$$E° = \frac{E_{pa}+E_{pc}}{2} \quad (15)$$

where *Epa* is the anodic (oxidative) peak potential, and *Epc* is the cathodic (reductive) peak potential.

High-Performance Liquid Chromatography

High-performance liquid chromatography (HPLC) is an analytical technique employed for the separation and quantification of a mixture of components. The mixture of components must be soluble in the liquid phase. The two major modes of HPLC are as follows: normal-phase HPLC (NP-HPLC) and reversed-phase HPLC (RP-HPLC). In NP-HPLC, the stationary phase is

more polar than the mobile phase, whereas in RP-HPLC, the stationary phase is less polar than the mobile phase. Currently, NP-HPLC has been rarely employed, while RP-HPLC is employed for almost all HPLC separations.[142] A typical HPLC instrument comprises a solvent (mobile phase), a high-pressure pump, an injector, a column (stationary phase), and a detector (Figure 11).

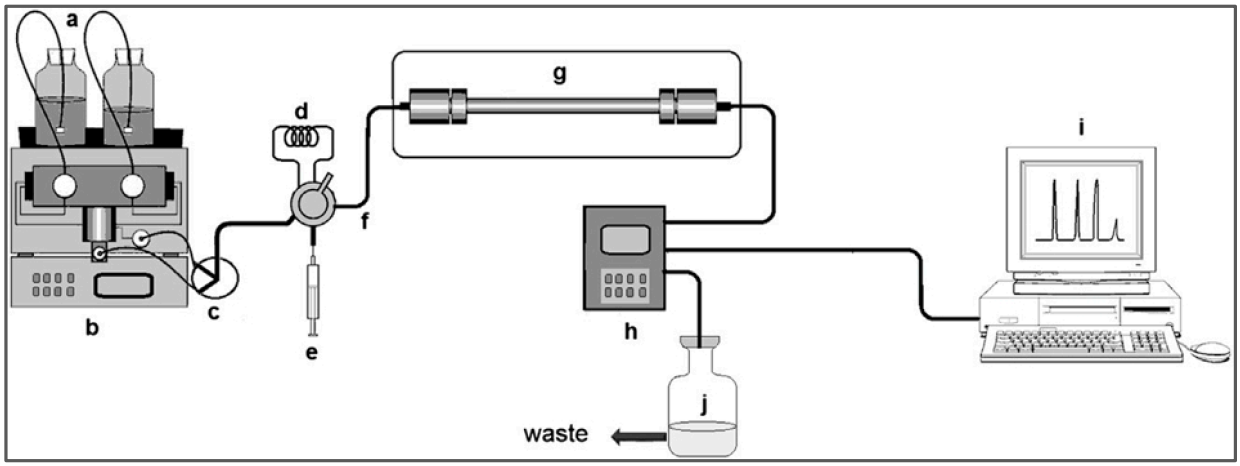

Figure 11. Schematic of high-performance liquid chromatography (HPLC). (a) solvents (mobile phases); (b) a pump to produce a high pressure; (c) a mixer for the homogenization of mobile phases; (d) a sample loop; (e) a syringe with a sample; (f) an injector valve; (g) an oven with the HPLC column; (h) a detector; (i) data acquisition; and (j) sample collection.[142]

During an HPLC experiment, after the mobile phase is pumped under high pressure, it is passed through an injector. In the injector, the mobile phase is mixed with the injected sample, followed by passing through the column. Then, the sample is separated into its components. Analytes are detected by the detector after their elution from the column. This information is recorded and processed by a computer. The column effluent is passed to a back-pressure filter and then to waste.[142-143] When the analyte passes through the column, it interacts between the stationary and mobile phases. The retention time of the analyte varies depending on the interaction between the molecules being analyzed, the stationary phase, and the solvent, or

solvent used. The analyte that exhibits the least interaction with the stationary phase separates first.[144-145]

The mobile phase comprises a nonpolar solvent, e.g., hexane or heptane mixed with a slightly more polar solvent such as isopropanol. On the other hand, a strongly polar stationary phase such as silica gel or alumina (Al_2O_3) is used.[146-147]

In RP-HPLC, stationary phases comprise nonpolar alkyl hydrocarbons, e.g., chains of C-8 or C-18 attached to silica as well as other inert supports. In fact, more than 60% of LC applications can be performed on C18 columns.[142, 148-149]

The two main HPLC pumps are as follows: constant pressure and constant flow pumps. Constant flow pumps have been widely used in HPLC applications because constant pressure pumps may change the flow rate, leading to the lack of accurate data and producing baseline noise. The mobile phase must be filtered and degassed before entering the pump as the pumping operation can be affected by any particulate matter and bubbles. Pumps are required to pump solvents at high pressure through the column under a constant, reproducible flow rate or pressure. [143, 146]

Two sample injection systems in HPLC are as follows: injection valves or automatic injection devices. Automatic injection devices are typically used to analyze up to 100 samples. The sample is injected into the sample loop using a syringe, and it is mixed with the stream of the mobile phase. Then, it passed into the column.[143, 146]

Two elution modes in HPLC are as follows: gradient and isocratic elution. In the gradient elution mode, the composition of the mobile phase is varied. In the isocratic separation mode, the composition of the mobile phase is maintained constant.[149-150] Gradient elution exhibits

advantages of a more rapid, better separation analysis, good reproducibility of retention times, and a wide range of applications due to the possibility of separating compounds with different polarities, molecular weights, and functionalities[142, 151]

Analyte detection is accomplished by using a detector with high sensitivity, a universal or a specific response, a wide linear range of dynamics, and a stable temperature and flow rate. Several detectors can be used in HPLC, including ultraviolet–visible (UV–vis), fluorescence, refractive index, and electrochemical detectors.[149] Typically, the UV–vis absorbance detector is used in HPLC as several compounds of interest absorb in the UV (or visible) range.[152]

UV–Visible Double Beam Spectrophotometer

Spectrophotometry is the quantitative measurement of the interaction of light with materials.[153] A spectrophotometer is a device that is utilized for measuring the absorbed light intensity as a function of wavelength. In UV–vis spectrophotometers, a light beam is transmitted from a UV and/or a visible light source via a prism or a diffraction grating monochromator. The light is passed through the sample to be measured before it reaches the detector. The UV–visible spectrophotometer is composed of five components: a light source, a monochromator, a sample holder, an interpreter, and a detector (Figure 12).

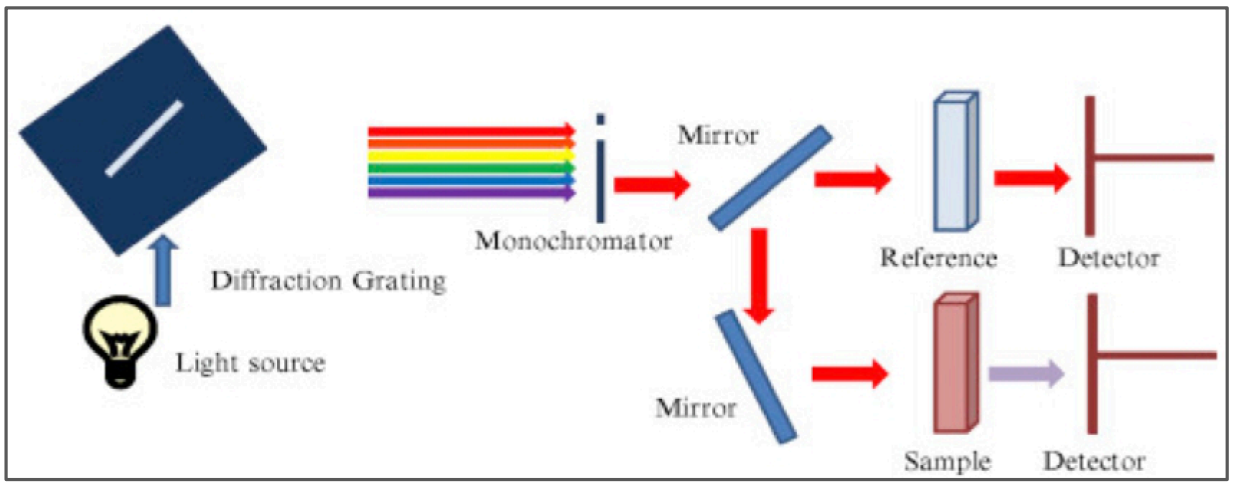

Figure 12. Schematic of a UV–visible double beam spectrophotometer, comprising a light source, diffraction grating, monochromator, sample, reference, and detector.[154]

The standard light source contains a deuterium arc (190–330 nm) and a tungsten filament lamp (330–800 nm). These two lamps generate a light beam that crosses the 190–800 nm spectral range. In the double-beam spectrophotometer, after the light passes through the monochromator, it is divided into two beams. One beam is used for the sample, while the other beam is used for reference measurement. This configuration is beneficial because it can be employed for simultaneously measuring the sample and reference, and the measurement is independent of the difference in the intensity and light source spectral composition.[154]

Olympus microscope Imaging

A compound light microscope is an optical instrument that utilizes visible light to create a magnified image of an object or specimen, which is projected onto the retina of an eye or an imaging device. The word compound refers to the presence of two lenses: objective lens and eyepiece (or ocular lens). Both lenses work together to afford the final magnification M of the image.

A compound light microscope comprises different components. Its main components include an eyepiece, an objective lens, a stage, a condenser lens, a condenser diaphragm, a condenser focusing knob, a field stop diaphragm, a specimen focusing knob, and a light source. Figure 13 shows the compound light microscope.

The compound light microscope comprises two key components that are responsible for image formation: objective lens and condenser lens. The objective lens collects light diffracted by the specimen and forms a magnified real image, which can be at a real intermediate image plane near the eyepieces or oculars. The condenser lens focuses light on a small area of the specimen from the illuminator.[155]

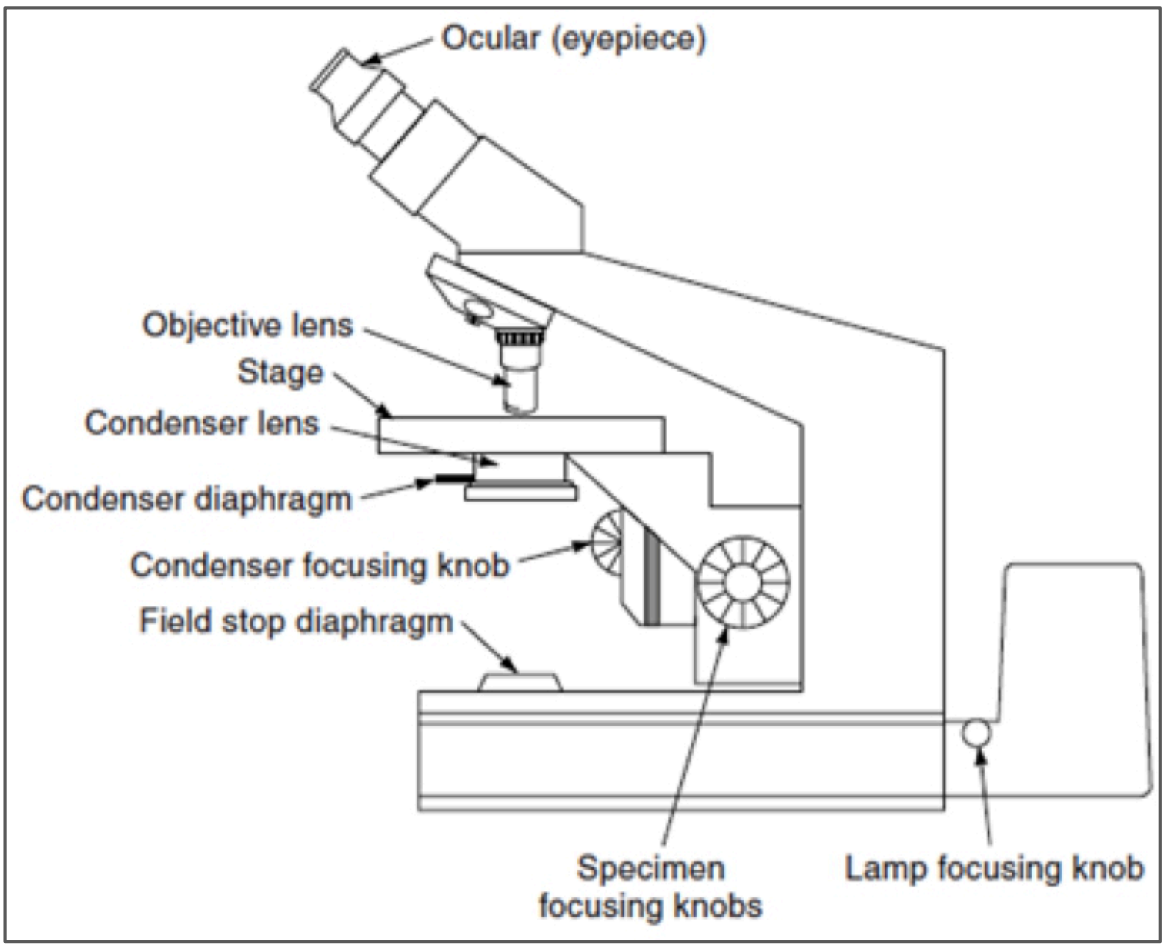

Figure 13. A typical compound light microscope, showing the location of the specimen focus knob, condenser focus knob, and collector lens focus dial on the lamp housing, as well as the location of two iris diaphragms: the field stop diaphragm at the illuminator and the condenser diaphragm at the condenser's front aperture.[155]

Scanning electron microscopy (SEM)

Scanning electron microscopy (SEM) is employed to analyze the microstructure and chemistry of various materials. The basic components of the SEM include a source of electrons, electromagnetic lenses to focus electrons, electron detectors, sample chambers, a computer, and displays (Figure 14). Electrons are emitted at the top using an electron gun, which are

accelerated down the column. The electrons pass through the lenses and apertures, which focus the beam down toward the sample. The electron beam scans the sample surface under vacuum, which provides information about a defined area of the sample. The emitted electrons are collected by a detector and converted into a signal, which is used to produce an image.[156]

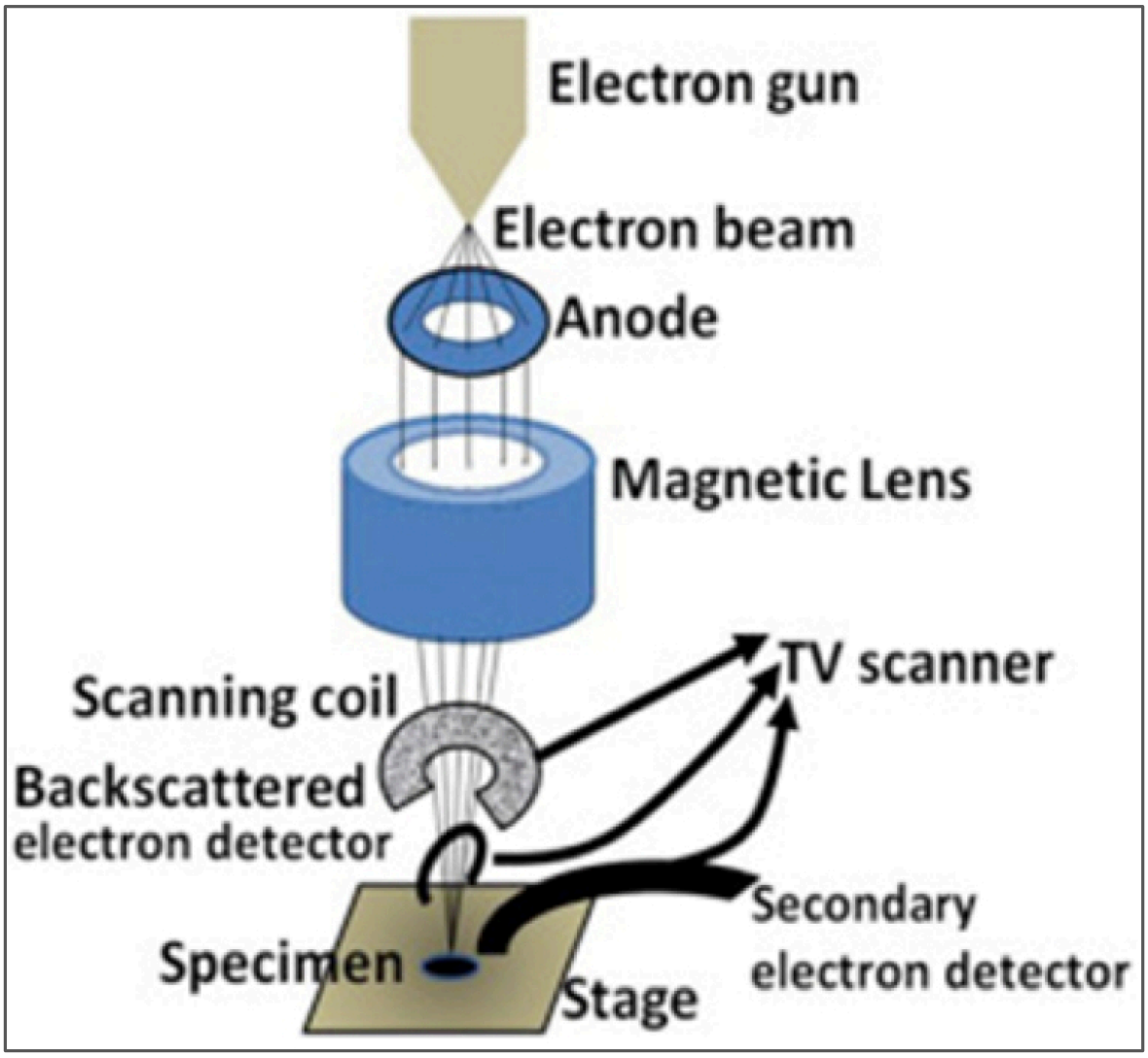

Figure 14. Components of a scanning electron microscopy (SEM) system. SEM comprises an electron source that produces an electron beam toward the specimen. The beam travels through the lenses, which control the electron beam. The specimen is manipulated by sample chambers, which can place the specimen at different angles and move it in all directions. SEM comprises different detectors, such as a secondary electron (SE) detector and a backscattered electron (BSE) detector.[156]

Microbes and Chemicals

Shewanella oneidensis MR-1 microbes were purchased from the Global Bioresource Center (ATCC) as a frozen culture. Microbiology-grade tryptic soy broth (TSB) growth medium was purchased from Sigma-Aldrich (Table1). Calcium chloride ($CaCl_2$), lead chloride ($PbCl_2$), cadmium chloride ($CdCl_2$), and magnesium dichloride ($MgCl_2$) were purchased from Sigma-Aldrich. Isopropyl alcohol (70% in H_2O), glutaraldehyde solution, pH7.0 phosphate buffer, and glycerol solution were purchased from Sigma-Aldrich. An indium tin oxide (ITO) glass slide was purchased from Thin Film Devices, Inc. The reference electrode (RE) Ag/AgCl was purchased from BASi. Sterilized vials of 1 mL were purchased from Fisher Scientific. Nanopure deionized water (DI, Barnstead Nanopure II) with a conductivity of 18 $M\Omega/cm^3$ was used to prepare all solutions.

Table 2. Composition of Tryptic Soy Broth (TSB) media (per liter).

Component	Composition (g)
Tryptone	17
Soytone	3
Glucose	2.5
Sodium Chloride	5
Potassium Phosphate Dibasic	2.5

Preparation of bacteria and culture condition

Shewanella oneidensis MR-1 (MicroBiologics Inc.) cultures were grown from a previously prepared stock that was kept frozen at −80 °C in 1-mL vials. The stock was prepared by mixing 500 µL of the culture and 500 µL of a 20% glycerol solution. A micropipette was used to measure the sample, and the tips were autoclaved. The stock was then frozen at −80 ° C until it was used.

A TSB solution was prepared by dissolving 30 g of dehydrated TSB powder in 1 L of DI. This solution was then autoclaved and cooled. The TSB solution was kept in a sealed 1-L bottle until use. TSB was chosen as one of the less nutrient-rich laboratory media, compared to another nutrient-rich media, such as brain heart infusion (BHI) or Luria-Bertani (LB). TSB culture medium is widely used in biofilm investigations.[157-158]

First, 1 mL of stock (*Shewanella oneidensis* MR-1) was added to 100 mL of TSB, followed by purging with N_2 for 1 h and incubation at 30 °C for 9 h until reaching a cell optical density of 0.2 at 650_{nm} (OD_{650}). The optical density of 0.2 was chosen because the bacteria grow rapidly during the exponential phase, and the growth rate exceeds the death rate. All cultures were grown in 250-mL Erlenmeyer flasks. The spectrophotometer (VMR UV6300PC double-beam) was set at 650 nm to measure the OD of the culture solution before harvesting.

Then, the culture was subjected to centrifugation at 5000 rpm for 10 min, and the resulting cell pellets were resuspended in TSB with different concentrations of $CaCl_2$, $PbCl_2$, $CdCl_2$, and $MgCl_2$ (50,100, 200, 400, 600, and 800 µM). They were dissolved in 1 L of DI, and this mixture was autoclaved and cooled, followed by purging with N_2 for 1 h. Next, three triplicates were placed in an ice bath for 1 h before being used for electrochemical experiments.

Electrochemical cell setup and measurements

The electrochemical cell setup comprises a three-electrode system: a working electrode (ITO), a reference electrode (Ag/AgCl), and a counter (Pt) electrode. The electrochemical cell was made from Delrin plastic (Abbott Development Shop). A metal oxide, such as indium tin oxide (ITO), has been chosen as the electrode surface for examining microbial adhesion.[159] Bacteria are known to attach to natural metal oxides.[160]

The electrochemical cell uses a total area of 9x2 cm^2 ITO glass slide (Thin Film Devices, Inc.). The exposed area of the ITO glass slide in contact with the analyte was 4.5×1 cm^2. Ag/AgCl (BASi Inc) was placed between the ends of the counter electrode (CE). A platinum wire (Pt) was parallel to the ITO glass slide surface. This electrochemical cell was able to hold 11 mL of the solution. The ITO glass slide was cleaned with 70% isopropyl alcohol before use, which was installed into the electrochemical cell. Figure 15 shows an image of the electrochemical cell.

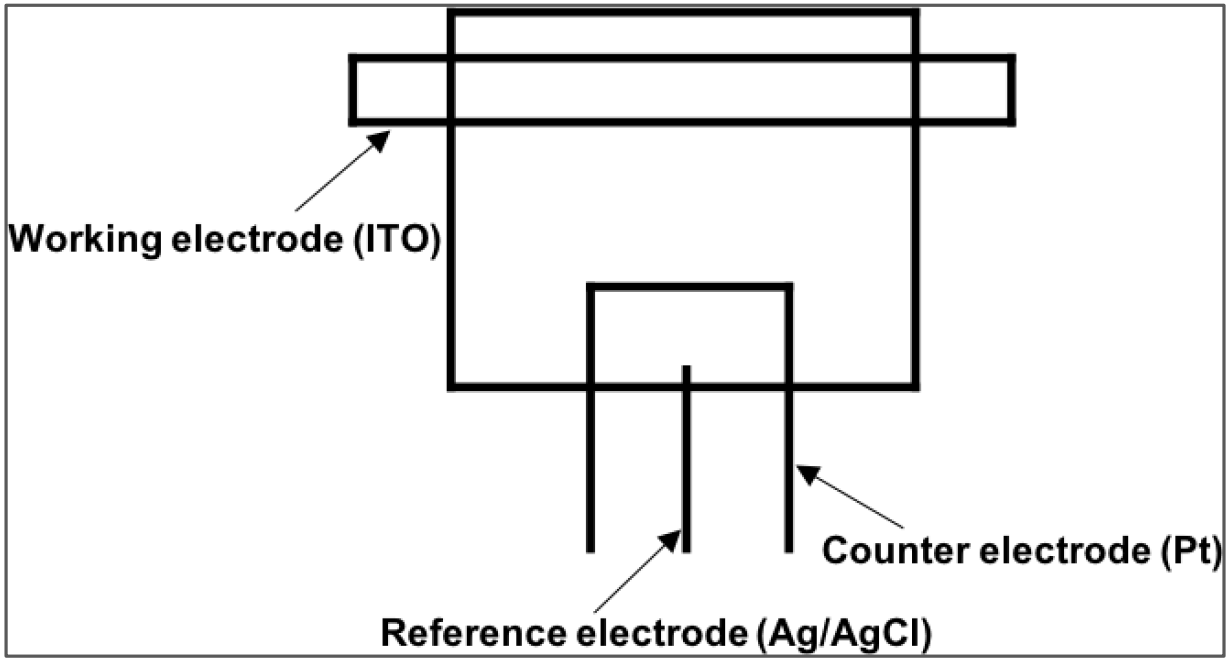

Figure 15. Electrochemical cell setup with a three-electrode system: working (ITO), reference (Ag/AgCl), and counter (Pt) electrodes.

A microbial sample was pumped in via Tygon tubes. The pump was stopped after the cell was filled with the microbial sample. The incoming and outgoing Tygon tubes were clamped shut by a tube space of 37 cm filled with the culture. The system was left for a loading of up to 2 h (BASI Epsilon) at an applied potential (potential step chronoamperometry (PSCA)) of +0.2 V vs. Ag/AgCl with continuous current sampling at 1-min intervals. After the 2-h period, six sequential cyclic voltammograms were recorded. CV comprised an initial negative potential scan at a rate of 5 mV/s applied between the initial potential E_i of +0.2 and the switching potential E_{sw} of –0.5 V vs Ag/AgCl.[159]

Olympus microscope imaging procedure

After the electrochemical experiment, the ITO slide was removed from the electrochemical cell and dried in air. The ITO slide was placed in a vertical drying position to minimize the pooling and drying of unattached microbes, followed by imaging using

an Olympus Compound Microscope BH2-RFCA by employing confocal microscopy. The NIH (*National Institutes of Health)* ImageJ program was used to count the percentage of bacteria covered on the electrode surface.

Scanning electron microscopy (SEM) and images processing

Shewanella oneidensis MR-1 cells attached to the ITO electrode were imaged by SEM (HITACHI, SU3500). After conducting electrochemical experiments, the ITO electrode was removed from the electrochemical cell and fixed with a 2.5% glutaraldehyde solution for 2 h. Fixed cells were washed three times with phosphate buffer (pH 7.0, 50 mM), dehydrated by a series of ethanol solutions (60, 70, 80, 90, 95, and 100%), and then dried in air.[161-163]

Analysis of glucose consumption and riboflavin production by HPLC

Instrumentation

Glucose consumption and riboflavin production were analyzed on an Agilent Technologies 1100 Series (HPLC) system. HPLC comprised a quaternary pump, an autosampler, a C18 analytical column YMC-Pack ODS-AQ (250 mm × 4.6 mm, 5 μM), and an ultraviolet–visible (UV–vis) detector. Derivatization reactions were performed on a Barnstead/Thermolyne Type 17600 Dri-Bath. Glucose was centrifuged on a Beckman Model J2-21 centrifuge, whereas riboflavin was centrifuged on a Marathon thermo IEC 21000R Model 120 centrifuge.

Chemicals and Reagents

ACS-grade glucose standard was purchased from Fisher Chemicals. The derivatization reagent 1-phenyl-3-methyl-5-pyrazolone (PMP), sodium hydroxide (NaOH), hydrochloric acid (HCl), chloroform, ammonium acetate (buffer), triethylamine, acetic acid, and a cellulose filter

membrane (0.22 μM) were purchased from Sigma-Aldrich. HPLC-grade acetonitrile as the mobile phase was purchased from Fisher Chemicals. Riboflavin standard was purchased from Sigma-Aldrich (≥ 98% purity). Nanopure deionized water (DI, Barnstead Nanopure II) with a conductivity of 18 MΩ/cm^3 was used to prepare all solutions.

Chromatographic method conditions and sample preparation of glucose consumption

Glucose consumption was analyzed by the HPLC/PMP derivatization method reported by Zhang et al.[164] using a YMC-Pack ODS-AQ (250 mm × 4.6 mm, 5 μm) column. Two solvents were used as the mobile phase for HPLC analysis: Solvent A comprised 0.4% triethylamine in a 20 mmol/L ammonium acetate buffer solution (pH 6.30 with acetic acid)–acetonitrile (9:1). Solvent B comprised 0.4% triethylamine in a 20 mmol/L ammonium acetate buffer solution (pH 6.30 with acetic acid)–acetonitrile (4:6). HPLC was monitored at 245 nm at a temperature of 25 °C and a flow rate of 1.0 mL. The injection volume was 5 μL. The gradient was 10%–14% in 9 min and 14%–64% from 9 min to 30 min, with an isocratic hold of 64% in the next 5 min.

Anodic culture suspensions were removed from the electrochemical cell during each experiment. The aliquots were subjected to centrifugation at 5000 rpm for 10 min. PMP–glucose was prepared by the reaction of 100 μL of a supernatant added to 100 μL of 0.5 M of PMP and 100 μL of 0.3 M of sodium hydroxide (NaOH). The mixture was incubated at 70 °C for 30 min. After derivatization, the reaction mixture was neutralized at 8°C with 0.3 M HCl, followed by the addition of 1 mL of chloroform to the solution. The solution was subjected to vortexing and centrifugation at 5000 rpm for 10 min at 6°C. The chloroform layer was removed, and the aqueous layer was extracted twice with chloroform. The final aqueous layer was injected into the HPLC.

Chromatographic method conditions and sample preparation of riboflavin production

Analysis of riboflavin production was performed according a previously reported method with some modifications.[99] A C18 analytical column YMC-Pack ODS-AQ (150 mm × 4.6 mm, 3 μM) was used as the HPLC column. The temperature and injection volume were 40 °C and 5 μL, respectively. The eluents comprised water and 50% acetonitrile at a flow rate of 1.0 mL min^{-1}. The HPLC profile was monitored at 266 nm.

The culture suspensions were removed from the electrochemical cell after six CVs of each experiment were recorded. The total amount was subjected to centrifugation (5000 rpm for 5 min). The supernatants were filtered using a 0.22 μM cellulose membrane and then injected for HPLC analysis.

CHAPTER THREE

RESULTS AND DISCUSSION

This chapter provides a detailed description of the results and discussion on the measurement of the current output by controlled potential electrolysis, scanning electron microscopy (SEM) imaging, and measurement of the percentage area coverage by Olympus compound microscopy, cyclic voltammetry (CV), and charge (Q) measurements, as well as research hypotheses, analyses of glucose consumption and riboflavin production by HPLC, and analysis of riboflavin production and glucose consumption via metal-ion enhancement in this Ph.D. project.

Metal Ion Effect on *Shewanella oneidensis* MR-1 Loading and Electrochemical Behavior at an ITO Electrode

Measurement of the current output via controlled potential electrolysis

Shewanella oneidensis MR-1 samples were injected into the electrochemical cell for a two-hour anodic loading period at the potential of +0.2 V vs. Ag/AgCl. The net current density was monitored during the loading process. Figure 16(a), shows a typical loading current density vs. time with blanks (no bacteria) tryptic soy broth (TSB) only, TSB with metal added, control (TSB with bacteria), and Cd^{2+} ion addition. Addition of new food source, as anticipated, allowed proliferation of the bacteria, Figure 16(b).

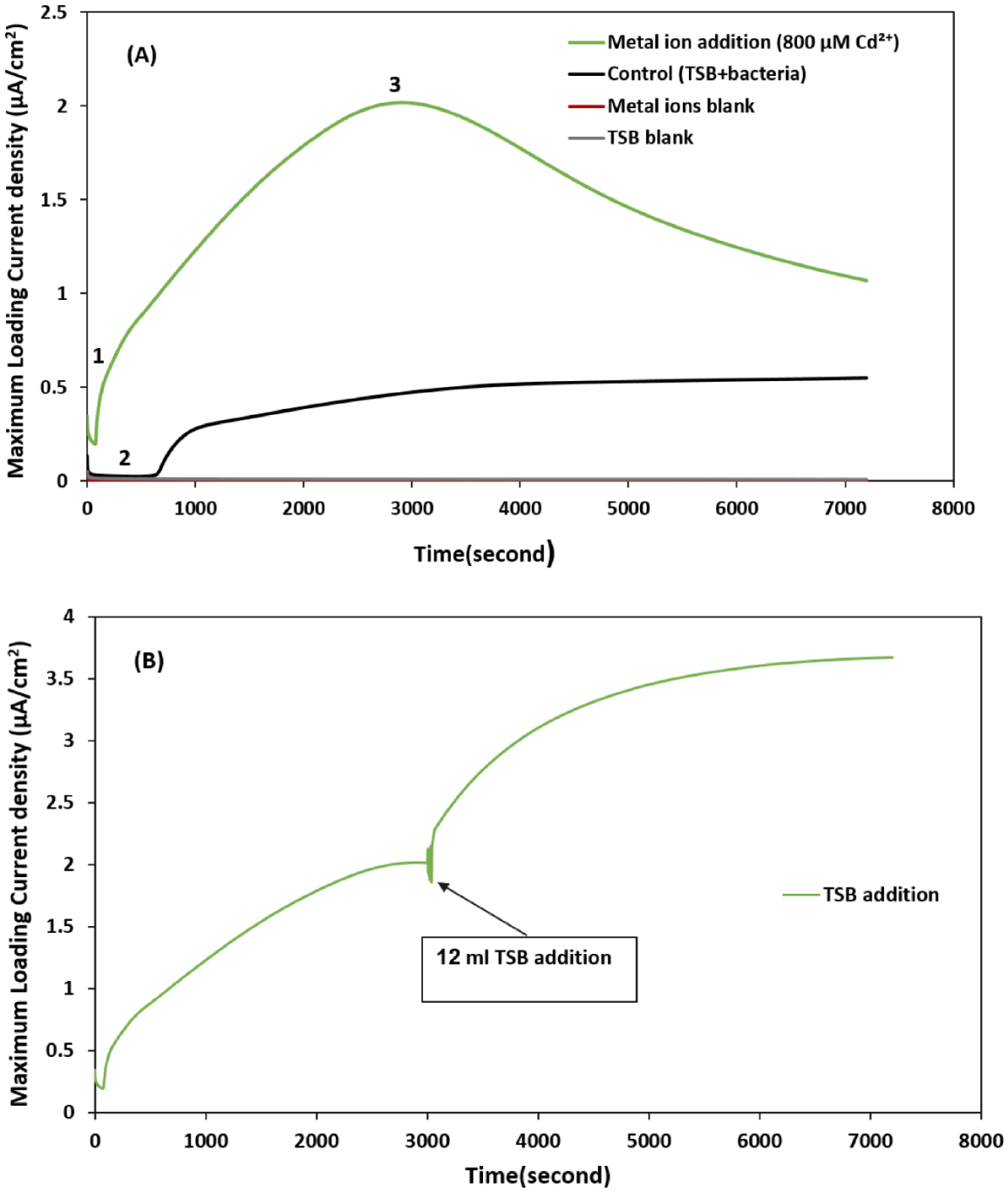

Figure 16. A typical loading current density vs. time. (a): the gray (TSB only) and red (TSB with metal ion added) lines are for blanks. The black line is for the control (TSB with bacteria). The green line is for Cd^{2+} addition. (b): Cd^{2+} experiment with an addition of 12 ml of TSB.

Figure 16(a) shows measurable features related to attachment. A rapid decay of current (Figure 16(a), feature 1) is associated with surface charging. This occurs within the first five

seconds. Feature 2 (lag phase of time (t_{lag}) with a nearly constant lag current (i_{lag})) has been observed elsewhere. Feature 3 is the maximum anodic loading currents density that occurs after the lag period grows. Feature 3 is followed by a decrease in current production. The drop can be altered by the addition of food source, Figure 16(b).

Figure 17 shows the effect of addition of metal ions Mg^{2}, Cd^{2+}, Pb^{2+}, and Ca^{2+} on start-up time and maximum loading current density compared to the control. It can be observed that both the concentration of metal ion and the species of the metal ion are important factors in altering the electrochemical behavior. An increase in the metal ion concentration decreased the start-up time and increased maximum loading current density. The type of ion also had a significant impact on start-up time and maximum loading current density compared to the control.

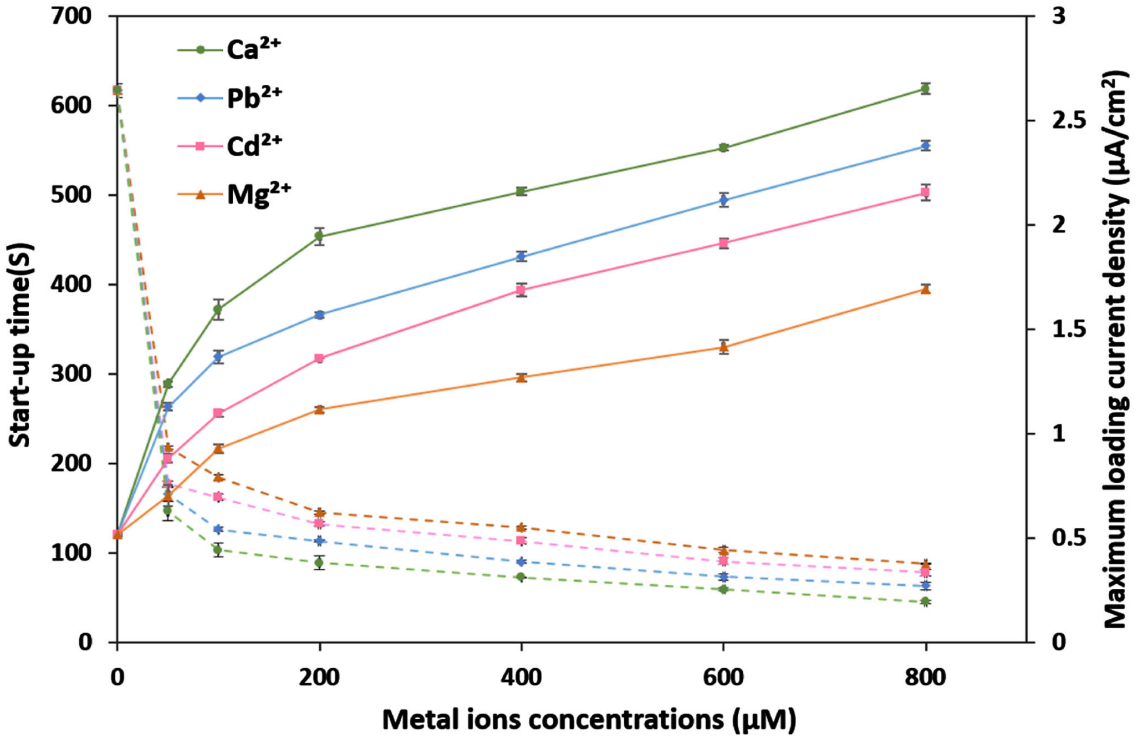

Figure 17. Start-up time (dashed line) and maximum loading current density (solid lines) vs. metal ion concentrations of Mg^{2+}, Cd^{2+}, Pb^{2+}, and Ca^{2+} for *Shewanella oneidensis* MR-1.

An increase in the metal ion concentration decreased the start-up time. This may be related to adhesion. The data show decreased start-up time consistent with literature experiments. The start-up phase depends on a a) electrochemical cell construction, b) substrate (i.e. glucose vs acetate), c) electron acceptor (fumarate, Fe^{3+}, O_2), and d) ionic strength.[165] For example (a), to reduce the start-up time Zhang et al.[166] used a glass fiber separator in MFC, as it has a low oxygen transfer coefficient and a low charge transfer resistances. Zou et al.[167] reported a much faster start-up rate for polymerized riboflavin (RF) onto carbon cloth (CC) electrode. In (d) the ionic strength can alter cell attachment by indirect means (see below). The addition of a metal ion concentration at 800 μM decreased the start-up times to 88 ± 1.00 s, 78 ± 3.60 s, 64 ± 4.16 s, and 45 ± 1.53 s for Mg^2, Cd^{2+}, Pb^{2+}, and Ca^{2+}, respectively, compared to the control of 617 ± 7.57 s.

Scanning electron microscope (SEM) imaging

The addition of metal ion concentrations improved the initial biofilm formation and increased the attachment of cells to the electrode. Bacterial adhesion to the ITO electrode was observed by the scanning electron microscope (SEM) (Figure 18). Figure 18(a) the control (TSB+Bacteria) shows that few bacteria are attached to the electrode surface in the presence of growth media only. In contrast, the addition of Mg^{2+}, Cd^{2+}, Pb^{2+}, and Ca^{2+} ions at 800 μM increased the bacterial attachment to the surface of the electrode Figures 18(b)-(e).

Measurement of the percentage area covered by Olympus compound microscopy

Olympus compound microscopy was used to measure the percentage surface covered by *Shewanella oneidensis* MR-1. The National Institutes of Health (NIH) ImageJ program was used to count the percentage coverage of cells attached to the electrode. ITO surface coverage was

significantly enhanced by the addition of metal ions Mg^{2+}, Cd^{2+}, Pb^{2+}, and Ca^{2+} compared to the control. The control resulted in a total of 10 ± 0.86% surface area coverage. The surface area coverage increased over the control to approximately 51.6 ± 0.25% for Mg^{2+}, 64.7 ± 0.94% for Cd^{2+}, 70.2 ± 0.45% for Pb^{2+}, and 78.5 ± 1.28% for Ca^{2+} at an ion concentration of 800 μM, as shown in Figure 19.

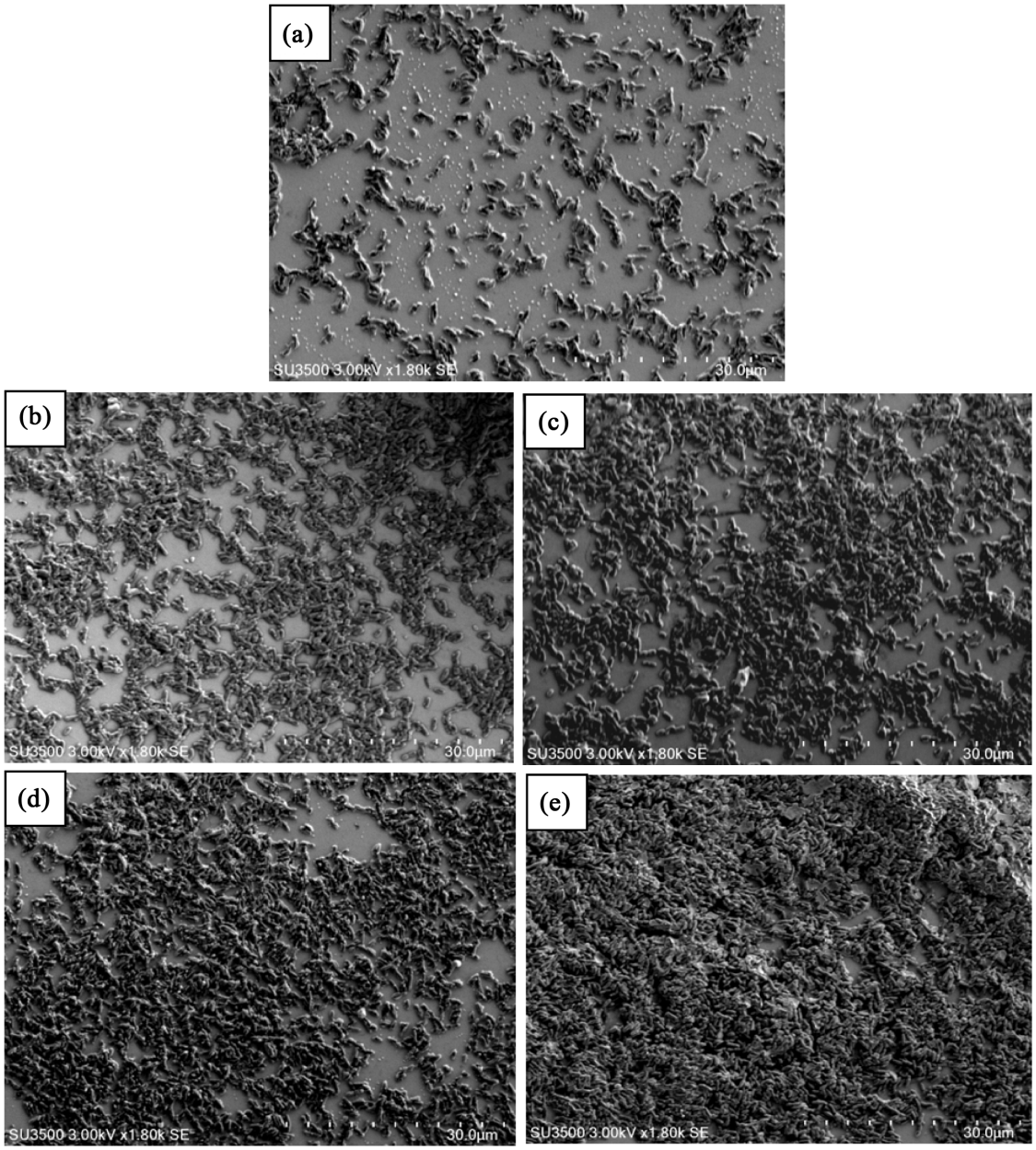

Figure 18. SEM of ITO electrode after an experiment for *Shewanella oneidensis* MR-1. (a) at control (TSB+Bacteria) and ((b), Mg^{2+}; (c), Cd^{2+}; (d), Pb^{2+}; and (e), Ca^{2+}) at 800 µM concentrations.

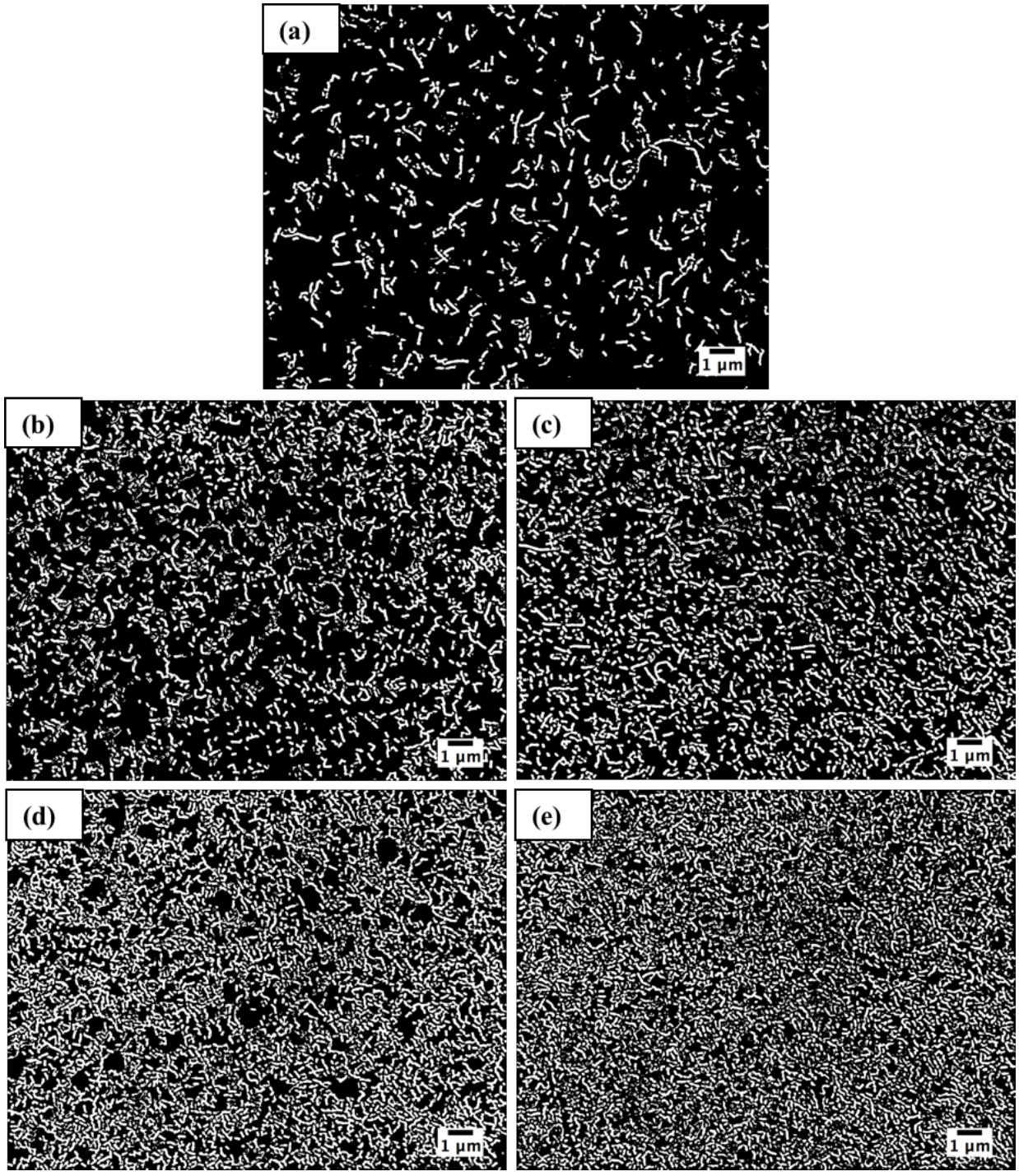

Figure 19. Olympus Compound Microscope BH2-RFCA of ITO electrode after an experiment for *Shewanella oneidensis* MR-1. (a) at control (TSB+Bacteria) and ((b), Mg^{2+}; (c), Cd^{2+}; (d), Pb^{2+}; and (e), Ca^{2+}) at 800 µM concentrations.

Effect of metal ions on current generation by *Shewanella oneidensis* MR-1

There is a direct relationship between maximum loading current density and bacterial coverage at the electrode surface (Figure 16(a), Feature 3). Figure 20 shows the average of triplicate maximum loading current density vs % bacterial coverages. The relationship between maximum loading current density and % bacterial coverages increases linearly ($R^2 = 0.99$). Once attached, at the same % coverage, the same linear maximum loading current density is observed between all metal ions. The effect is not metal ion-specific. F test values are larger than 0.05 showing that this relationship.

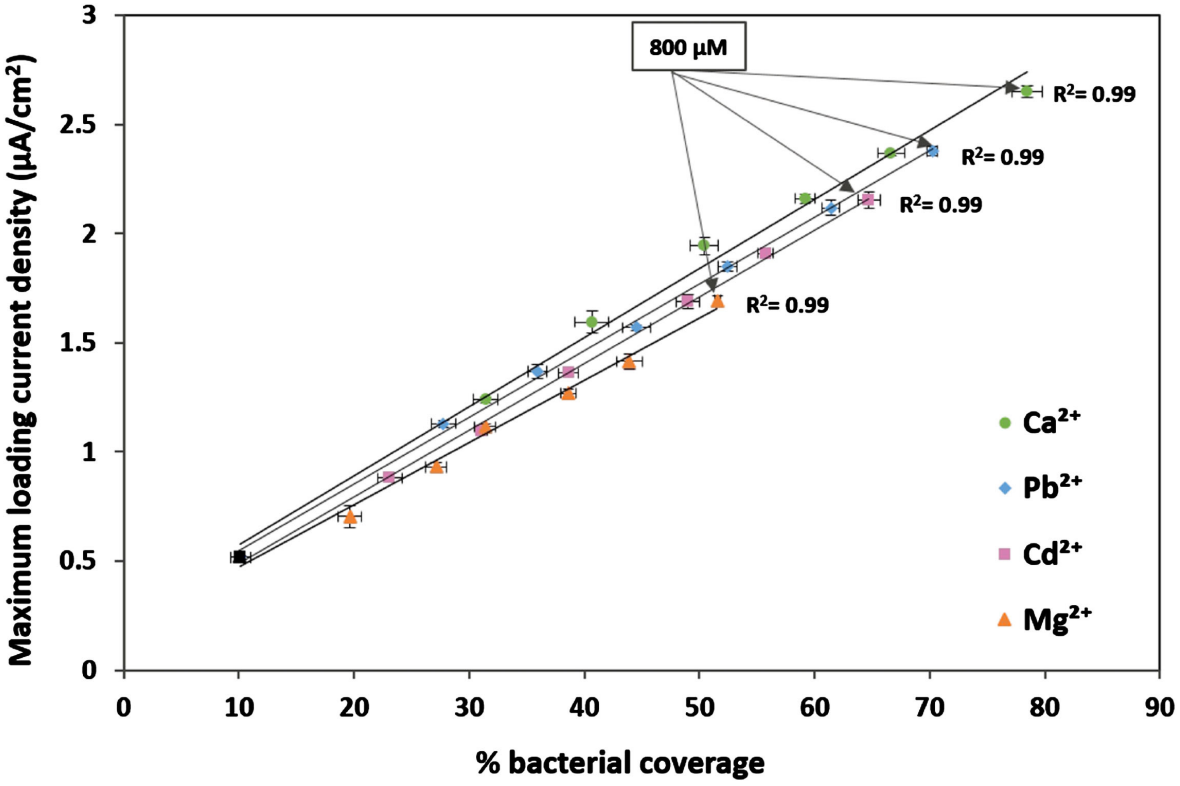

Figure 20. Maximum loading current density vs. percentage of *Shewanella oneidensis* MR-1 coverage at control (TSB+Bacteria) and Mg^2, Cd^{2+}, Pb^{2+}, and Ca^{2+} metal ion concentrations.

The metal ions, however, also show a specific effect on loading current. The maximum loading currents density obtained (for coverages at 800 μM) for Mg^{2+} was 1.69 ± 0.02, approximately 2.25 times higher than that of the control; for Cd^{2+} it was 2.15 ± 0.03, which is approximately 3.13 times higher than that of the control; and for Pb^{2+} it was 2.38 ± 0.02, approximately 3.58 times higher than that of the control. For Ca^{2+} 2.65 ± 0.02, it was approximately 4.09 times higher than that of the control. F tests show that these values were significantly different.

Cyclic Voltammetry (CV) and Charge (Q) measurements

A second set of electrochemical data belongs to cyclic voltammetry obtained after electrode loading at +0.2 V vs Ag/AgCl for two hours. The first of 6 CVs are shown in Figure 21. The TSB only and metal ion blanks show no discernible peaks, as expected. It is observed that the reduction peak current is increased over the control when Mg^{2+}, Cd^{2+}, Pb^{2+}, and Ca^{2+} are added. The CV shows redox peaks with a midpoint potential of -0.17 V and consistent with the outer membrane Cyt-c, which had a potential range of -0.27–0.13V.[9, 67] The shape of the CV suggests an adsorbed species.[159, 168-169] In the cyclic voltammetry, the highest reduction peak current density obtained for Ca^{2+} was 4.16 ± 0.13 μA/cm^2, while for Pb^{2+}, Cd^{2+}, and Mg^{2+}, it was 3.70 ± 0.13 μA/cm^2, 2.90 ± 0.12 μA/cm^2, and 2.27 ± 0.12 μA/cm^2, respectively; this is compared with the control of 0.99 ± 0.09 μA/cm^2. These results were consistent with those of the controlled potential electrolysis experiments shown in Figure 16.

The integrated peaks area under the reduction peak gives the amount of material that attached to the electrode surface (equation 16).

$$Q(C) = nFN \quad (16)$$

where (n) is the number of electrons transferred per molecule, (F) is Faraday's constant (96,485 $C \cdot mol^{-1}$), and N is the amount of material electrolyzed in moles of either and or both the outer membrane cytochrome and the mediator flavin. Total Q should be related to the percent coverage.

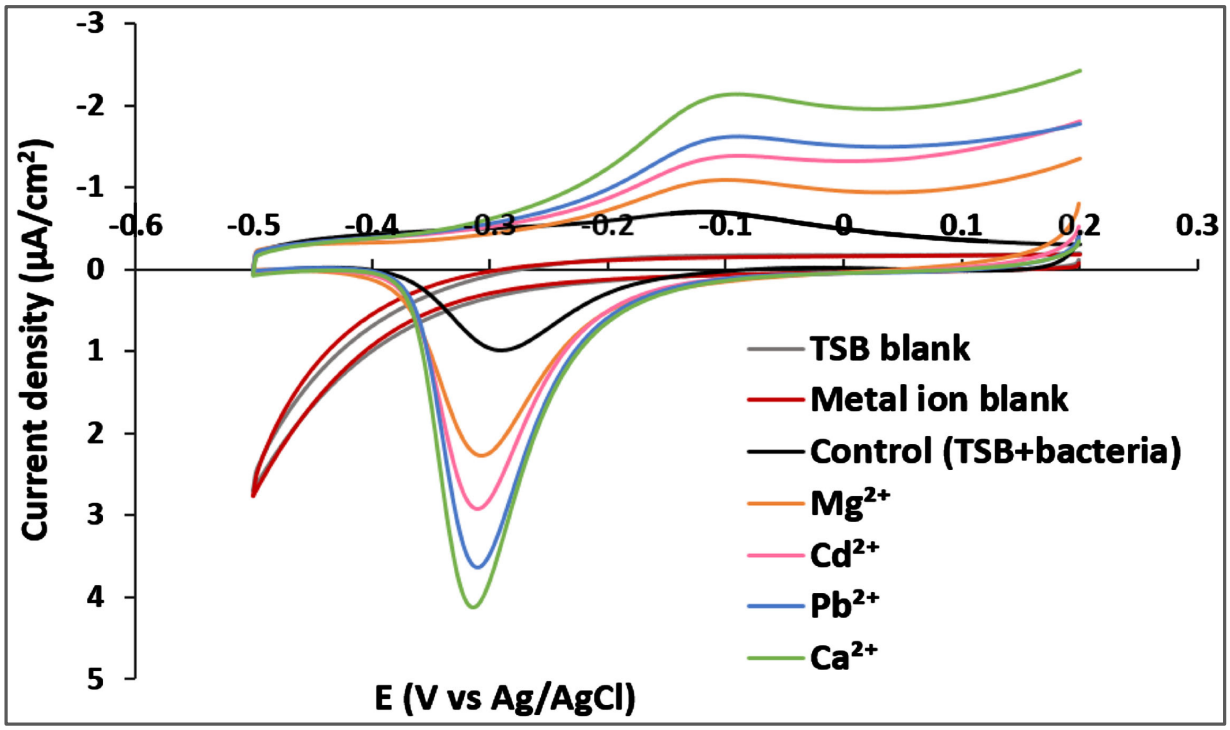

Figure 21. Cyclic voltammetry after electrode loading at +0.2 V vs Ag/AgCl for two-hours of *Shewanella oneidensis* MR-1. The gray (TSB only) and red (TSB with metal ion added) lines are for blanks. The black line is for the control (TSB with bacteria). The orange, pink, blue and green lines represent metal ion of Mg^{2+}, Cd^{2+}, Pb^{2+}, and Ca^{2+} concentrations at 800 µM, respectively.

In Figure 22, the Q value obtained for the control (TSB+Bacteria) was equal to 78 ± 4.29µC. The Q values for Mg^{2+}, Cd^{2+}, Pb^{2+}, and Ca^{2+} were found to be 216 ± 1.89, 260 ± 1.5, 296 ± 2.47, and 346 ± 2.89 µC, respectively. Consistent with Figure 20, the increase in the measured cathodic peak charge vs. percentage of *Shewanella oneidensis* MR-1 coverage was linear ($R^2 = 0.99$) for each metal (Figure 22). There is a slight difference in linearity as measured

by the slope on charge and the type metal ion. F ratio values are less than 0.05 indicating that there is a difference in the slopes between charge and % bacterial coverage. Above it was concluded when the cells are attached to the electrode surface, at a given total surface coverage, current output is non-specific between metal ions. Here it is noted that the ability to accept a charge (cathodic process) is slightly a metal ion-specific.

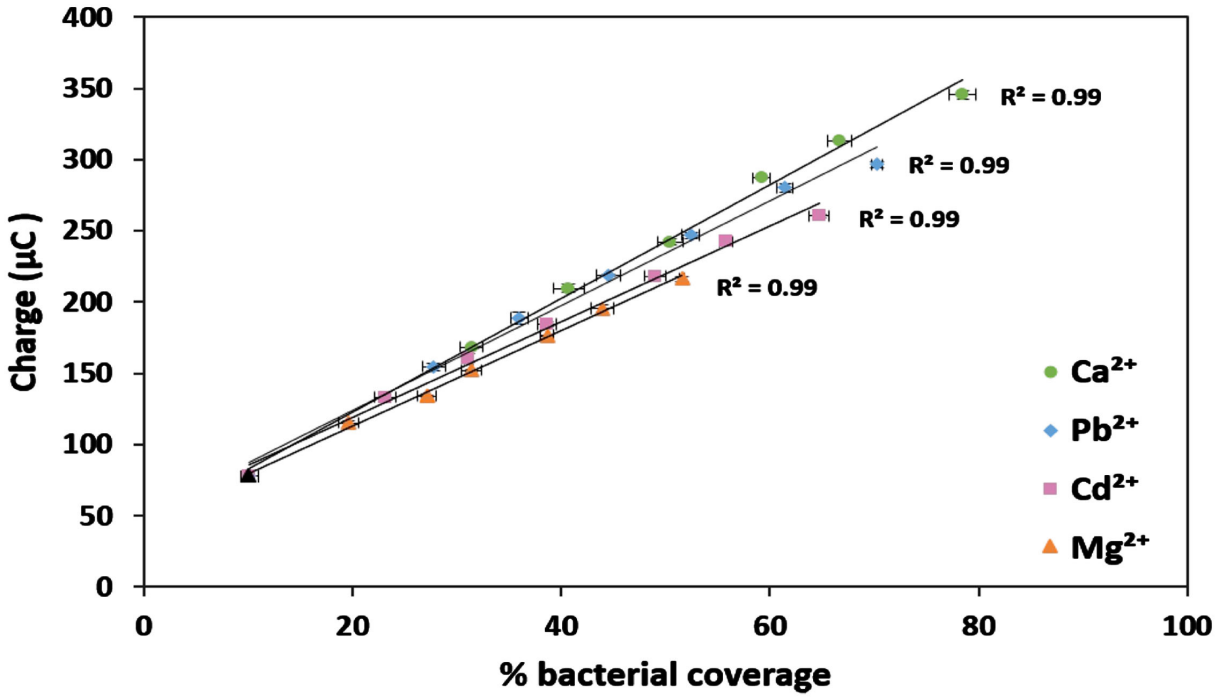

Figure 22. The cathodic peak charge vs. percentage of *Shewanella oneidensis* MR-1 coverage at control (TSB+Bacteria) and Mg^{2+}, Cd^{2+}, Pb^{2+}, and Ca^{2+} metal ion concentrations.

Research discussion

There are several hypotheses related to the increase in the metal ion concentration could increase bacterial attachment. Firstly, *Shewanella* surfaces are negatively charged at pH 7[170] due to EPS structural anionic groups. Non-specific electrostatic forces may be applicable. Researchers have applied classical Derjaguin, Landau, Vervey, and Overbeek (DLVO) double

layer theory to describe bacterial attachment to inorganic surfaces. The classical DLVO theory is described as the net interaction between a cell and a flat surface, which results from attractive van der Waals interactions and repulsive interactions between the electrical double layer of the cell and the substratum.[106] Choi et al.[115] studied the attachment and detachment of bacteria during various ionic strengths by using quartz sand surface. They found that increasing the ionic strength of the solution increased attachment. Similarly, Loosdrecht et al.[117] adhesion at polystyrene surfaces increased with increasing ionic strength of the electrolyte.

However, the theory does not adequately describe all of the observed behavior. Rijnaarts et al.[112] attempted to apply classical DLVO theory by controlling for the ionic strength and found only a moderate adherence to the theory. Rijnaarts et al.[112] study of bacterial adhesion on Teflon and glass surfaces hydrophobicity found different behavior at low ionic strength (0.001 M) and high ionic strength (0.1 M). At low ionic strength attachment was inhibited by DLVO-type electrostatic repulsion, but at high concentration attachment was controlled by steric interactions.

We also found that classical DLVO theory failed to explain all the data in two ways. Firstly, ionic strength was held constant (0.09 M), which should have resulted in no alteration of adhesion. DLVO theory would suggest that at similar concentrations there would be no effect in changing the cation species. Thus, like Rijnaarts classical DLVO theory was found insufficient to explain the results.

Secondly, DLVO theory can be altered by considering the hydrophobicity. Extracellular polymeric substance (EPS) is an important component in controlling the hydrophobicity of the bacterial cell surface. Tsuneda et al.[171] reported that if the amount of EPS is small, cell adhesion

onto solid surfaces is inhibited by electrostatic interaction, and if the amount of EPS is large, cell adhesion is promoted by polymeric interaction.

An explanation for the results relates to metal ion binding within the EPS. Metal ions are known to bind to EPS[172-173] and, therefore, likely affect the properties of the EPS. EPS on the bacteria may extend through the barrier into a region where attraction can dominate. As an example, Redman et al.[174] suggested that when the bacteria have attached from the pili or flagellum that can occur across the barrier when the microbe lies within the secondary minimum. Different adhesion effects result when the configuration of EPS is either tight or loose.

In addition to the interaction of metal ions with EPS Wei et al.[126] have found carboxyl and phosphate groups were mostly responsible for Cd^{2+} adsorption on bacterial cells and affect the affinity between the bacterial cells and metal ions. Dobrowolski et al.[175] found vibration band alterations associated with carboxylic acids and alcohols when Cd^{2+} and Pb^{2+} were bound extracellular substances obtained from bacteria. These effects are, in the literature, also predicted to be non-specific and related to trends in hydrated ionic radii, hydrated radii, and hydration energies.[176-177]

Thirdly, a supplemental explanation for the differences between metal ions is the impact of their water of hydration on binding to the EPS sites. This mechanism varies based on ion size and charge, and coordination with water. As predicted, for a non-specific electrostatic mechanism, attachment increases with ionic radii, Figure 23. Mg^{2+}, Cd^{2+}, and Ca^{2+} follow the expected trend well. For these ions, bacterial coverage is linear with ionic radii ($R^2 = 0.99$). As expected, Ca^{2+} results in the highest current density. Pb^{2+} is out of sequence between Mg^{2+}, Cd^{2+}, and Ca^{2+}.

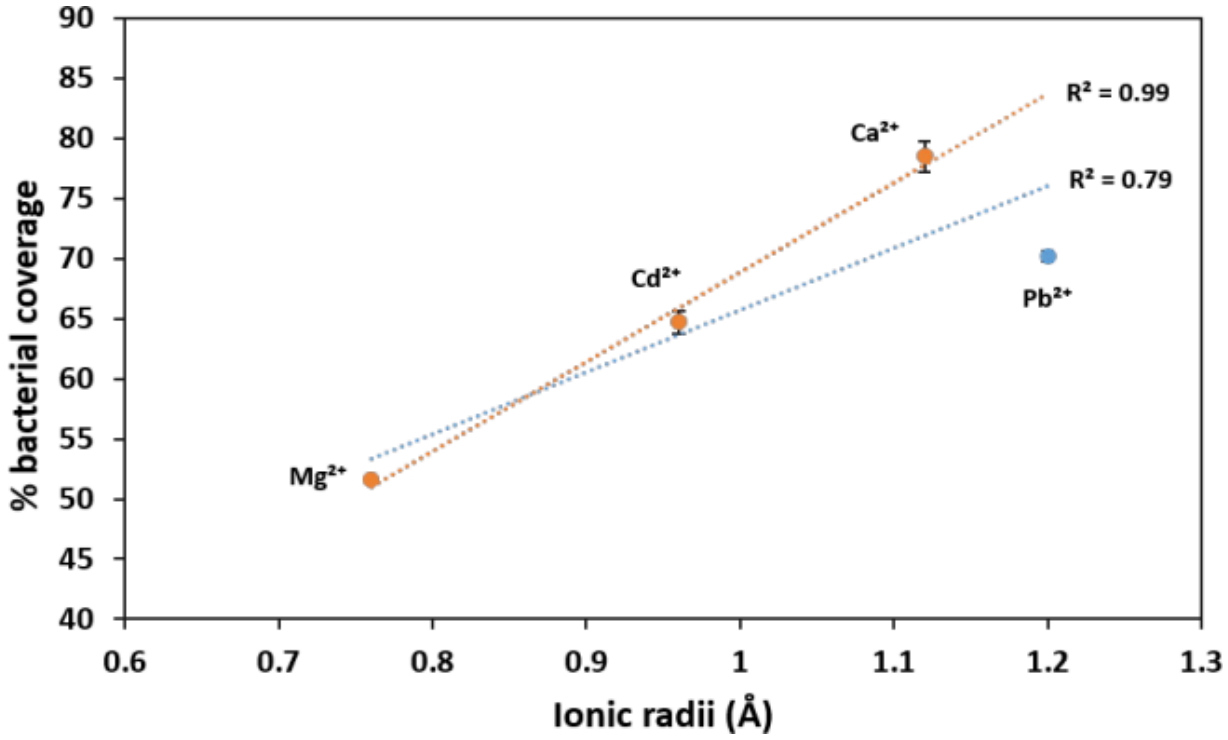

Figure 23. % bacterial electrode coverage vs Ionic radii (Å) of Mg^{2+}, Cd^{2+}, Pb^{2+}, and Ca^{2+} metal ions.

Inclusion of Pb^{2+} into the sequence resulted in a significantly poorer correlation between % bacterial coverage and ionic radii ($R^2 = 0.79$). This difference may be related to alterations in valence shell electrons. The structure of the hydrated Pb^{2+} ion is affected by the lone electron pair, which is giving complex hemi-directed in aqueous solution.[178]

Analysis of Glucose Consumption and Riboflavin Production from *Shewanella oneidensis* MR-1 by Using HPLC

Analysis of glucose consumption by HPLC

Glucose is a major source of both carbon and energy for bacteria. The ability of *Shewanella* to consume glucose has been debated in the literature. Choi et al.[179] and Howard et al.[180] have reported that *Shewanella oneidensis* MR-1 can utilize glucose as a carbon source.

Tryptic soy broth (TSB) is a growth medium for microorganisms, which is composed of 2.5 g of glucose as a source of both carbon and energy for microorganisms.

Monosaccharides cannot be directly identified by absorption due to the lack of chromophores in their molecular structure.[164] Honda et al.[181] were the first to propose the development of 1-phenyl-3-methyl-5-pyrazolone (PMP), a pre-column derivative reagent that provides a high yield for high absorbent single derivatives. The Honda method includes a derivatization reaction of glucose with PMP to form a PMP reducing sugar (Figure 24).

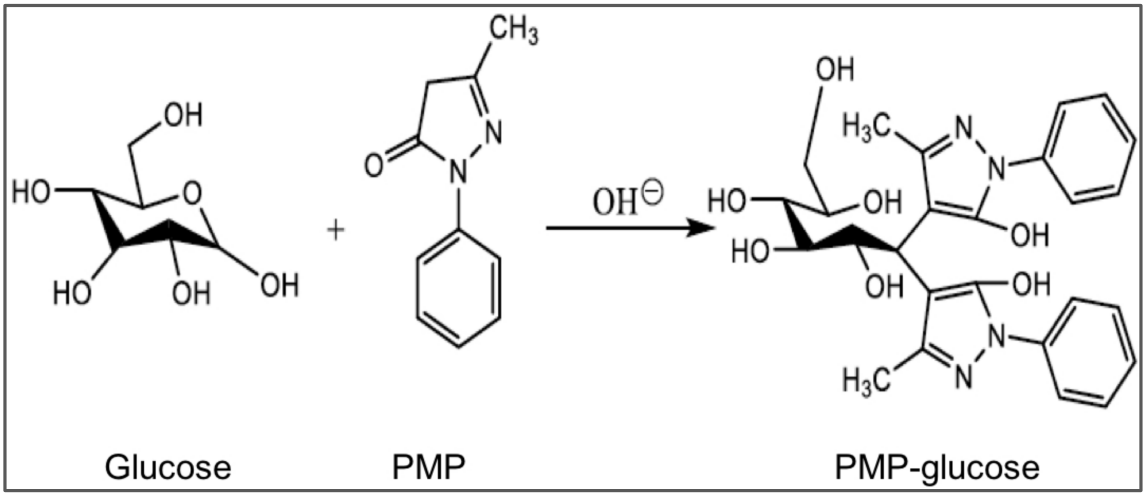

Figure 24. Formation principle of the glucose–PMP derivative by the reaction of PMP with glucose.

The RP-HPLC method proposed by Zhang et al.[164] has been applied for the determination of PMP-glucose, which has been found to be accurate due to the absence of excipient interference during separation. Concentrations of glucose standards and glucose consumed by microbial samples were measured. The PMP-glucose standard was prepared in different concentrations of 0.5, 1.0, 1.5, 2, and 2.5 g/L. After the conversion of glucose to PMP-glucose, 5 μL was injected into the HPLC system for triplet experiments. The peak area of PMP-glucose (intensity mAU) was analyzed and plotted against the retention time (min). Figure 25 shows the

analysis of the PMP-glucose standard by HPLC at a short retention time of approximately 16.826 min.

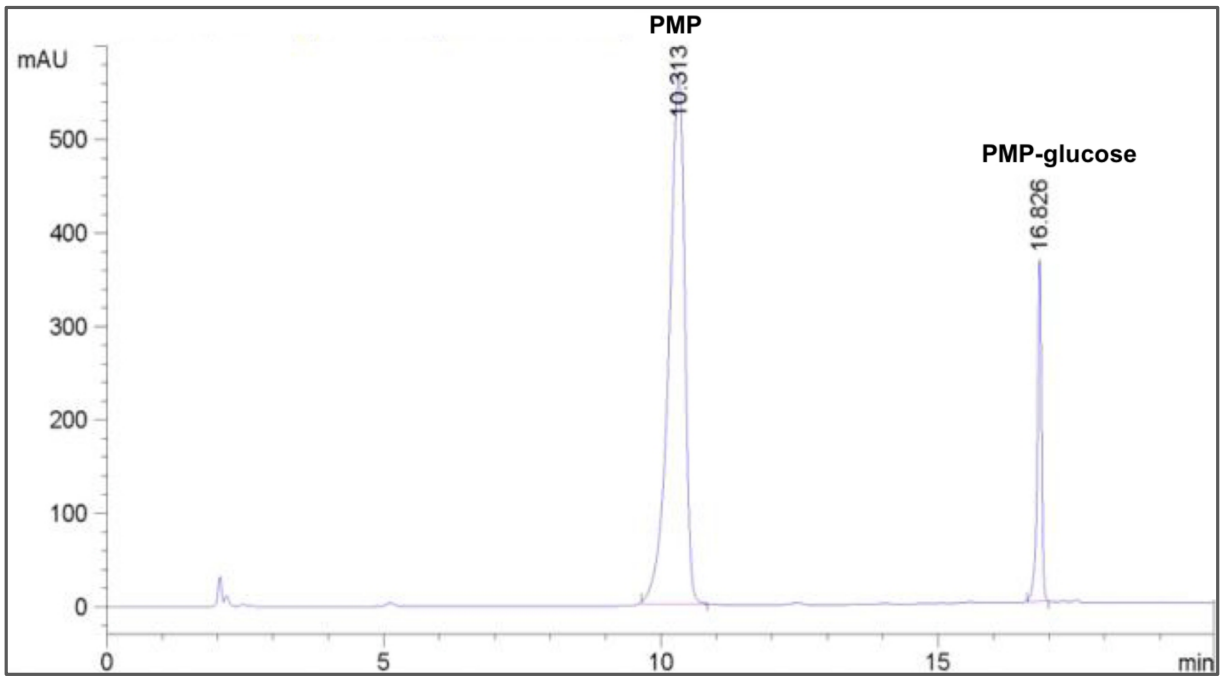

Figure 25. Chromatogram showing the separation of PMP-glucose from a microbial sample supernatant at 16.826 min, and the peak corresponding to PMP residues is observed at 10.313 min.

Different sets of microbial samples were derivatized in the same manner as that performed for the glucose standard samples. The supernatants of microbial samples including bacteria without the added metal ions and bacteria with added metal ions, such as Ca^{2+}, Pb^{2+}, Cd^{2+}, and Mg^{2+}, were injected into the HPLC system for triplet experiments. The retention time was 35 min for the complete reaction. By HPLC analysis, the peak area of PMP-glucose was observed at a short retention time of approximately 16.806 min (Figure 26).

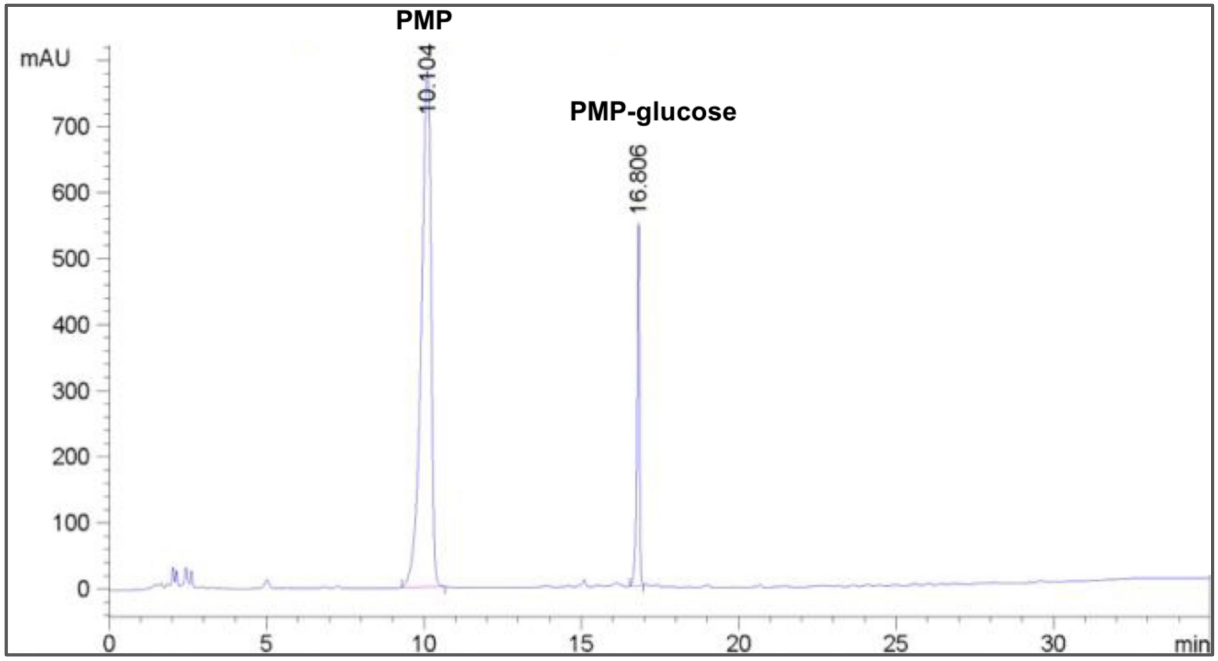

Figure 26. Chromatogram showing the separation of PMP-glucose from a microbial sample supernatant at 16.806 min, and the peak corresponding to PMP residues is observed at 10.104 min.

To validate any analytical procedure, it is imperative to determine the linearity of the calibration curve.[182] A set of experiments with the different concentrations of glucose standards were performed, followed by HPLC analysis. Linearity was measured on the basis of the relationship between the peak area of the compound and its concentration. Typically, to investigate linearity, five concentrations of glucose standard solutions covering the range of 0.5-2.5 g/L are required to obtain a regression line of the calibration curve. The 2.5 g/L concentration of glucose is the expected glucose concentration of a microbial sample. The coefficient of determination (R^2) was 0.99, satisfying the criterion of ≥ 0.99. The results demonstrated good linearity between the peak area and glucose standard solution concentrations (Figure 27).

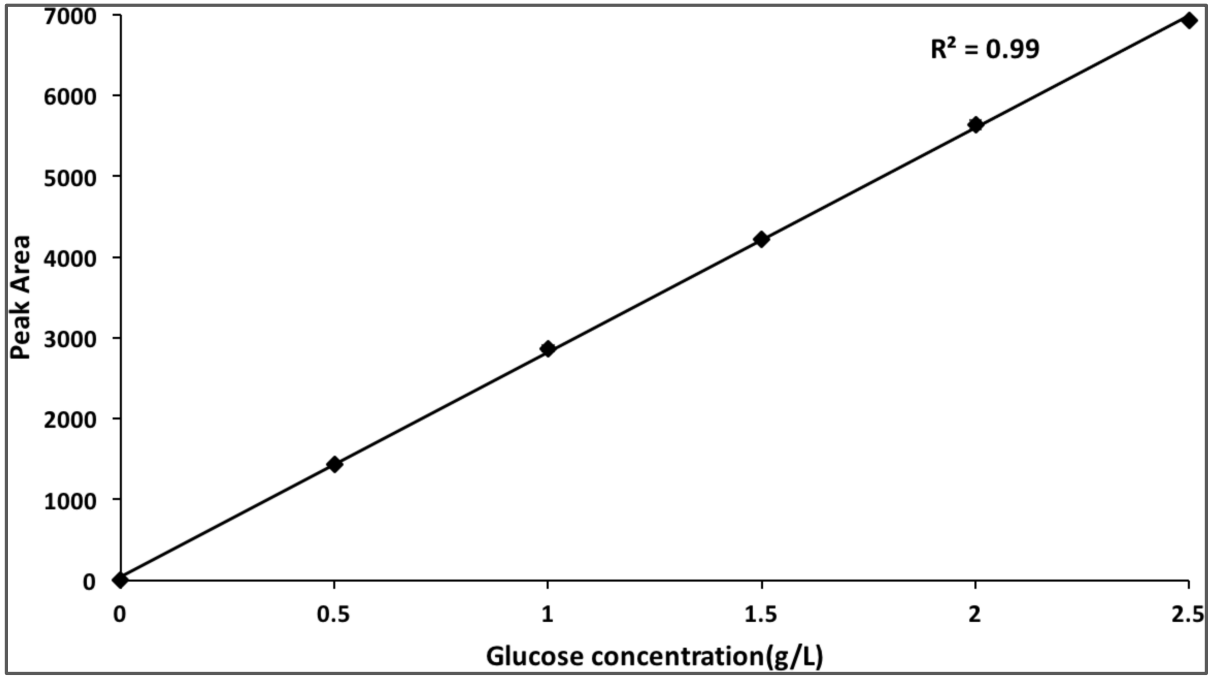

Figure 27. Calibration curve for the glucose standard solutions consumed in the microbial samples in the range of 0.5–2.5 g/L on the HPLC system.

Analysis of riboflavin production by HPLC

Production of riboflavin by various bacteria can be affected by several factors, including medium pH[96, 183-184] and metal ions.[99, 102] Riboflavin production was analyzed by using an HPLC system. The wavelength at maximum absorbance (λmax) of riboflavin was selected by the utilized UV–Vis Spectrophotometer. First, 0.5 µg/mL of the riboflavin standard was prepared and scanned in the range from 400 to 190 nm. Figure 28 shows the absorbance spectrum of riboflavin at two wavelengths in the visible and UV regions. The λmax values were 222 nm and 266 nm in the UV and visible regions, respectively. A wavelength of 266 nm for riboflavin was selected which can enhance detection.

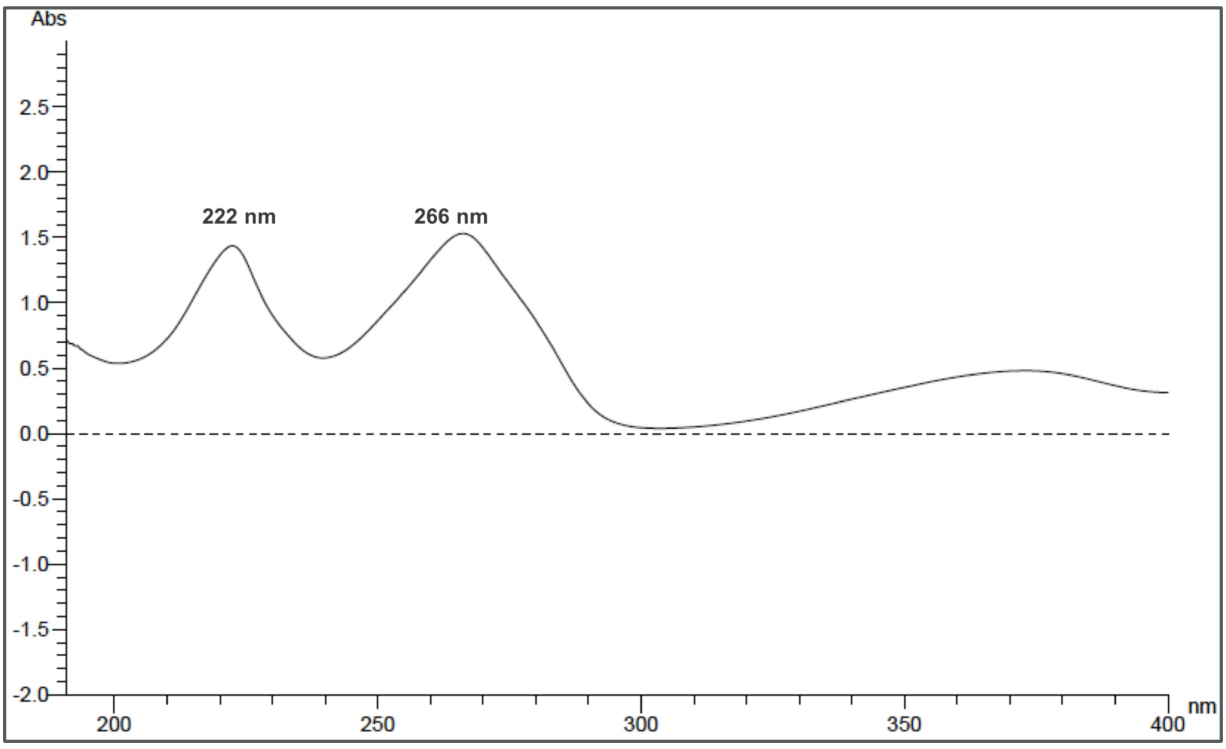

Figure 28. UV–vis spectrum of riboflavin. Maximum absorbance values of 222 nm and 266 nm were observed in the UV and visible regions, respectively.

Acetonitrile was selected as the eluting solvent for riboflavin analysis due to its water miscibility, low viscosity, and elution efficiency. The mobile phase composition is one of the key parameters for controlling and optimizing the separation of eluted compounds in HPLC. Different sets of riboflavin standards of 0.5. 1, 1.5, 2, 2.5, and 3 µg/mL were prepared and injected into the HPLC system. A good resolution and short run time were achieved after 5.639 min by using 50% acetonitrile (Figure 29).

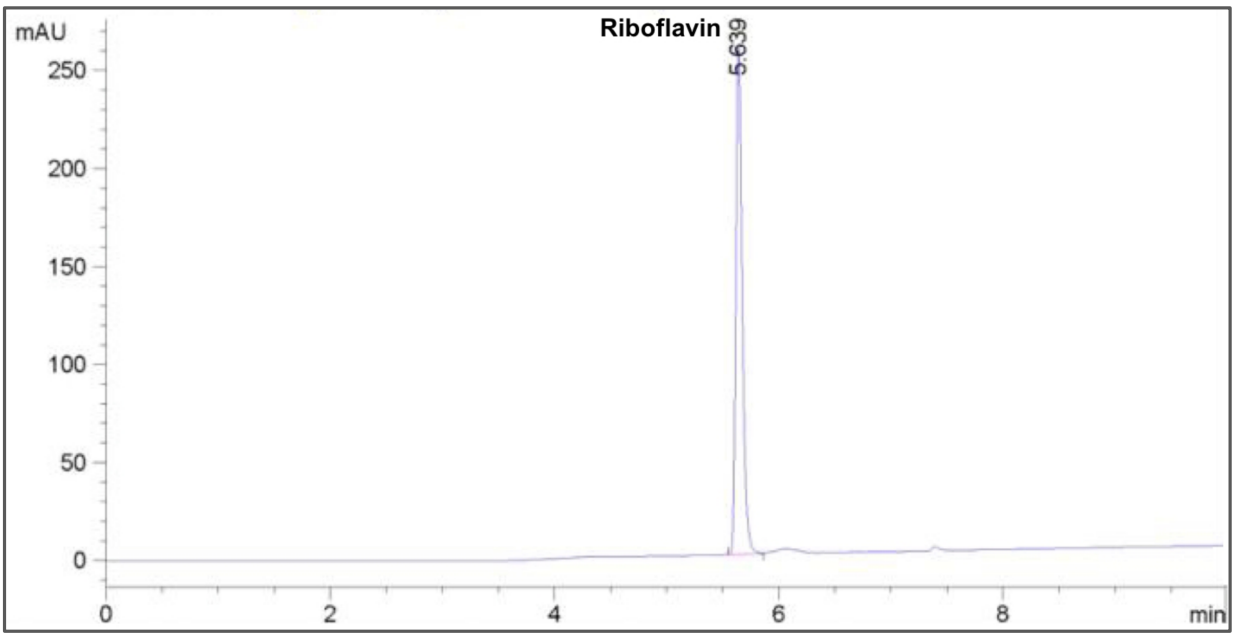

Figure 29. Chromatogram showing the separation of riboflavin at 5.639 min in the standard sample.

The supernatants of the microbial samples were prepared for bacteria without the added metal ions and bacteria with added metal ions, such as Ca^{2+}, Pb^{2+}, Cd^{2+}, and Mg^{2+}. First, 5 µL of the sample was injected into the HPLC system for triplet experiments. The retention time was 10 min for the complete reaction. By HPLC analysis, the peak of riboflavin in the microbial sample was observed at a short retention time of approximately 5.639 min (Figure 30).

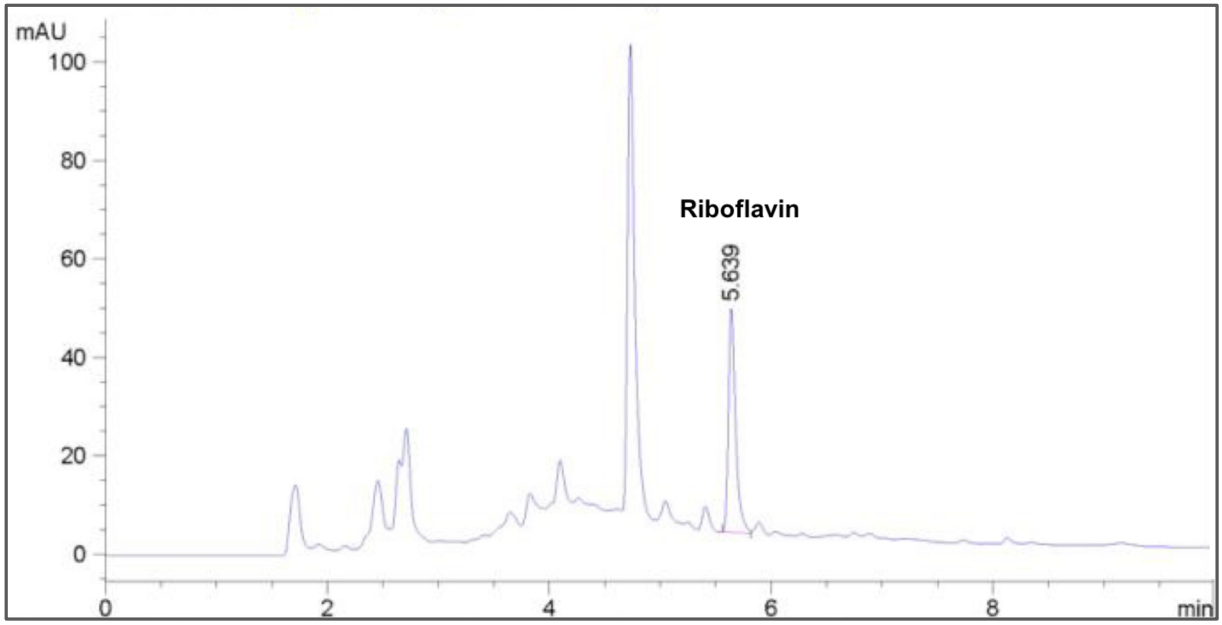

Figure 30. Chromatogram showing the separation of riboflavin at 5.639 min in the microbial sample supernatant.

Limit of detection (LOD) is the lowest concentration of an analyte in a sample that can be measured and distinguished from zero or the noise level of the system. Limit of quantification (LOQ) is the lowest analyte concentration in a sample that can be determined with an acceptable precision and accuracy under experimental conditions. LOD and LOQ can be measured on the basis of the signal-to-noise ratio of the analyte, affording a response 3 and 10 times greater than the noise level of the detection system respectively.[185] The lowest LOD and lower LOQ of riboflavin in solution were determined. LOD and LOQ were estimated to be 0.01 μg/mL and 0.05 μg/mL, respectively (Figure 31). LOD and LOQ values were estimated by triplicate injections.

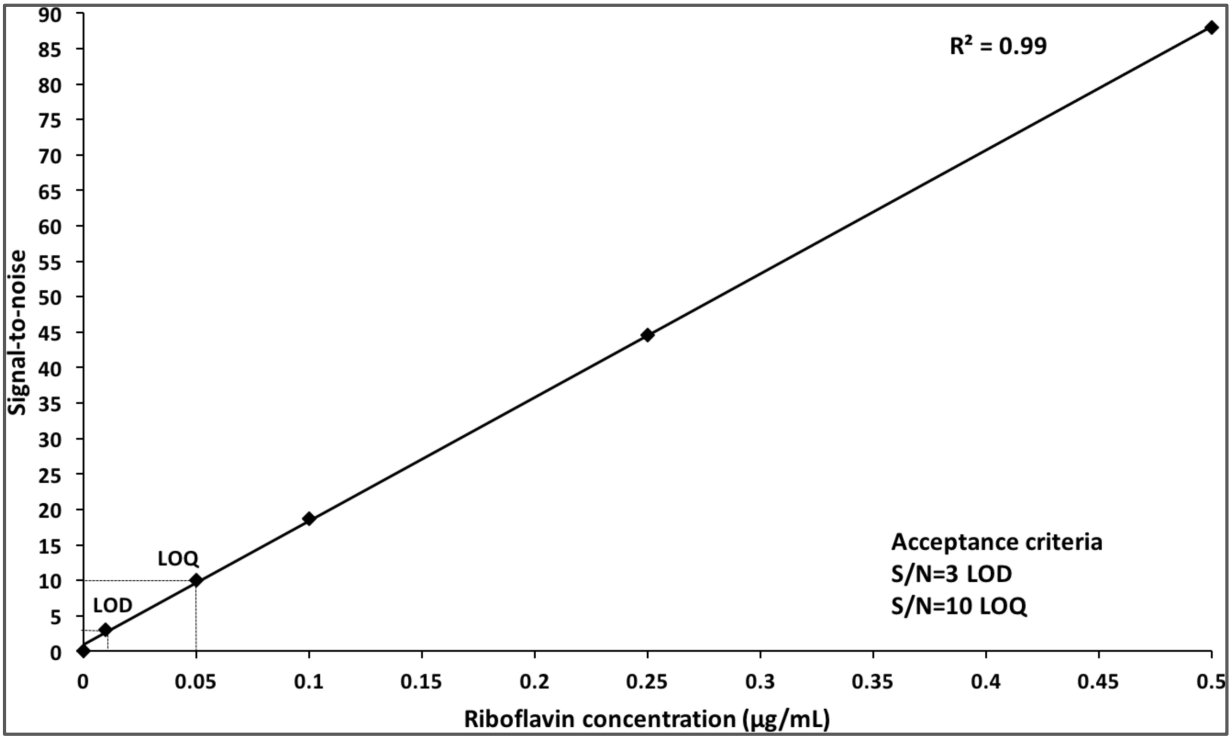

Figure 31. Calibration curve showing the limit of detection (LOD) and limit of quantification (LOQ) for riboflavin concentrations.

The linearity of the calibration curve was determined by six concentrations in the range from 0.5 to 3 µg/mL of riboflavin standards. Different concentrations of riboflavin standards were injected into the HPLC system for triplicate experiments. The calibration curve exhibited a good linearity for the method, which was verified by $R^2 \geq 0.99$. Figure 32 shows the calibration curve of six concentration ranges of riboflavin.

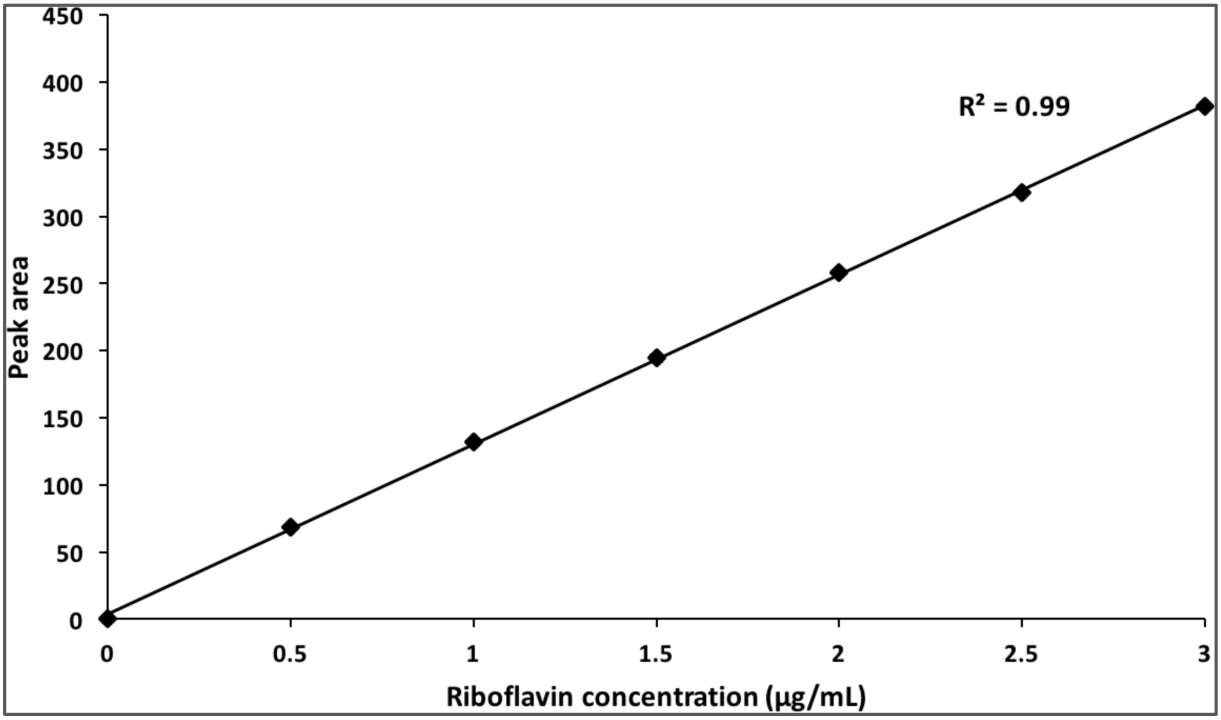

Figure 32. Calibration curve for the riboflavin standard solutions produced in the microbial samples in the range of 0.5–3 µg/mL on the HPLC system.

Effects of metal ions on metabolism

Final hypothesis, metal ions may affect the metabolism of the bacteria. Cd^{2+} is known to be far more toxic than Pb^{2+}. As the minimal inhibitory concentration (MIC) is 0.5 g/cm^3 for Cd^{2+} compared to 5.0 g/cm^3 for Pb^{2+}. The effect is suggested to be a metabolic one in Cd^{2+} where Cd^{2+} interferes with both Ca^{2+} and Zn^{2+} related sulfhydryl group.[127]

In order to check metabolism, several experiments were performed. First, the optical density (O.D.) was measured from the extracted volume of growth media in the electrochemical cell (Figure 33). There is no observed difference in the optical density from the beginning to the end of the experiment between metal ions. This suggests that there is no toxic effect inhibiting

microbial growth in solution. This is despite the difference in minimum inhibitory concentration (MIC) for the metal ions.

Second, HPLC was utilized to measure the glucose consumed during the electrochemical experiment (Figure 33). Glucose consumption was dependent on the type of metal ions in the cultures. Glucose concentrations found in solutions of 800 μM Mg^{2+}, Cd^{2+}, Pb^{2+}, and Ca^{2+} were 0.45 ± 0.10, 0.67 ± 0.15, 0.85 ± 0.06, and 1.53 ± 0.15 g/L, respectively. These values were much higher than those consumed by the control, 0.14 ± 0.05 g/L. Fitzgerald et al.[102] found that the lactate consumed was independent of the concentration of $CaCl_2$ in the medium.

Third, riboflavin production was monitored. Extracellular electron transfer (EET) efficiency is considered to be the limiting parameter that determines the performance of a microbial fuel cell (MFC).[85] Electron shuttle mediators are one of the most important EET pathways in MFCs. Electron shuttles facilitate the transfer of an electron between microbes, from substances that donate electrons to microbes, and/or from microbes to substances that accept electrons.[45, 96, 186-187] Riboflavin has been identified as an indirect extracellular electron transfer (EET) mediator, serving as an electron shuttle for the EET of *Shewanella oneidensis* MR-1 in MFCs.[45, 96, 188] There is a difference between metal ions which may be metabolitic.[102, 189] Xu et al.[99] found that the riboflavin was increased with Cu^{2+} and Cd^{2+} (1.78 and 1.73 μM) compared to the control (1.46 μM). The concentration of riboflavin was measured by HPLC (Figure 33). Riboflavin concentrations found in solutions of 800 μM for Mg^{2+}, Cd^{2+}, Pb^{2+}, and Ca^{2+} were 2.28 ± 0.10, 3.08 ± 0.15, 4.27 ± 0.06, and 6.23 ± 0.13 μM, respectively. These values were much higher than those produced by the control, 0.26 ± 0.06 μM.

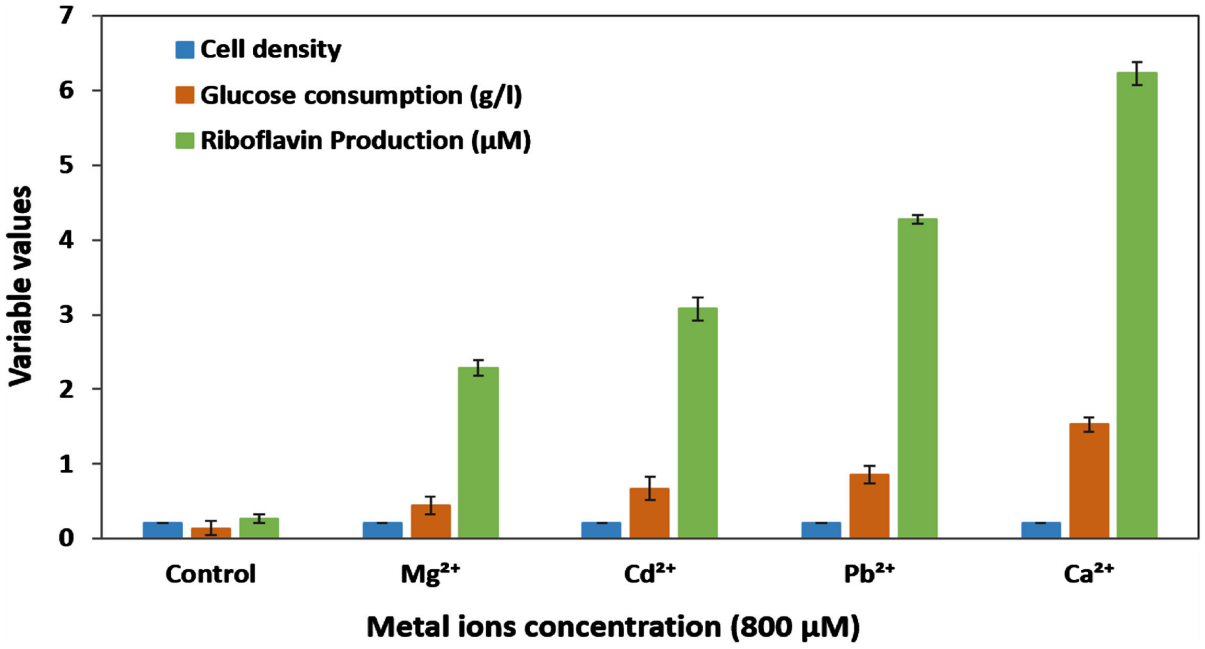

Figure 33. Cell density on exit of electrochemical cell (blue), glucose consumption (orange), and riboflavin production (green) vs. control (TSB+Bacteria) and Mg^{2+}, Cd^{2+}, Pb^{2+}, and Ca^{2+} metal ion concentrations at 800 µM for *Shewanella oneidensis* MR-1.

As riboflavin is a mediator for electron transfer, increased riboflavin product should increase electrochemical activity of the bacteria. The trends were consistent with all of the electrochemical trends observed above. Both sets of experiments indicate that glucose (consumed) and riboflavin (produced) follow the same trends in the electrochemical behavior shown above.

The results implied that metal ions Mg^{2+}, Cd^{2+}, Pb^{2+}, and Ca^{2+} enhanced bacteria attachment to the electrode surface and that might, in part, contribute to current output improvement. There are other factors related to the current output. For example, cellular metabolism and activity of electron transfer chain (e.g., c-type cytochrome). These factors might be influenced by metal ions Mg^{2+}, Cd^{2+}, Pb^{2+}, and Ca^{2+} and might play a role in current output improvement.

CHAPTER FOUR

CONCLUSION AND FUTURE WORK

Conclusion

The aim of this Ph.D. project was to study the effect of metal ions on the efficiency of bacterial extracellular electron transfer (EET) in *Shewanella* oneidensis MR-1. This was achieved by enhancing bacterial adhesion to the ITO electrode surface to improve the current output of microbial fuel cells. In this study, electrochemistry and analytical chemistry technologies were used to evaluate the enhanced activity of the bacteria.

The study showed that the current output generated by *Shewanella oneidensis* MR-1 was affected by the addition of metal ions. The initial surface coverage of the bacteria was measured with respect to the start-up time, the maximum loading current density during the loading of the ITO surface at +0.2 V, and the cyclic voltammetry peak current. Our results clearly reveal a major difference in the attachment and behavior of *Shewanella oneidensis* MR-1 for Mg^{2+}, Cd^{2+}, Pb^{2+}, and Ca^{2+} compared with those observed for the control.

Major differences in the attachments were observed for the loading current measurements. The start-up time was considerably decreased, and the maximum loading current density considerably increased for Mg^{2+}, Cd^{2+}, Pb^{2+}, and Ca^{2+} compared with that observed for the control. The highest maximum loading current density at 800 μM was found to be 2.65 ± 0.02 (Ca^{2+}), which was approximately 4.09 times higher; 2.38 ± 0.02 (Pb^{2+}), approximately 3.58 times higher; 2.15 ± 0.03 (Cd^{2+}), approximately 3.13 times higher; and 1.69 ± 0.02 (Mg^{2+})

$\mu A/cm^2$ approximately 2.25 times higher than that of the control. The lowest decreased start-up times for 800 μM were found at 88 ± 1.00 (Mg^{2+}), 78 ± 3.60 (Cd^{2+}), 64 ± 4.16 (Pb^{2+}), and 45 ± 1.53 (Ca^{2+}), compared to the control of 617 ± 7.57 s. The addition of Mg^{2+}, Cd^{2+}, Pb^{2+}, and Ca^{2+} led to the significant increase in the current output compared with that of the control.

As measured by SEM, confocal microscopy, and the cathodic peak charge in cyclic voltammetry (Q_{pc}), the final surface coverage of bacteria increases with the increase in the metal ion concentrations. In the cyclic voltammetry, it was observed that the reduction peak current density increased with the addition of 800 μM of Ca^{2+}, Pb^{2+}, Cd^{2+}, and Mg^{2+} to 4.16 ± 0.13, 3.70 ± 0.13, 2.90 ± 0.12, and 2.27 ± 0.12 μA/cm2, respectively, compared with the control (0.99 ± 0.09 μA/cm2). Increased metal ion concentrations increased the number of cells attached to the electrode to a greater extent in the order $Ca^{2+} > Pb^{2+} > Cd^{2+} > Mg^{2+}$ compared with the control. Metal ion concentrations of 800 μM increased the surface area coverage by approximately 51.6 ± 0.25% for (Mg^{2+}), 64.7 ± 0.94% (Cd^{2+}), 70.2 ± 0.45% (Pb^{2+}), and 78.5 ± 1.28% (Ca^{2+}), compared with the control (10 ± 0.86%).

The area under the reduction peak was used to determine the amount of material attached to the surface as measured by the integrated peaks current. The cathodic peak charge values were increased to 216 ± 1.89 (Mg^{2+}), 260 ± 1.5 (Cd^{2+}), 296 ± 2.47 (Pb^{2+}), and 346 ± 2.89 (Ca^{2+}) μC at a higher concentration of 800 μM, whereas the control was found to be 78 ± 4.29 μC. The relationship between cathodic peak charge and % bacterial coverages increased linearly (R^2 = 0.99). There was a slight difference in slopes between the charge and % bacterial coverage. These differences were indicated as statistically related to a metal ion-specific effect. This result established that the addition of metal ions led to a more significant impact on bacterial cell

attachment to the electrodes.

Metal ions have a non-specific effect on repulsion between the surface and bacteria, ionic radii, and the structure of extracellular polysaccharides (EPSs). In this study, the ionic strength was maintained constant, thus it should not have resulted in an alteration of bacterial adhesion to the electrode's surface.

Ionic radii are known to cause non-specific differences in the behaviors of bacterial adhesion. Bacterial adhesion to an electrode's surface increases with ionic radii. Bacterial coverage for Mg^{2+}, Cd^{2+}, and Ca^{2+} was linear with ionic radii ($R^2 = 0.99$). As expected, Ca^{2+} resulted in the highest current density, compared with Pb^{2+}, Cd^{2+}, and Mg^{2+}. The Pb^{2+} was out of sequence between Mg^{2+}, Cd^{2+}, and Ca^{2+} and resulted in a poorer correlation between % bacterial coverage and ionic radii ($R^2 = 0.79$). This difference may be due to the hydrated Pb^{2+} ion structure influenced by the lone electron pair, which is giving complex hemi-directed in aqueous solution.[178]

It was indicated that metal ions increased the anodic biofilm formation. Once attached, a linear relationship was observed between the percentage of bacterial coverage and electrochemical performance, which may have been related to alterations in the structures of the extracellular polysaccharides (EPSs), as observed in the literature.[126, 175]

The effect of metal ions on glucose consumption and riboflavin production was analyzed using an HPLC system. The HPLC chromatograms of glucose consumption and riboflavin production showed peaks with good shape and stable retention time. Interfering peaks were found at (16.81 min) for glucose consumption, whereas for riboflavin, they were found at (5.64 min) retention times. The obtained R^2 values resulted the linearity being acceptable for glucose

consumption and riboflavin production for the different concentration ranges tested. Good linearity of glucose consumption and riboflavin production was confirmed according to the coefficient of determination ($R^2 \geq 0.99$). The limit of detection (LOD) values for riboflavin were approximately 0.01 μg/mL, whereas the limit of quantification (LOQ) values were approximately 0.05 μg/mL. These results demonstrate that metal ions have a specific effect on glucose consumption, riboflavin production, and toxicity. Glucose consumption and riboflavin production were enhanced by the addition of metal ions, which can affect the current output generated by *Shewanella oneidensis* MR-1.

Heavy metals ions were expected to have a toxic effect on bacterial growth; however, in this study, heavy metals had no effect on the optical density of the extracted solutions, which indicated that the bacterial growth in the solutions was unaffected. Metabolic activity mirrored the same order of activity for the electrochemical results.

Glucose consumption was found to be dependent on the type of metal ions present in the culture's solutions. Glucose concentrations obtained in solutions of 800 μM for Mg^{2+}, Cd^{2+}, Pb^{2+}, and Ca^{2+} were 0.45 ± 0.10, 0.67 ± 0.15, 0.85 ± 0.06, and 1.53 ± 0.15 g/L, respectively. These values were much higher than those for the glucose consumed by the control of (0.14 ± 0.05 g/L). The concentrations of riboflavin in solutions of 800 μM were 2.28 ± 0.10 (Mg^{2+}), 3.08 ± 0.15 (Cd^{2+}), 4.27 ± 0.06 (Pb^{2+}), and 6.23 ± 0.13 μM (Ca^{2+}). These values were higher than those produced by the control (0.26 ± 0.06 μM). Mg^{2+}, Cd^{2+}, Pb^{2+}, and Ca^{2+} significantly increased the current output compared with that of the control. These results suggest avenues of research on the improvement of performance and operation of MFCs.

Future work

The following recommendations are made for future research. Computational modeling can be used to study the binding of metal ions to lipopolysaccharide (LPS). Molecular modeling programs are one of the approaches used to study the behavior of metal ions that bind to the LPS. This can be done via collaborations with the department of chemistry and biochemistry at Loyola University Chicago, or with other labs at different universities or various corporate groups.

Molecular modeling is widely used to study the behavior of the molecular structures in chemical or biological systems.[190-191] Molecular modeling is a computerized work that applies the laws of physics, supported by experimental data. This approach can be used to analyze atom types and numbers, the nature of the bonds, bond lengths, angles, and dihedral angles, and molecular energy. It can also be employed to determine electrostatic potentials and molecular and biological properties, which are predicted for understanding the activity of the structure.[191-192]

A molecular model for rough LPS can be designed based on structural information which determined via experiments. Lins and Straatsma[193] have designed an LPS model for *Pseudomonas aeruginosa*, as shown in Figure 34. A single LPS molecule and a single phospholipid molecule were replicated from the bacterial membrane exterior. The model could start with this LPS structure as a gram-negative bacteria, or a new structure could be built for *Shewanella oneidensis* MR-1. There are several steps in computational chemistry methods that could be used to complete the set of force field parameters required for the molecular simulations of the system. First, a molecular model for the LPS membrane can be built from single molecules of LPS and a phospholipid chain. Second, Ca^{2+}, Pb^{2+}, Cd^{2+}, and Mg^{2+} can be distributed near the

structure to neutralize the original charge of the LPS unit. Third, an electrostatic model can be used to calculate partial atomic charges for the complete LPS molecule. Fourth, molecular dynamics simulations can be used with the rough LPS to analyze the energetic and structural factors.

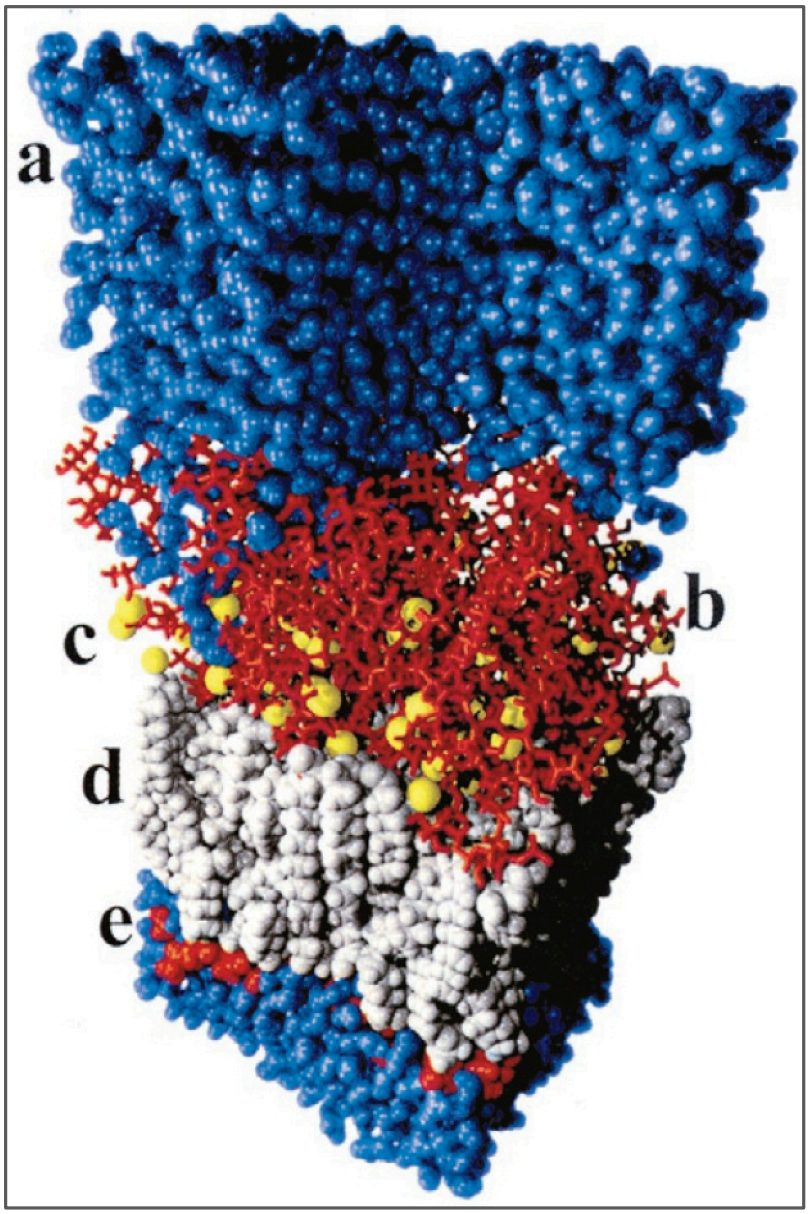

Figure 34. Molecular model of the rough lipopolysaccharide of *Pseudomonas aeruginosa*. (a) The water layer. (b) The top of the sugars. (c) The yellow spheres are Ca^{2+} ions. (d) The phospholipid layer. (e) Polar head groups immersed in water.[193]

There are two important functional groups, the carboxyl and phosphate groups; these are the most responsible for metal ions binding to LPS. Lins and Straatsma[193] found that all Ca^{2+} ions' coordination sites interact with phosphate groups on the LPS structure. One of the Ca^{2+} ion coordination sites is coordinated with carboxyl groups, and another is interaction with hydroxyl groups. The molecular modeling analysis of the rough LPS of *Shewanella oneidensis* MR-1 with metal ions could provide further details about bacterial adhesion to the surface and a function of the LPS membrane's composition. Divalent cations lead to significant changes in physicochemical behaviors, such as hydration, ionic valence, and the structure of the aggregates of LPS membranes.[194] Accordingly, the electrochemical results clarified that the Pb^{2+} was out of sequence between Mg^{2+}, Cd^{2+}, and Ca^{2+} in the linear relationship between bacterial coverage and the ionic radii. Through LPS modeling, it may be possible to determine if the Pb^{2+} results lead to the same or different enhancement effects compared to electrochemical behaviors. This may be due to the hydrated Pb^{2+} ion structure and how it is effected by the lone electron pair.[178]

Trivalent cations could also affect cell adhesion to the surface of an electrode and enhance the current output generation from *Shewanella oneidensis* MR-1. Controlling the ionic strength should make non-specific effects (e.g., ion size) minimal. Molecular modeling could be performed simultaneously with electrochemical experiments in the laboratory.

REFERENCE LIST

1. Kim, I.-S.; Chae, K.-J.; Choi, M.-J.; Verstraete, W., Microbial fuel cells: recent advances, bacterial communities and application beyond electricity generation. *Environmental Engineering Research* **2008,** *13* (2), 51-65.

2. Slate, A. J.; Whitehead, K. A.; Brownson, D. A.; Banks, C. E., Microbial fuel cells: An overview of current technology. *Renewable and Sustainable Energy Reviews* **2019,** *101*, 60-81.

3. Santoro, C.; Arbizzani, C.; Erable, B.; Ieropoulos, I., Microbial fuel cells: from fundamentals to applications. A review. *Journal of Power Sources* **2017,** *356*, 225-244.

4. Bhargavi, G.; Venu, V.; Renganathan, S. In *Microbial fuel cells: recent developments in design and materials*, IOP Conference Series: Materials Science and Engineering, IOP Publishing: 2018; p 012034.

5. Du, Z.; Li, H.; Gu, T., A state of the art review on microbial fuel cells: a promising technology for wastewater treatment and bioenergy. *Biotechnology advances* **2007,** *25* (5), 464-482.

6. Rabaey, K.; Lissens, G.; Siciliano, S. D.; Verstraete, W., A microbial fuel cell capable of converting glucose to electricity at high rate and efficiency. *Biotechnology letters* **2003,** *25* (18), 1531-1535.

7. Logan, B. E.; Hamelers, B.; Rozendal, R.; Schröder, U.; Keller, J.; Freguia, S.; Aelterman, P.; Verstraete, W.; Rabaey, K., Microbial fuel cells: methodology and technology. *Environ Sci Technol* **2006,** *40* (17), 5181-5192.

8. Kim, H. J.; Park, H. S.; Hyun, M. S.; Chang, I. S.; Kim, M.; Kim, B. H., A mediator-less microbial fuel cell using a metal reducing bacterium, Shewanella putrefaciens. *Enzyme Microb Tech* **2002,** *30* (2), 145-152.

9. Kim, B. H.; Kim, H. J.; Hyun, M. S.; Park, D. H., Direct electrode reaction of Fe (III)-reducing bacterium, Shewanella putrefaciens. *Journal of Microbiology and Biotechnology* **1999,** *9*, 127-131.

10. Kim, H. J.; Hyun, M. S.; Chang, I. S.; Kim, B. H., A microbial fuel cell type lactate biosensor using a metal-reducing bacterium, Shewanella putrefaciens. *Journal of Microbiology and Biotechnology* **1999,** *9* (3), 365-367.

11. Jiang, Y.; Xu, Y.; Yang, Q.; Chen, Y.; Zhu, S.; Shen, S., Power generation using polyaniline/multi-walled carbon nanotubes as an alternative cathode catalyst in microbial fuel cells. *International Journal of Energy Research* **2014,** *38* (11), 1416-1423.

12. Fornero, J. J.; Rosenbaum, M.; Angenent, L. T., Electric power generation from municipal, food, and animal wastewaters using microbial fuel cells. *Electroanalysis: An International Journal Devoted to Fundamental and Practical Aspects of Electroanalysis* **2010,** *22* (7-8), 832-843.

13. Kumar, R.; Singh, L.; Zularisam, A.; Hai, F. I., Microbial fuel cell is emerging as a versatile technology: a review on its possible applications, challenges and strategies to improve the performances. *International Journal of Energy Research* **2018,** *42* (2), 369-394.

14. Rabaey, K.; Verstraete, W., Microbial fuel cells: novel biotechnology for energy generation. *Trends Biotechnol* **2005,** *23* (6), 291-298.

15. Yong, X.-Y.; Feng, J.; Chen, Y.-L.; Shi, D.-Y.; Xu, Y.-S.; Zhou, J.; Wang, S.-Y.; Xu, L.; Yong, Y.-C.; Sun, Y.-M., Enhancement of bioelectricity generation by cofactor manipulation in microbial fuel cell. *Biosensors and Bioelectronics* **2014,** *56*, 19-25.

16. Lovley, D. R., Microbial fuel cells: novel microbial physiologies and engineering approaches. *Current opinion in biotechnology* **2006,** *17* (3), 327-332.

17. Li, M.; Zhou, M.; Tian, X.; Tan, C.; McDaniel, C. T.; Hassett, D. J.; Gu, T., Microbial fuel cell (MFC) power performance improvement through enhanced microbial electrogenicity. *Biotechnology advances* **2018,** *36* (4), 1316-1327.

18. Huang, L.; Logan, B. E., Electricity generation and treatment of paper recycling wastewater using a microbial fuel cell. *Applied microbiology and biotechnology* **2008,** *80* (2), 349-355.

19. Kumar, R.; Singh, L.; Zularisam, A.; Hai, F. I., Potential of porous Co3O4 nanorods as cathode catalyst for oxygen reduction reaction in microbial fuel cells. *Bioresource Technol* **2016,** *220*, 537-542.

20. Logan, B. E.; Hamelers, B.; Rozendal, R. A.; Schrorder, U.; Keller, J.; Freguia, S.; Aelterman, P.; Verstraete, W.; Rabaey, K., Microbial fuel cells: Methodology and technology. *Environ Sci Technol* **2006,** *40* (17), 5181-5192.

21. Chaudhuri, S. K.; Lovley, D. R., Electricity generation by direct oxidation of glucose in mediatorless microbial fuel cells. *Nature biotechnology* **2003,** *21* (10), 1229.

22. Rahimnejad, M.; Adhami, A.; Darvari, S.; Zirepour, A.; Oh, S.-E., Microbial fuel cell as new technology for bioelectricity generation: a review. *Alex Eng J* **2015,** *54* (3), 745-756.

23. Kracke, F.; Vassilev, I.; Krömer, J. O., Microbial electron transport and energy conservation–the foundation for optimizing bioelectrochemical systems. *Frontiers in microbiology* **2015,** *6*, 575.

24. Logan, B. E.; Regan, J. M., Microbial fuel cells—challenges and applications. ACS Publications: **2006**.

25. Okamoto, A.; Kalathil, S.; Deng, X.; Hashimoto, K.; Nakamura, R.; Nealson, K. H., Cell-secreted flavins bound to membrane cytochromes dictate electron transfer reactions to surfaces with diverse charge and pH. *Scientific reports* **2014,** *4*, 5628.

26. Pirbadian, S.; Barchinger, S. E.; Leung, K. M.; Byun, H. S.; Jangir, Y.; Bouhenni, R. A.; Reed, S. B.; Romine, M. F.; Saffarini, D. A.; Shi, L., Shewanella oneidensis MR-1 nanowires are outer membrane and periplasmic extensions of the extracellular electron transport components. *Proceedings of the National Academy of Sciences* **2014,** *111* (35), 12883-12888.

27. Liu, H.; Grot, S.; Logan, B. E., Electrochemically assisted microbial production of hydrogen from acetate. *Environ Sci Technol* **2005,** *39* (11), 4317-4320.

28. Logan, B. E., *Microbial fuel cells*. John Wiley & Sons: 2008.

29. Mohan, Y.; Kumar, S. M. M.; Das, D., Electricity generation using microbial fuel cells. *International Journal of Hydrogen Energy* **2008,** *33* (1), 423-426.

30. Sharma, Y.; Li, B., The variation of power generation with organic substrates in single-chamber microbial fuel cells (SCMFCs). *Bioresource Technol* **2010,** *101* (6), 1844-1850.

31. Izadi, P.; Rahimnejad, M., Simultaneous electricity generation and sulfide removal via a dual chamber microbial fuel cell. *Biofuel Research Journal* **2014,** *1* (1), 34-38.

32. Pant, D.; Van Bogaert, G.; Diels, L.; Vanbroekhoven, K., A review of the substrates used in microbial fuel cells (MFCs) for sustainable energy production. *Bioresource Technol* **2010,** *101* (6), 1533-1543.

33. Habermann, W.; Pommer, E., Biological fuel cells with sulphide storage capacity. *Applied microbiology and biotechnology* **1991,** *35* (1), 128-133.

34. Kumar, R.; Singh, L.; Wahid, Z. A.; Din, M. F. M., Exoelectrogens in microbial fuel cells toward bioelectricity generation: a review. *International Journal of Energy Research* **2015,** *39* (8), 1048-1067.

35. Shantaram, A.; Beyenal, H.; Veluchamy, R. R. A.; Lewandowski, Z., Wireless sensors powered by microbial fuel cells. *Environ Sci Technol* **2005,** *39* (13), 5037-5042.

36. Chang, I. S.; Jang, J. K.; Gil, G. C.; Kim, M.; Kim, H. J.; Cho, B. W.; Kim, B. H., Continuous determination of biochemical oxygen demand using microbial fuel cell type biosensor. *Biosensors and Bioelectronics* **2004,** *19* (6), 607-613.

37. Liu, Z.; Liu, J.; Zhang, S.; Xing, X.-H.; Su, Z., Microbial fuel cell based biosensor for in situ monitoring of anaerobic digestion process. *Bioresource Technol* **2011,** *102* (22), 10221-10229.

38. Potter, M. C., Electrical effects accompanying the decomposition of organic compounds. *Proceedings of the Royal Society of London. Series B, Containing Papers of a Biological Character* **1911,** *84* (571), 260-276.

39. Carmona-Martínez, A. A.; Harnisch, F.; Kuhlicke, U.; Neu, T. R.; Schröder, U., Electron transfer and biofilm formation of Shewanella putrefaciens as function of anode potential. *Bioelectrochemistry* **2013,** *93*, 23-29.

40. Megonigal, J. P.; Hines, M.; Visscher, P., Anaerobic metabolism: linkages to trace gases and aerobic processes. *Biogeochemistry* **2004**.

41. Lovley, D. R.; Holmes, D. E.; Nevin, K. P., Dissimilatory fe (iii) and mn (iv) reduction. **2004**.

42. Logan, B. E.; Regan, J. M., Electricity-producing bacterial communities in microbial fuel cells. *TRENDS in Microbiology* **2006,** *14* (12), 512-518.

43. Kumar, R.; Singh, L.; Zularisam, A., Exoelectrogens: recent advances in molecular drivers involved in extracellular electron transfer and strategies used to improve it for microbial fuel cell applications. *Renewable and Sustainable Energy Reviews* **2016,** *56*, 1322-1336.

44. Fitzgerald, L. A.; Petersen, E. R.; Leary, D. H.; Nadeau, L. J.; Soto, C. M.; Ray, R. I.; Little, B. J.; Ringeisen, B. R.; Johnson, G. R.; Vora, G. J., Shewanella frigidimarina microbial fuel cells and the influence of divalent cations on current output. *Biosensors and Bioelectronics* **2013,** *40* (1), 102-109.

45. Marsili, E.; Baron, D. B.; Shikhare, I. D.; Coursolle, D.; Gralnick, J. A.; Bond, D. R., Shewanella secretes flavins that mediate extracellular electron transfer. *Proceedings of the National Academy of Sciences* **2008,** *105* (10), 3968-3973.

46. Bretschger, O.; Cheung, A. C.; Mansfeld, F.; Nealson, K. H., Comparative microbial fuel cell evaluations of Shewanella spp. *Electroanalysis: An International Journal Devoted to Fundamental and Practical Aspects of Electroanalysis* **2010,** *22* (7-8), 883-894.

47. Okamoto, A.; Nakamura, R.; Ishii, K.; Hashimoto, K., In vivo Electrochemistry of C-Type Cytochrome-Mediated Electron-Transfer with Chemical Marking. *ChemBioChem* **2009,** *10* (14), 2329-2332.

48. Li, S.-L.; Freguia, S.; Liu, S.-M.; Cheng, S.-S.; Tsujimura, S.; Shirai, O.; Kano, K., Effects of oxygen on Shewanella decolorationis NTOU1 electron transfer to carbon-felt electrodes. *Biosensors and Bioelectronics* **2010,** *25* (12), 2651-2656.

49. Biffinger, J. C.; Fitzgerald, L. A.; Ray, R.; Little, B. J.; Lizewski, S. E.; Petersen, E. R.; Ringeisen, B. R.; Sanders, W. C.; Sheehan, P. E.; Pietron, J. J., The utility of Shewanella japonica for microbial fuel cells. *Bioresource Technol* **2011,** *102* (1), 290-297.

50. Pankhurst, K. L.; Mowat, C. G.; Rothery, E. L.; Hudson, J. M.; Jones, A. K.; Miles, C. S.; Walkinshaw, M. D.; Armstrong, F. A.; Reid, G. A.; Chapman, S. K., A proton delivery pathway in the soluble fumarate reductase from Shewanella frigidimarina. *J Biol Chem* **2006,** *281* (29), 20589-20597.

51. Huang, J.; Sun, B.; Zhang, X., Electricity generation at high ionic strength in microbial fuel cell by a newly isolated Shewanella marisflavi EP1. *Applied microbiology and biotechnology* **2010,** *85* (4), 1141-1149.

52. Hau, H. H.; Gralnick, J. A., Ecology and biotechnology of the genus Shewanella. *Annu. Rev. Microbiol.* **2007,** *61*, 237-258.

53. Venkateswaran, K.; Moser, D. P.; Dollhopf, M. E.; Lies, D. P.; Saffarini, D. A.; MacGregor, B. J.; Ringelberg, D. B.; White, D. C.; Nishijima, M.; Sano, H., Polyphasic taxonomy of the genus Shewanella and description of Shewanella oneidensis sp. nov. *International Journal of Systematic and Evolutionary Microbiology* **1999,** *49* (2), 705-724.

54. Heidelberg, J. F.; Paulsen, I. T.; Nelson, K. E.; Gaidos, E. J.; Nelson, W. C.; Read, T. D.; Eisen, J. A.; Seshadri, R.; Ward, N.; Methe, B., Genome sequence of the dissimilatory metal ion–reducing bacterium Shewanella oneidensis. *Nature biotechnology* **2002,** *20* (11), 1118.

55. Alshahrani, A.; Fitch, A.; Al-Bazi, J., Metal Ions Impact on Shewanella Oneidensis MR-1 Adhesion to ITO Electrode and the Enhancement of Current Output. *American Journal of Analytical Chemistry* **2019,** *10* (09), 428.

56. Gram, C., Ueber die isolirte Farbung der Schizomyceten in Schnitt-und Trockenpraparaten. *Fortschritte der Medicin* **1884,** *2*, 185-189.

57. Vadillo-Rodríguez, V.; Dutcher, J. R., Viscoelasticity of the bacterial cell envelope. *Soft Matter* **2011,** *7* (9), 4101-4110.

58. Cabeen, M. T.; Jacobs-Wagner, C., Bacterial cell shape. *Nature Reviews Microbiology* **2005,** *3* (8), 601.

59. Beveridge, T., Ultrastructure, chemistry, and function of the bacterial wall. In *International review of cytology*, Elsevier: **1981**; Vol. 72, pp 229-317.

60. Myers, C. R.; Myers, J. M., Localization of cytochromes to the outer membrane of anaerobically grown Shewanella putrefaciens MR-1. *J Bacteriol* **1992,** *174* (11), 3429-3438.

61. Ogawa, T.; Asai, Y.; Makimura, Y.; Tamai, R., Chemical structure and immunobiological activity of Porphyromonas gingivalis lipid A. *Front Biosci* **2007,** *12*, 3795-3812.

62. Nikaido, H., Molecular basis of bacterial outer membrane permeability revisited. *Microbiol. Mol. Biol. Rev.* **2003,** *67* (4), 593-656.

63. Li, B.; Logan, B. E., Bacterial adhesion to glass and metal-oxide surfaces. *Colloids and Surfaces B: Biointerfaces* **2004,** *36* (2), 81-90.

64. Patrauchan, M. A.; Sarkisova, S.; Sauer, K.; Franklin, M. J., Calcium influences cellular and extracellular product formation during biofilm-associated growth of a marine Pseudoalteromonas sp. *Microbiology* **2005,** *151* (9), 2885-2897.

65. Kierek, K.; Watnick, P. I., The Vibrio cholerae O139 O-antigen polysaccharide is essential for Ca2+-dependent biofilm development in sea water. *Proceedings of the National Academy of Sciences* **2003,** *100* (24), 14357-14362.

66. Zhou, A. Y.; Zajdel, T. J.; TerAvest, M. A.; Maharbiz, M. M. In *A miniaturized monitoring system for electrochemical biosensing using Shewanella oneidensis in environmental applications*, 2015 37th Annual International Conference of the IEEE Engineering in Medicine and Biology Society (EMBC), IEEE: **2015**; pp 7518-7521.

67. Meitl, L. A.; Eggleston, C. M.; Colberg, P. J.; Khare, N.; Reardon, C. L.; Shi, L., Electrochemical interaction of Shewanella oneidensis MR-1 and its outer membrane cytochromes OmcA and MtrC with hematite electrodes. *Geochimica et Cosmochimica Acta* **2009,** *73* (18), 5292-5307.

68. Hartshorne, R. S.; Jepson, B. N.; Clarke, T. A.; Field, S. J.; Fredrickson, J.; Zachara, J.; Shi, L.; Butt, J. N.; Richardson, D. J., Characterization of Shewanella oneidensis MtrC: a cell-surface decaheme cytochrome involved in respiratory electron transport to extracellular electron acceptors. *JBIC Journal of Biological Inorganic Chemistry* **2007,** *12* (7), 1083-1094.

69. Grobbler, C.; Virdis, B.; Nouwens, A.; Harnisch, F.; Rabaey, K.; Bond, P. L., Effect of the anode potential on the physiology and proteome of Shewanella oneidensis MR-1. *Bioelectrochemistry* **2018,** *119*, 172-179.

70. Kane, A. L.; Brutinel, E. D.; Joo, H.; Maysonet, R.; VanDrisse, C. M.; Kotloski, N. J.; Gralnick, J. A., Formate metabolism in Shewanella oneidensis generates proton motive force and prevents growth without an electron acceptor. *J Bacteriol* **2016,** *198* (8), 1337-1346.

71. Kim, B. H.; Ikeda, T.; Park, H. S.; Kim, H. J.; Hyun, M. S.; Kano, K.; Takagi, K.; Tatsumi, H., Electrochemical activity of an Fe (III)-reducing bacterium, Shewanella putrefaciens IR-1, in the presence of alternative electron acceptors. *Biotechnology Techniques* **1999,** *13* (7), 475-478.

72. Urry, L. A.; Cain, M. L.; Wasserman, S. A.; Minorsky, P. V.; Reece, J. B., *Campbell biology*. Pearson Education, Incorporated: 2017.

73. Kalathil, S.; Hashimoto, K.; Okamoto, A., Effect of Ionic Strength on the Rate of Extracellular Electron Transport in Shewanella oneidensis MR-1 through Bound-Flavin Semiquinones. *ChemElectroChem* **2014,** *1* (11), 1840-1843.

74. Nakamura, R.; Kai, F.; Okamoto, A.; Hashimoto, K., Mechanisms of long-distance extracellular electron transfer of metal-reducing bacteria mediated by nanocolloidal semiconductive iron oxides. *Journal of Materials Chemistry A* **2013,** *1* (16), 5148-5157.

75. Nakamura, R.; Ishii, K.; Hashimoto, K., Electronic absorption spectra and redox properties of C type cytochromes in living microbes. *Angewandte Chemie International Edition* **2009,** *48* (9), 1606-1608.

76. Zhao, Y.; Watanabe, K.; Nakamura, R.; Mori, S.; Liu, H.; Ishii, K.; Hashimoto, K., Three-dimensional conductive nanowire networks for maximizing anode performance in microbial fuel cells. *Chemistry–A European Journal* **2010,** *16* (17), 4982-4985.

77. Goldbeck, C. P.; Jensen, H. M.; TerAvest, M. A.; Beedle, N.; Appling, Y.; Hepler, M.; Cambray, G.; Mutalik, V.; Angenent, L. T.; Ajo-Franklin, C. M., Tuning promoter strengths for improved synthesis and function of electron conduits in Escherichia coli. *ACS synthetic biology* **2013,** *2* (3), 150-159.

78. Gralnick, J. A.; Newman, D. K., Extracellular respiration. *Molecular microbiology* **2007,** *65* (1), 1-11.

79. Chouler, J.; Di Lorenzo, M., Water quality monitoring in developing countries; can microbial fuel cells be the answer? *Biosensors* **2015,** *5* (3), 450-470.

80. Rinaldi, A.; Mecheri, B.; Garavaglia, V.; Licoccia, S.; Di Nardo, P.; Traversa, E., Engineering materials and biology to boost performance of microbial fuel cells: a critical review. *Energy & Environmental Science* **2008,** *1* (4), 417-429.

81. Pandit, S.; Das, D., Principles of microbial fuel cell for the power generation. In *Microbial fuel cell*, Springer: 2018; pp 21-41.

82. Pandit, S.; Chandrasekhar, K.; Kakarla, R.; Kadier, A.; Jeevitha, V., Basic principles of microbial fuel cell: technical challenges and economic feasibility. In *Microbial Applications Vol. 1*, Springer: 2017; pp 165-188.

83. Breuer, M.; Rosso, K. M.; Blumberger, J.; Butt, J. N., Multi-haem cytochromes in Shewanella oneidensis MR-1: structures, functions and opportunities. *Journal of The Royal Society Interface* **2015,** *12* (102), 20141117.

84. Lower, B. H.; Hochella, M. F.; Lower, S. K., Putative mineral-specific proteins synthesized by a metal reducing bacterium. *American Journal of Science* **2005,** *305* (6-8), 687-710.

85. Yang, Y.; Xu, M.; Guo, J.; Sun, G., Bacterial extracellular electron transfer in bioelectrochemical systems. *Process Biochemistry* **2012,** *47* (12), 1707-1714.

86. Meyer, T. E.; Tsapin, A. I.; Vandenberghe, I.; De Smet, L.; Frishman, D.; Nealson, K. H.; Cusanovich, M. A.; Van Beeumen, J. J., Identification of 42 possible cytochrome c genes in the Shewanella oneidensis genome and characterization of six soluble cytochromes. *Omics: a journal of integrative biology* **2004,** *8* (1), 57-77.

87. Shi, L.; Chen, B.; Wang, Z.; Elias, D. A.; Mayer, M. U.; Gorby, Y. A.; Ni, S.; Lower, B. H.; Kennedy, D. W.; Wunschel, D. S., Isolation of a high-affinity functional protein complex between OmcA and MtrC: two outer membrane decaheme c-type cytochromes of Shewanella oneidensis MR-1. *J Bacteriol* **2006,** *188* (13), 4705-4714.

88. Gorby, Y. A.; Yanina, S.; McLean, J. S.; Rosso, K. M.; Moyles, D.; Dohnalkova, A.; Beveridge, T. J.; Chang, I. S.; Kim, B. H.; Kim, K. S., Electrically conductive bacterial nanowires produced by Shewanella oneidensis strain MR-1 and other microorganisms. *Proceedings of the National Academy of Sciences* **2006,** *103* (30), 11358-11363.

89. Velasquez-Orta, S. B.; Head, I. M.; Curtis, T. P.; Scott, K.; Lloyd, J. R.; von Canstein, H., The effect of flavin electron shuttles in microbial fuel cells current production. *Applied microbiology and biotechnology* **2010,** *85* (5), 1373-1381.

90. Stams, A. J.; De Bok, F. A.; Plugge, C. M.; Van Eekert, M. H.; Dolfing, J.; Schraa, G., Exocellular electron transfer in anaerobic microbial communities. *Environmental Microbiology* **2006,** *8* (3), 371-382.

91. Hernandez, M.; Newman, D., Extracellular electron transfer. *Cellular and Molecular Life Sciences CMLS* **2001,** *58* (11), 1562-1571.

92. Liao, Z.-H.; Sun, J.-Z.; Sun, D.-Z.; Si, R.-W.; Yong, Y.-C., Enhancement of power production with tartaric acid doped polyaniline nanowire network modified anode in microbial fuel cells. *Bioresource Technol* **2015,** *192*, 831-834.

93. Qiao, Y.; Bao, S.-J.; Li, C. M.; Cui, X.-Q.; Lu, Z.-S.; Guo, J., Nanostructured polyaniline/titanium dioxide composite anode for microbial fuel cells. *Acs Nano* **2007,** *2* (1), 113-119.

94. Logan, B. E.; Wallack, M. J.; Kim, K.-Y.; He, W.; Feng, Y.; Saikaly, P. E., Assessment of microbial fuel cell configurations and power densities. *Environmental Science & Technology Letters* **2015,** *2* (8), 206-214.

95. Miyahara, M.; Kouzuma, A.; Watanabe, K., Effects of NaCl concentration on anode microbes in microbial fuel cells. *AMB Express* **2015,** *5* (1), 1-9.

96. Yong, Y.-C.; Cai, Z.; Yu, Y.-Y.; Chen, P.; Jiang, R.; Cao, B.; Sun, J.-Z.; Wang, J.-Y.; Song, H., Increase of riboflavin biosynthesis underlies enhancement of extracellular electron transfer of Shewanella in alkaline microbial fuel cells. *Bioresource Technol* **2013,** *130*, 763-768.

97. Nimje, V. R.; Chen, C.-Y.; Chen, C.-C.; Tsai, J.-Y.; Chen, H.-R.; Huang, Y. M.; Jean, J.-S.; Chang, Y.-F.; Shih, R.-C., Microbial fuel cell of Enterobacter cloacae: Effect of anodic pH microenvironment on current, power density, internal resistance and electrochemical losses. *international journal of hydrogen energy* **2011,** *36* (17), 11093-11101.

98. Zhuang, L.; Zhou, S.; Li, Y.; Yuan, Y., Enhanced performance of air-cathode two-chamber microbial fuel cells with high-pH anode and low-pH cathode. *Bioresource Technol* **2010,** *101* (10), 3514-3519.

99. Xu, Y.-S.; Zheng, T.; Yong, X.-Y.; Zhai, D.-D.; Si, R.-W.; Li, B.; Yu, Y.-Y.; Yong, Y.-C., Trace heavy metal ions promoted extracellular electron transfer and power generation by Shewanella in microbial fuel cells. *Bioresource Technol* **2016,** *211*, 542-547.

100. Wu, D.; Xing, D.; Lu, L.; Wei, M.; Liu, B.; Ren, N., Ferric iron enhances electricity generation by Shewanella oneidensis MR-1 in MFCs. *Bioresource Technol* **2013,** *135*, 630-634.

101. Kim, J. R.; Min, B.; Logan, B. E., Evaluation of procedures to acclimate a microbial fuel cell for electricity production. *Applied microbiology and biotechnology* **2005,** *68* (1), 23-30.

102. Fitzgerald, L. A.; Petersen, E. R.; Gross, B. J.; Soto, C. M.; Ringeisen, B. R.; El-Naggar, M. Y.; Biffinger, J. C., Aggrandizing power output from Shewanella oneidensis MR-1 microbial fuel cells using calcium chloride. *Biosensors and Bioelectronics* **2012,** *31* (1), 492-498.

103. Lu, Z.; Chang, D.; Ma, J.; Huang, G.; Cai, L.; Zhang, L., Behavior of metal ions in bioelectrochemical systems: A review. *Journal of Power Sources* **2015,** *275*, 243-260.

104. Liu, H.; Cheng, S.; Logan, B. E., Power generation in fed-batch microbial fuel cells as a function of ionic strength, temperature, and reactor configuration. *Environ Sci Technol* **2005,** *39* (14), 5488-5493.

105. Lefebvre, O.; Tan, Z.; Kharkwal, S.; Ng, H. Y., Effect of increasing anodic NaCl concentration on microbial fuel cell performance. *Bioresource Technol* **2012,** *112*, 336-340.

106. Hermansson, M., The DLVO theory in microbial adhesion. *Colloids and Surfaces B: Biointerfaces* **1999,** *14* (1-4), 105-119.

107. Park, S.-J.; Seo, M.-K., *Interface science and composites*. Academic Press: 2011; Vol. 18.

108. Hunter, K.; Liss, P., Organic matter and the surface charge of suspended particles in estuarine waters 1. *Limnology and Oceanography* **1982,** *27* (2), 322-335.

109. Jucker, B. A.; Harms, H.; Zehnder, A., Adhesion of the positively charged bacterium Stenotrophomonas (Xanthomonas) maltophilia 70401 to glass and Teflon. *J Bacteriol* **1996,** *178* (18), 5472-5479.

110. Werwey, E.; Overbeek, J. T. G., Theory of the Stability of Lyophobic Colloid, Elsevier. *Amsterdam-New York* **1948,** *34*.

111. Zhang, H.; Olson, M. S., Effect of heavy metals on bacterial attachment in soils. *Journal of Environmental Engineering* **2012,** *138* (11), 1106-1113.

112. Rijnaarts, H. H.; Norde, W.; Lyklema, J.; Zehnder, A. J., DLVO and steric contributions to bacterial deposition in media of different ionic strengths. *Colloids and Surfaces B: Biointerfaces* **1999,** *14* (1-4), 179-195.

113. Sheng, X.; Ting, Y. P.; Pehkonen, S. O., The influence of ionic strength, nutrients and pH on bacterial adhesion to metals. *Journal of Colloid and Interface Science* **2008,** *321* (2), 256-264.

114. Gordon, A. S.; Millero, F. J., Electrolyte effects on attachment of an estuarine bacterium. *Appl Environ Microb* **1984,** *47* (3), 495-499.

115. Choi, N.-C.; Choi, J.-W.; Kwon, K.-S.; Lee, S.-G.; Lee, S., Quantifying bacterial attachment and detachment using leaching solutions of various ionic strengths after bacterial pulse. *AMB Express* **2017,** *7* (1), 38.

116. McEldowney, S.; Fletcher, M., Variability of the influence of physicochemical factors affecting bacterial adhesion to polystyrene substrata. *Appl Environ Microb* **1986,** *52* (3), 460-465.

117. van Loosdrecht, M. C.; Lyklema, J.; Norde, W.; Zehnder, A. J., Bacterial adhesion: a physicochemical approach. *Microbial Ecology* **1989,** *17* (1), 1-15.

118. McLean, J. S.; Pinchuk, G. E.; Geydebrekht, O. V.; Bilskis, C. L.; Zakrajsek, B. A.; Hill, E. A.; Saffarini, D.; Romine, M. F.; Gorby, Y. A.; Fredrickson, J. K., Oxygen-dependent autoaggregation in Shewanella oneidensis MR-1. *Environmental microbiology* **2008,** *10* (7), 1861-1876.

119. Clarke, T. A.; Edwards, M. J.; Gates, A. J.; Hall, A.; White, G. F.; Bradley, J.; Reardon, C. L.; Shi, L.; Beliaev, A. S.; Marshall, M. J., Structure of a bacterial cell surface decaheme electron conduit. *Proceedings of the National Academy of Sciences* **2011,** *108* (23), 9384-9389.

120. Richardson, D. J.; Butt, J. N.; Fredrickson, J. K.; Zachara, J. M.; Shi, L.; Edwards, M. J.; White, G.; Baiden, N.; Gates, A. J.; Marritt, S. J., The 'porin–cytochrome'model for microbe-to-mineral electron transfer. *Molecular microbiology* **2012,** *85* (2), 201-212.

121. Guvensen, N. C.; Demir, S.; Ozdemir, G., Effects of magnesium and calcium cations on biofilm formation by Sphingomonas Paucimobilis from an industrial environment. *Fresenius Environ. Bull* **2012,** *21*, 3685-3692.

122. Körstgens, V.; Flemming, H.-C.; Wingender, J.; Borchard, W., Influence of calcium ions on the mechanical properties of a model biofilm of mucoid Pseudomonas aeruginosa. *Water science and technology* **2001,** *43* (6), 49-57.

123. Thomas, K. J.; Rice, C. V., Revised model of calcium and magnesium binding to the bacterial cell wall. *Biometals* **2014,** *27* (6), 1361-1370.

124. Bazaka, K.; Crawford, R. J.; Nazarenko, E. L.; Ivanova, E. P., Bacterial extracellular polysaccharides. In *Bacterial adhesion*, Springer: 2011; pp 213-226.

125. Johnson, K.; Ams, D.; Wedel, A.; Szymanowski, J.; Weber, D.; Schneegurt, M.; Fein, J., The impact of metabolic state on Cd adsorption onto bacterial cells. *Geobiology* **2007,** *5* (3), 211-218.

126. Wei, X.; Fang, L.; Cai, P.; Huang, Q.; Chen, H.; Liang, W.; Rong, X., Influence of extracellular polymeric substances (EPS) on Cd adsorption by bacteria. *Environmental pollution* **2011,** *159* (5), 1369-1374.

127. Nies, D. H., Microbial heavy-metal resistance. *Applied microbiology and biotechnology* **1999,** *51* (6), 730-750.

128. Sharma, R. K.; Agrawal, M., Biological effects of heavy metals: an overview. *Journal of environmental Biology* **2005,** *26* (2), 301-313.

129. Bard, A., J.; Faulkner, L., R. *Electrochemical methods Fundamentals and Applications* **2001**.

130. Scholz, F., *Electroanalytical methods*. Springer: 2010; Vol. 1.

131. Bard, A. J.; Faulkner, L. R., Fundamentals and applications. *Electrochemical Methods* **2001,** *2*, 482.

132. Skoog, D. A.; Holler, F. J.; Crouch, S. R., *Principles of instrumental analysis*. Cengage learning: 2017.

133. Andrienko, D., Cyclic voltammetry. *John Wiely & Sons publication, New York* **2008**, 3-12.

134. Bard, A. J.; Faulkner, L. R.; Leddy, J.; Zoski, C. G., *Electrochemical methods: fundamentals and applications*. wiley New York: 1980; Vol. 2.

135. Moretto, L. M.; Seeber, R., Controlled Potential Techniques in Amperometric Sensing. In *Environmental Analysis by Electrochemical Sensors and Biosensors*, Springer: 2014; pp 239-282.

136. McCleverty, J. A.; Meyer, T. J., *Comprehensive coordination chemistry II: from biology to nanotechnology*. Elsevier Pergamon: 2004.

137. Elgrishi, N.; Rountree, K. J.; McCarthy, B. D.; Rountree, E. S.; Eisenhart, T. T.; Dempsey, J. L., A practical beginner's guide to cyclic voltammetry. *Journal of Chemical Education* **2017,** *95* (2), 197-206.

138. Kissinger, P. T.; Heineman, W. R., Cyclic voltammetry. *Journal of Chemical Education* **1983,** *60* (9), 702.

139. Andrade, C.; Oliveira, M. D.; Faulin, T.; Hering, V.; Abdalla, D. S. P., Biosensors for detection of Low-Density Lipoprotein and its modified forms. In *Biosensors for Health, Environment and Biosecurity*, IntechOpen: 2011.

140. Mandler, D., Fritz Scholz (Ed.): Electroanalytical methods. Guide to experiments and applications. *Analytical and Bioanalytical Chemistry* **2010,** *398* (7-8), 2771-2772.

141. Jeanmonod, D.; Suzuki, K., We are IntechOpen the world's leading publisher of Open Access books Built by scientists for scientists TOP 1% Control of a Proportional Hydraulic System. *Intech open* **2018,** *2*, 64.

142. de Castro Vasconcellos, P.; da Rocha, G. O.; Caramão, E. B.; Machado, M. E.; Krause, L. C., Chromatographic Techniques for Organic Analytes. In *Comprehensive Analytical Chemistry*, Elsevier: 2015; Vol. 70, pp 267-309.

143. Snyder, L. R.; Kirkland, J. J.; Dolan, J. W., *Introduction to modern liquid chromatography*. John Wiley & Sons: 2011.

144. Corradini, D., *Handbook of HPLC*. CRC Press: 2016.

145. Barceló, D., Comprehensive Analytical Chemistry. *Elsevier* **2006,** *49*, 87-100.

146. Barnes, J., *High performance liquid chromatography*. John Wiley & Sons: 1992.

147. Robinson, J. W.; Frame, E. M. S., *Undergraduate Instrumental Analysis*. CRC Press: 2004.

148. Galea, C.; Mangelings, D.; Vander Heyden, Y., Characterization and classification of stationary phases in HPLC and SFC–a review. *Analytica chimica acta* **2015,** *886*, 1-15.

149. Forgács, E.; Cserháti, T., CHROMATOGRAPHY| Principles. **2003**.

150. Bélanger, J. M.; Paré, J. J.; Sigouin, M., High performance liquid chromatography (HPLC): principles and applications. In *Techniques and Instrumentation in Analytical Chemistry*, Elsevier: 1997; Vol. 18, pp 37-59.

151. McCalley, D. V., The challenges of the analysis of basic compounds by high performance liquid chromatography: some possible approaches for improved separations. *Journal of Chromatography A* **2010,** *1217* (6), 858-880.

152. Swartz, M., HPLC detectors: a brief review. *Journal of Liquid Chromatography & Related Technologies* **2010,** *33* (9-12), 1130-1150.

153. Germer, T. A.; Zwinkels, J. C.; Tsai, B. K., Theoretical concepts in spectrophotometric measurements. In *Experimental Methods in the Physical Sciences*, Elsevier: 2014; Vol. 46, pp 11-66.

154. Nilapwar, S. M.; Nardelli, M.; Westerhoff, H. V.; Verma, M., Absorption spectroscopy. In *Methods in enzymology*, Elsevier: 2011; Vol. 500, pp 59-75.

155. Murphy, D. B., *Fundamentals of light microscopy and electronic imaging*. John Wiley & Sons: 2002.

156. Singh, A., Chapter 4-Experimental Methodologies for the Characterization of Nanoparticles. *Engineered Nanoparticles: Structure, Properties and Mechanisms of Toxicity, Singh, AK (Ed.)., Academic Press, New York* **2016**, 125-170.

157. Nyenje, M.; Green, E.; Ndip, R., Evaluation of the effect of different growth media and temperature on the suitability of biofilm formation by Enterobacter cloacae strains isolated from food samples in South Africa. *Molecules* **2013,** *18* (8), 9582-9593.

158. Sezonov, G.; Joseleau-Petit, D.; d'Ari, R., Escherichia coli physiology in Luria-Bertani broth. *J Bacteriol* **2007,** *189* (23), 8746-8749.

159. Muscolino, J., Building and Optimizing a Spectroelectrochemical System for the Study of Shewanella Putrefaciens. **2016**.

160. Bose, S.; Hochella Jr, M. F.; Gorby, Y. A.; Kennedy, D. W.; McCready, D. E.; Madden, A. S.; Lower, B. H., Bioreduction of hematite nanoparticles by the dissimilatory iron reducing bacterium Shewanella oneidensis MR-1. *Geochimica et Cosmochimica Acta* **2009,** *73* (4), 962-976.

161. Wu, W.; Yang, F.; Liu, X.; Bai, L., Influence of substrate on electricity generation of Shewanella loihica PV-4 in microbial fuel cells. *Microbial cell factories* **2014,** *13* (1), 69.

162. Wu, W.; Niu, H.; Yang, D.; Wang, S.; Jiang, N.; Wang, J.; Lin, J.; Hu, C., Polyaniline/carbon nanotubes composite modified anode via graft polymerization and self-assembling for microbial fuel cells. *Polymers* **2018,** *10* (7), 759.

163. Deng, X.; Okamoto, A., Electrode potential dependency of single-cell activity identifies the energetics of slow microbial electron uptake process. *Frontiers in Microbiology* **2018,** *9*, 2744.

164. Zhang, J.; Zhang, Q.; Wang, J.; Shi, X.; Zhang, Z., Analysis of the monosaccharide composition of fucoidan by precolumn derivation HPLC. *Chinese Journal of Oceanology and Limnology* **2009,** *27* (3), 578-582.

165. Liu, G.; Yates, M. D.; Cheng, S.; Call, D. F.; Sun, D.; Logan, B. E., Examination of microbial fuel cell start-up times with domestic wastewater and additional amendments. *Bioresource Technol* **2011,** *102* (15), 7301-7306.

166. Zhang, X.; Liang, P.; Shi, J.; Wei, J.; Huang, X., Using a glass fiber separator in a single-chamber air-cathode microbial fuel cell shortens start-up time and improves anode performance at ambient and mesophilic temperatures. *Bioresource Technol* **2013,** *130*, 529-535.

167. Zou, L.; Wu, X.; Huang, Y.; Ni, H.; Long, Z.-e., Promoting Shewanella Bidirectional Extracellular Electron Transfer for Bioelectrocatalysis by Electropolymerized Riboflavin Interface on Carbon Electrode. *Frontiers in microbiology* **2018,** *9*, 3293.

168. Steentjes, T.; Jonkheijm, P.; Huskens, J., Electron Transfer Processes in Ferrocene-Modified Poly (ethylene glycol) Monolayers on Electrodes. *Langmuir* **2017,** *33* (43), 11878-11883.

169. Laviron, E., General expression of the linear potential sweep voltammogram in the case of diffusionless electrochemical systems. *Journal of Electroanalytical Chemistry and Interfacial Electrochemistry* **1979,** *101* (1), 19-28.

170. Sokolov, I.; Smith, D. S.; Henderson, G. S.; Gorby, Y. A.; Ferris, F. G., Cell surface electrochemical heterogeneity of the Fe(III)-reducing bacteria Shewanella putrefaciens. *Environ Sci Technol* **2001,** *35* (2), 341-347.

171. Tsuneda, S.; Aikawa, H.; Hayashi, H.; Yuasa, A.; Hirata, A., Extracellular polymeric substances responsible for bacterial adhesion onto solid surface. *FEMS microbiology letters* **2003,** *223* (2), 287-292.

172. Beveridge, T.; Fyfe, W., Metal fixation by bacterial cell walls. *Canadian Journal of Earth Sciences* **1985,** *22* (12), 1893-1898.

173. Guiné, V.; Spadini, L.; Sarret, G.; Muris, M.; Delolme, C.; Gaudet, J.-P.; Martins, J., Zinc sorption to three gram-negative bacteria: combined titration, modeling, and EXAFS study. *Environ Sci Technol* **2006,** *40* (6), 1806-1813.

174. Redman, J. A.; Walker, S. L.; Elimelech, M., Bacterial adhesion and transport in porous media: Role of the secondary energy minimum. *Environ Sci Technol* **2004,** *38* (6), 1777-1785.

175. Dobrowolski, R.; Szcześ, A.; Czemierska, M.; Jarosz-Wikołazka, A., Studies of cadmium (II), lead (II), nickel (II), cobalt (II) and chromium (VI) sorption on extracellular polymeric substances produced by Rhodococcus opacus and Rhodococcus rhodochrous. *Bioresource Technol* **2017,** *225*, 113-120.

176. Rivera-Utrilla, J.; Bautista-Toledo, I.; Ferro-García, M. A.; Moreno-Castilla, C., Activated carbon surface modifications by adsorption of bacteria and their effect on aqueous lead adsorption. *Journal of Chemical Technology & Biotechnology* **2001,** *76* (12), 1209-1215.

177. Ferris, F. G.; Beveridge, T., Physicochemical roles of soluble metal cations in the outer membrane of Escherichia coli K-12. *Canadian journal of microbiology* **1986,** *32* (7), 594-601.

178. Persson, I., Hydrated metal ions in aqueous solution: How regular are their structures? *Pure and Applied Chemistry* **2010,** *82* (10), 1901-1917.

179. Choi, D.; Lee, S. B.; Kim, S.; Min, B.; Choi, I.-G.; Chang, I. S., Metabolically engineered glucose-utilizing Shewanella strains under anaerobic conditions. *Bioresource Technol* **2014,** *154*, 59-66.

180. Howard, E. C.; Hamdan, L. J.; Lizewski, S. E.; Ringeisen, B. R., High frequency of glucose-utilizing mutants in Shewanella oneidensis MR-1. *FEMS microbiology letters* **2012,** *327* (1), 9-14.

181. Honda, S.; Akao, E.; Suzuki, S.; Okuda, M.; Kakehi, K.; Nakamura, J., High-performance liquid chromatography of reducing carbohydrates as strongly ultraviolet-absorbing and electrochemically sensitive 1-phenyl-3-methyl5-pyrazolone derivatives. *Analytical biochemistry* **1989,** *180* (2), 351-357.

182. Green, J. M., Peer reviewed: a practical guide to analytical method validation. *Analytical chemistry* **1996,** *68* (9), 305A-309A.

183. Yamane, Y.; Ooshima, H.; Kato, J., Overproduction of riboflavin by an Arthrobacter sp. mutant resistant to 5-fluorouracil. *Enzyme Microb Tech* **1993,** *15* (10), 877-880.

184. Kolonne, S.; Seviour, R.; McDougall, B., Effect of pH on exocellular riboflavin production byEremothecium ashbyii. *Biotechnol Lett* **1994,** *16* (1), 79-84.

185. Shrivastava, A.; Gupta, V. B., Methods for the determination of limit of detection and limit of quantitation of the analytical methods. *Chronicles of young scientists* **2011,** *2* (1), 21.

186. Lovley, D. R., Bug juice: harvesting electricity with microorganisms. *Nature Reviews Microbiology* **2006,** *4* (7), 497.

187. Watanabe, K.; Manefield, M.; Lee, M.; Kouzuma, A., Electron shuttles in biotechnology. *Current Opinion in Biotechnology* **2009,** *20* (6), 633-641.

188. Carmona-Martinez, A. A.; Harnisch, F.; Fitzgerald, L. A.; Biffinger, J. C.; Ringeisen, B. R.; Schröder, U., Cyclic voltammetric analysis of the electron transfer of Shewanella oneidensis MR-1 and nanofilament and cytochrome knock-out mutants. *Bioelectrochemistry* **2011,** *81* (2), 74-80.

189. Fitzgerald, L. A.; Petersen, E. R.; Leary, D. H.; Nadeau, L. J.; Soto, C. M.; Ray, R. I.; Little, B. J.; Ringeisen, B. R.; Johnson, G. R.; Vora, G. J.; Biffinger, J. C., Shewanella

frigidimarina microbial fuel cells and the influence of divalent cations on current output. *Biosens Bioelectron* **2013,** *40* (1), 102-109.

190. Leach, A. R.; Leach, A. R., *Molecular modelling: principles and applications*. Pearson education: 2001.

191. Saleh, N. A.; Elhaes, H.; Ibrahim, M., Design and development of some viral protease inhibitors by QSAR and molecular modeling studies. In *Viral proteases and their inhibitors*, Elsevier: 2017; pp 25-58.

192. Cohen, N. C., *Guidebook on molecular modeling in drug design*. Elsevier: 1996.

193. Lins, R. D.; Straatsma, T., Computer simulation of the rough lipopolysaccharide membrane of Pseudomonas aeruginosa. *Biophysical journal* **2001,** *81* (2), 1037-1046.

194. Nascimento, A.; Pontes, F. J.; Lins, R. D.; Soares, T. A., Hydration, ionic valence and cross-linking propensities of cations determine the stability of lipopolysaccharide (LPS) membranes. *Chemical communications* **2014,** *50* (2), 231-233.

VITA

Dr. Aisha Awad Al Shahrani is the daughter of Awad Abdullah Alshahrani and Huda Ahmad Alasiri. Dr. Aisha Awad Al Shahrani was born and raised in Abha, Saudi Arabia.

She was enrolled in the Graduate Program of the Chemistry Department at Texas A&M University-Commerce and received her M.S. Degree in Chemistry in August 2014. She was awarded a full scholarship from Albaha University to complete the Ph.D. program. In August 2014, she was enrolled in Ph.D. Program of the Chemistry Department at Loyola University Chicago. While at Loyola University Chicago, Dr. Aisha participated in several conferences and presented posters as well as a presentation.

Currently, Dr. Aisha Awad Al Shahrani is an Assistant Professor of Chemistry at Albaha University in Al Baha, Saudi Arabia. Dr. Aisha intends to continue to develop her research in the field of analytical chemistry and in a wide range in chemistry and science fields.